Title
Molecular mechanism of cotransin action

Permalink
https://escholarship.org/uc/item/4bt2x57f

Author
MacKinnon, Andrew L.

Publication Date
2011

Peer reviewed|Thesis/dissertation

Molecular mechanism of cotransin action

by

Andrew L. MacKinnon

DISSERTATION

Submitted in partial satisfaction of the requirements for the degree of

DOCTOR OF PHILOSOPHY

in

Chemistry and Chemical Biology

in the

GRADUATE DIVISION

of the

UNIVERSITY OF CALIFORNIA, SAN FRANCISCO

Dedicated to my family.

Acknowledgments

I would like to thank Jack for guidance; Manu for technical support and reagents; Dan and Jen for their friendship; and my brothers Matt and Evan, and my mom, Susan MacKinnon for always being there.

Molecular mechanism of cotransin action

by

Andrew L. MacKinnon

Abstract

Cotransins are a class of cyclic-heptadepsi-peptides that potently inhibits translocation of a subset of proteins across the membrane of the endoplasmic reticulum (ER). Sensitivity or resistance to cotransins depends on the identity of a protein's N-terminal ER-targeting sequence. However, the precise mechanism of action of cotransins is unknown. Motivated by cotransins' unprecedented ability to block an essential step in the biogenesis of several therapeutically relevant secretory and membrane proteins, we sought to clarify their precise mechanism of action.

We discovered that cotransins directly target a highly conserved protein-conducting channel in the ER membrane known as Sec61. Sec61 mediates the translocation of secretory proteins across the ER membrane and the insertion of most integral membrane proteins into the ER membrane. Despite directly binding to a channel utilized by all proteins entering the ER, cotransins block passage of only a select few. These findings lead us to hypothesize that cotransins could be used as chemical probes into the underlying molecular mechanism of Sec61 function.

To test this possibility, we determined how cotransins block Sec61-mediated insertion of a model protein into the ER membrane. We found that cotransin-bound Sec61 impedes passage of a hydrophobic transmembrane domain (TMD) from the pore of Sec61 into the surrounding lipid bilayer, thereby permitting analysis of a previously uncharacterized pre-integration intermediate. Site-specific crosslinking studies of this intermediate revealed an α-helical TMD docked near the cytosolic face of the lateral gate in Sec61. Progression through the cotransin-stabilized stage was strongly influenced by biophysical properties of the TMD, such as α-helical propensity and hydrophobicity. Cotransins therefore reveal that direct interactions between the TMD and the lateral gate of Sec61 precede TMD transfer into the membrane.

Taken together, these findings identify Sec61 as a possible therapeutic target and provide a mechanistic framework in which to judge the therapeutic potential of cotransins. Future studies will seek to define the entire subset of human proteins whose expression is inhibited by cotransins and the efficacy of cotransins in different models of human disease.

Table of Contents

List of Tables

List of Figures and Schemes

Chapter 1: Introduction

1.1 Abstract

Cotranslational translocation across the membrane of the endoplasmic reticulum (ER) is an essential step in the biogenesis of most eukaryotic secretory and integral membrane proteins. This process occurs at a multi-subunit protein complex embedded in the ER membrane, termed the translocon, the minimal component of which comprises the Sec61 channel. Sec61 mediates the translocation of soluble polypeptides across the ER membrane and the integration of hydrophobic polypeptides into the ER membrane, concurrent with their synthesis by a membrane-bound ribosome. However, many mechanistic details of cotranslational translocation remain poorly understood. Cotransins (CTs) are a class of small molecules that potently blocks translocation across the ER membrane in a substrate-selective manner. These inhibitors therefore potentially represent a set of chemical tools that can be used to dissect the mechanism of translocation. In this chapter, I first summarize what is known about the mechanism of translocation across the ER membrane. I then discuss the discovery, development, and initial characterization of CTs. Finally, I propose using CTs as probes for the mechanism Sec61-mediated translocation.

1.2 Overview of protein sorting and the secretory pathway

Nearly all proteins are synthesized in the cytosol, yet many perform their function in a different cellular compartment. Protein sorting is the process by which proteins are selectively delivered to their respective compartments. Proper protein sorting requires

both a signal that specifies delivery to a particular compartment and specialized cellular

machinery to carry out the physical process of protein delivery.[1]

Secreted and cell surface membrane proteins represent ~30% of the human proteome and

mediate many essential cellular processes.[2] These proteins, as well as proteins of the

endoplasmic reticulum (ER) and Golgi, are sorted to these locations by the secretory

pathway. Recognition of secreted and cell surface proteins is conferred by the presence of

a hydrophobic signal sequence near the N-terminus of the nascent polypeptide. Delivery

into the secretory pathway is mediated by a highly conserved cystosolic targeting

machinery that is coupled with a protein-conducting channel in the ER membrane.[3] The

major steps leading into the secretory pathway can be summarized as follows: 1)

recognition of the signal sequence of a nascent secretory or membrane protein during its

synthesis in the cytosol, 2) delivery of the ribosome-nascent polypeptide complex to the

cytosolic face of the ER membrane, and 3) cotranslational translocation of the nascent

protein across or integration into the ER membrane. These three steps, discussed in more

detail in the following sections, both commit a protein to the secretory pathway, and are

required for their subsequent delivery to internal organelles, the cell membrane, or for

secretion from the cell.

1.3 Overview of cotranslational translocation

Entry into the secretory pathway requires the recognition and delivery of nascent

secretory and membrane proteins to the cytosolic face of the endoplasmic reticulum (ER)

(**Figure 1-1**). This begins in the cytosol, when a hydrophobic signal sequence or internal

transmembrane (TM) domain of a nascent secretory or membrane protein emerges from a translating ribosome and is recognized by the signal recognition particle (SRP). SRP targets the ribosome-nascent polypeptide complex (RNC) to the cytosolic face of the ER membrane via a GTP-dependent interaction between SRP and its membrane-bound receptor known as SR.[4] The interaction between SRP and SR results in GTP hydrolysis and transfer of the RNC from SRP to a multi-subunit integral membrane protein complex embedded in the ER membrane. The minimal component of this complex is the highly conserved Sec61 complex,[5] which forms a protein-conducting channel across the ER membrane.[6,7] Sec61 directly binds the signal sequence,[8,9] an event that is thought to "gate" the channel toward the ER lumen and thereby provide a continuous pathway for the nascent polypeptide to translocate directly across or integrate into the ER membrane, concurrent with its synthesis.[7] While a great deal is known about the mechanism of SRP-mediated delivery of the RNC to the membrane,[10-12] less is known about how the RNC is transferred from SRP to Sec61, the precise role of Sec61 in this process,[13] and whether or not discrete intermediates exist after RNC transfer but before signal sequence-mediated gating of Sec61.
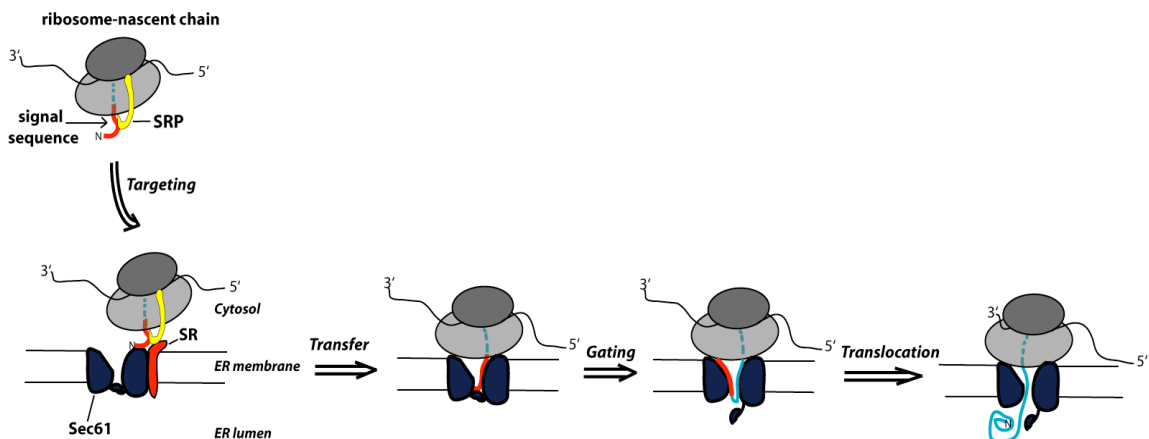
Figure 1-1. Overview of cotranslational translocation.
The N-terminal signal sequence of a nascent secretory protein is recognized by the signal recognition particle (SRP) as it emerges from the ribosome in the cytosol. SRP targets the ribosome-nascent chain complex (RNC) to the ER membrane via an interaction between SRP and the SRP receptor (SR). The RNC is then transferred to the Sec61 complex in the ER membrane. Following transfer, the signal sequence induces a conformational change in Sec61, termed "gating", which opens the channel toward the ER lumen. The nascent polypeptide is then translocated through Sec61 and across the membrane where it is folded and processed by ER lumenal enzymes.

1.4 Diverse signal sequences mediate targeting to the ER

N-terminal signal sequences are strikingly diverse in terms of their length, charge, and overall hydrophobicity, yet all mediate sorting to the ER. Signal sequences do share a common architecture characterized by a basic N-domain, a stretch of 6–20 hydrophobic amino acids, and a slightly polar C-region.[14] The hydrophobic core of the signal sequence appears to be the most critical structural feature that confers SRP-mediated entry into the secretory pathway.[15] The first hydrophobic transmembrane domain (TMD) of an integral membrane protein can also direct SRP-mediated targeting to the ER. In this case, the targeting sequence is referred to as a signal anchor (SA), reflecting both its ability to direct targeting as well as its ability to anchor the protein in the lipid bilayer. The SA domain can adopt either a type I (N_{lumen}/C_{cyto}) or type II (N_{cyto}/C_{lumen}) orientation with

respect to the plane of the membrane. The topology of the SA is largely determined by the hydrophobicity of the SA and by charged residues flanking the SA.[16,17] Like signal sequences, SAs are not strictly conserved in primary amino acid sequence, but since they must ultimately span the lipid bilayer, they appear to be generally more hydrophobic.[15]

Despite the lack of primary sequence similarity, signal sequences all interact with the same targeting and translocation machinery. Structural studies have revealed that recognition of the signal sequence by the 54 kDa subunit of SRP occurs in a deep, hydrophobic groove that is lined with methionine residues.[18,19] The conformational flexibility of the methionine side chain was proposed to account for the broad range of signal sequences that are recognized by SRP. While a minimal number of hydrophobic amino acids in the signal sequence appears to be required for SRP binding,[20] once bound by SRP, RNC delivery to the ER membrane is ensured.

Following SRP-mediated delivery to the ER membrane, signal sequences must also be recognized by the Sec61 channel. Signal sequence recognition by Sec61 appears to be highly variable and more stringent than recognition by SRP. For example, signals that are equally efficient in directing SRP-mediated targeting to the ER can vary greatly in the ability to mediate formation of a stable RNC-Sec61 junction,[21] and in the ability to "gate" the Sec61 channel and to initiate transport across the membrane.[22] These differences are also reflected by the requirement for some signal sequences (but not others) of accessory factors such as TRAP[23] and TRAM[24] to promote efficient translocation. Interestingly, signal sequences appear to be fairly well conserved across species,[22] and functionally

matched with their respective mature domains to minimize production of mis-translocated species.[22,23] The structural diversity among signal sequences therefore appears to underlie important functional differences that are revealed at the membrane. This was dramatically demonstrated in cell culture models where entry into the ER was modulated in a signal sequence-dependent manner in response to changing culture conditions.[25] These results imply that signal sequence recognition by Sec61 may represent an underappreciated point of regulatory control in the secretory pathway.

It is important to emphasize that the mechanism by which signal sequences "gate" Sec61 to initiate transport across the membrane is unknown. Furthermore, while it is commonly assumed that all signal sequences interact with a common binding site in Sec61, this remains to be formally demonstrated. Indeed, many aspects of Sec61 function remain poorly understood. In the following sections, I summarize what is known about the architecture of the Sec61 channel and the conformational changes of Sec61 that are thought to underlie protein translocation.

1.5 Sec61-mediated translocation across the ER membrane

The highly conserved Sec61 complex mediates the translocation of secretory proteins across the ER membrane and the integration of membrane proteins into the lipid bilayer. To accomplish this task, Sec61 recognizes functional signal sequences,[9,26] orients the signal sequence and TMDs with respect to the membrane,[17] and mediates the retention, translocation, or membrane integration of nascent polypeptide segments.[27,28] Remarkably, these events occur while the nascent polypeptide is being translated by a membrane-

7

bound ribosome. Sec61 must therefore be highly dynamic and flexible and must respond to structural features of the incoming nascent polypeptide. These conformational changes of the Sec61 complex and how these changes are coordinated with translation are poorly understood.

Sec61 is a heterotrimer comprised of α, β, and γ subunits. A single copy of the trimer is thought to form the functional channel in the membrane.[29,30] Sec61α, the largest subunit, contains ten TMDs (TMD 1–10) and forms the structural core of the channel (**Figure 1-2)**. The crystal structure of the archeal homolog of Sec61α (known as SecY) reveals an hourglass shaped pore in the membrane which is sealed at the lumenal end by a short α-helix, termed the plug.[31] To allow translocation of nascent polypeptides across the membrane, the plug must be removed from the central pore, opening the channel toward the ER lumen. This "lumenal gating" event is proposed to occur upon recognition of the signal sequence via its intercalation into the walls of Sec61α. Signal sequence recognition would destabilize the position of the plug,[32] expand the diameter of the channel, and allow the nascent polypeptide to insert into the channel in a looped conformation for translocation of its C-terminal domain across the membrane.[28,29,32] This idea is supported by the observation that a signal sequence can photo-crosslink to TMD 2 and TMD 7 of Sec61.[8] The coordination of lumenal gating with ongoing translation may be regulated by both the identity of the signal sequence[21,22] and nascent polypeptide structure within the ribosome.[34] This implies the existence of a mechanism for direct communication between the ribosome and Sec61, which has been demonstrated both experimentally[35] and in computational simulations.[36] Accessory proteins such as TRAP

and TRAM may further regulate lumenal gating in a signal sequence-dependent manner.[23,24]
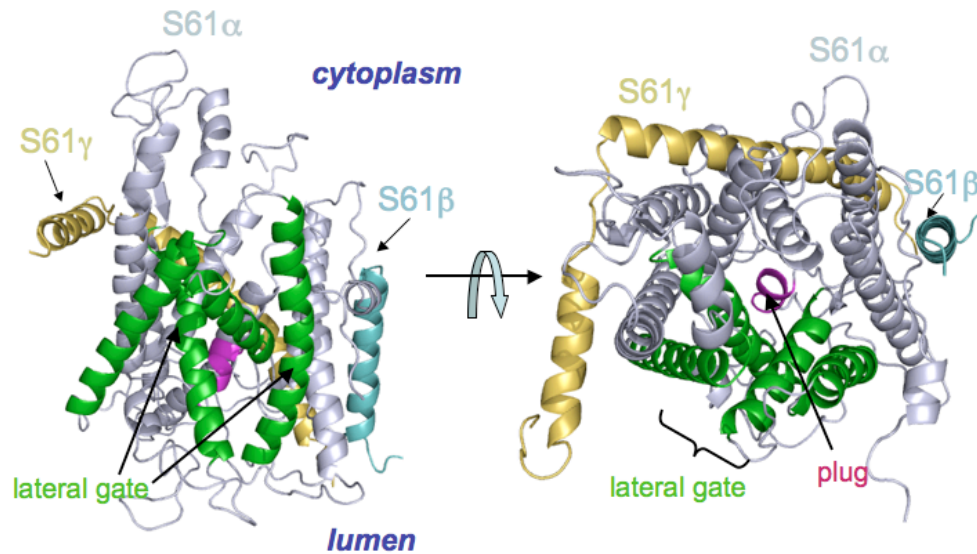
Figure 1-2. Mammalian homology model of the Sec61 translocation channel.
The plug domain is colored magenta and helices forming the lateral gate are colored green. The model is derived from the crystal structure of the archeal channel.[31]

Sec61 is also proposed to open laterally within the plane of the membrane by at least 12 Å to allow TMDs of integral membrane proteins to cotranslationally enter the lipid bilayer directly from the channel pore (**Figure 1-3**). This is thought to occur through a seam in the channel walls, termed the "lateral gate", which is formed at the interface of TMD 2/3 and TMD 7/8 of Sec61α, the same region shown to photo-crosslink to signal sequences. Different structures of Sec61 complexes have revealed the lateral gate in a continuum of partially open states,[37-39] implicating the lateral gate as a potential site of TMD exit into the lipid bilayer. However, the functional significance of these structural changes, and the role of the lateral gate during TMD integration remain speculative. At

least two models have been proposed for the mechanism of lateral gating and TMD integration. In one model, which is based on the strong correlation observed between hydrophobicity and membrane integration efficiency of model TMDs, the lateral gate was proposed to fluctuate between open and closed conformations, allowing the TMD to thermodynamically equilibrate with the lipid bilayer.[40-42] In another model, which is based on the observation that TMDs can be held in a fixed orientation at the Sec61 channel,[43,44] and that mutations to Sec61 can affect integration efficiency,[45] lateral gating was proposed to be kinetically controlled by direct, substrate-specific interactions between Sec61 and the TMD. The extent to which both models may hold true under different conditions is unknown. Indeed, the lack of appropriate methods to stabilize this intrinsically dynamic process has greatly limited our understanding of this fundamental step of protein biogenesis.
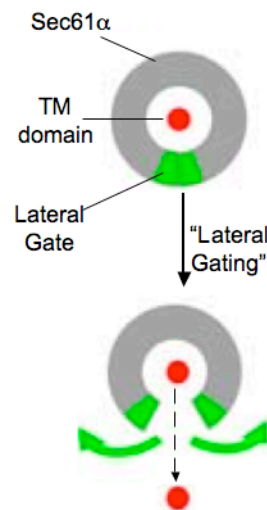
Figure 1-3. Proposed mechanism of lateral gating.
Sec61α may open laterally from within the plane of the membrane to allow integration of hydrophobic transmembrane (TM) domains into the lipid bilayer. Adapted from reference 54.

Sec61 also orients TMDs with respect to the plane of the membrane. This is thought to largely be controlled by the structure of the incoming nascent polypeptide according to the "positive inside rule". This rule is based on the observation that the more positive end of a TMD is typically retained on the cytoplasmic side of the membrane.[17] Two conserved, positively charged residues in the plug domain of Sec61α, and one conserved negatively charged residue in TMD 8 of Sec61α were shown to contribute to TMD orientation.[46] These residues may help topologically orient the incoming TMD through electrostatic forces. During the integration of a polytopic membrane protein, Sec61 must direct the cytosolic or lumenal loops of the nascent protein to opposite sides of the membrane, as well as laterally open to allow integration of TMDs into the membrane.[27] The channel must therefore alternate between several different open and closed conformations, and coordinate these structural changes based on the properties of the incoming nascent polypeptide. The molecular mechanisms that direct these changes are only beginning to be appreciated.

To summarize, Sec61 must necessarily function as a highly dynamic and flexible protein-conducting channel, yet relatively little is known about the conformational changes that underlie this flexibility. While structures of the Sec61 channel have led to compelling hypotheses about what these changes might be, these ideas remain largely untested. Furthermore, while it is clear that structural features of the nascent chain can regulate conformational changes in Sec61 to achieve proper topology in the membrane, how this occurs is unknown. New tools and experimental approaches are required to gain new molecular-level insights into these processes.

1.6 Cotransins: substrate-selective inhibitors of cotranslational translocation

The fungal cyclic-heptadepsi-peptide natural product known as HUN-7293 (**Figure 1-4**) was first discovered in a screen for inhibitors of the expression of vascular cell adhesion molecule (VCAM).[47] HUN-7293 potently inhibited VCAM expression in stimulated primary human cell lines by an unknown mechanism. Guided by structure-activity relationships (SAR) of the HUN-7293 scaffold,[48] a simplified derivative known as cotransin (CT1) was prepared for mechanistic studies.[49] These studies revealed that CT1 did not block the transcription or translation of VCAM, but instead prevented its translocation into the endoplasmic reticulum (ER), leading to proteasome-dependent degradation in the cytosol. Mechanistic studies in a reconstituted system with truncated VCAM-ribosome-nascent chain complexes (RNCs) showed that inhibition of translocation occurs after RNC-targeting to the ER membrane but before access of the nascent polypeptide to the ER lumen (**Figure 1-5**). Similar results were obtained with CAM-741, a related cyclopeptide.[50]
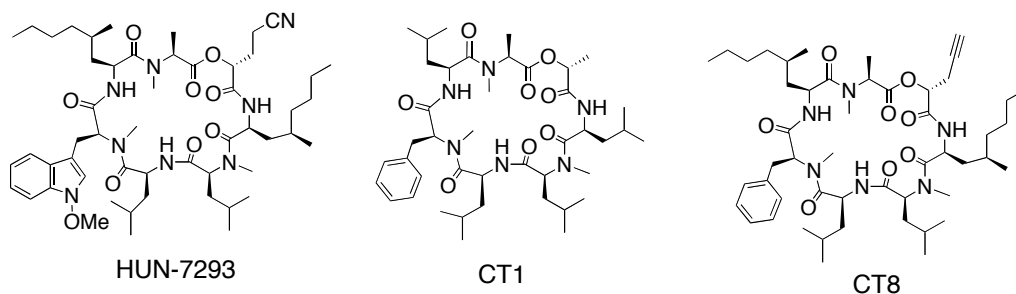
Figure 1-4. Structures of HUN-7293, CT1, and CT8.

Domain swapping experiments revealed that the VCAM signal sequence alone was necessary and sufficient to confer sensitivity to the action of CT1. However, comparison of the signal sequences of all known CT1-sensitive proteins did not reveal an obvious consensus sequence.[49] Furthermore, systematic mutagenesis of the VCAM or VEGF signal peptides failed to uncover a clear set of "rules" governing sensitivity to CTs.[51,52] To add to the mystery, it was recently demonstrated that chemical changes to the CT scaffold can modulate the range of inhibited proteins, yielding more selective or more promiscuous inhibitors.[53]
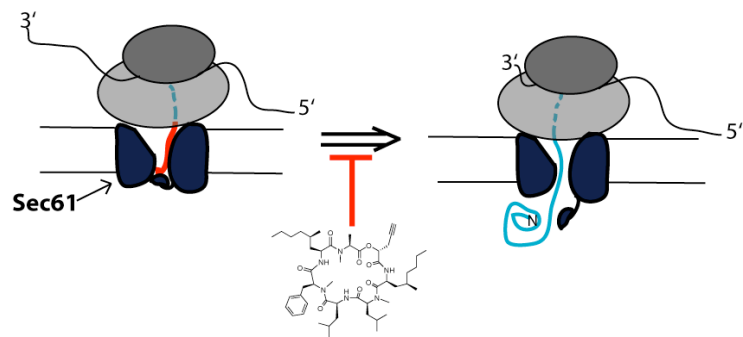
Figure 1-5. Proposed mechanism of action of CTs.
CTs block signal sequence-mediated "gating" of the Sec61 channel by an unknown mechanism.

Taken together, these studies suggest a cryptic mechanism of action wherein CT blocks signal sequence-dependent "gating" of the Sec61 channel (**Figure 1-5**). However, the direct molecular target of CT, the mechanism by which CT blocks translocation across the membrane, and the basis for its substrate selectivity are unknown. A greater understanding of the mechanism of action of CT could therefore reveal new insights into how signal sequences mediate functional changes to Sec61, and the mechanism of translocation across the ER membrane.

1.7 Conclusions

Cotranslational translocation across the ER membrane is a fundamental step in the biogenesis of secretory and membrane proteins, yet many of the events occurring at the membrane remain poorly characterized. A greater understanding of these dynamic events requires new experimental methods and tools. Small-molecule inhibitors such as CTs may provide a unique set of tools to dissect the process of cotranslational translocation. In my dissertation, I more fully characterize the mode of action of CTs, revealing new insight into the mechanism of Sec61-mediated translocation. In chapter 2, I describe the design, synthesis, and application of a CT photo-affinity probe used to identify the direct molecular target of CT in the ER membrane. In chapter 3, I use CT and a model membrane protein to mechanistically dissect the process of Sec61-mediated transmembrane domain integration.

1.8 References

1. Wickner, W., and Schekman, R. (2005). Protein translocation across biological membranes. Science *310*, 1452–1456.

2. Liu, J., and Rost, B. (2001). Comparing function and structure between entire proteomes. Protein Sci. *10*, 1970-1979.

3. Zimmermann, R., Eyrisch, S., Ahmad, M., and Helmsb, V. (2011). Protein translocation across the ER membrane. Biochim. Biophys. Acta *1808*, 912–924.

4. Luirink, J., and Sinning, I. (2004). SRP-mediated protein targeting: structure and function revisited. Biochim. Biophys. Acta *1694*, 17–35.

5. Görlich, D., and Rapoport, T.A. (1993). Protein translocation into proteoliposomes reconstituted from purified components of the endoplasmic reticulum membrane. Cell *75*, 615–630.

6. Mothes, W., Prehn, S., and Rapoport, T.A. (1994). Systematic probing of the environment of a translocating secretory protein during translocation through the ER membrane. EMBO J. *13*, 3973–3982.

7. Crowley, K.S., Reinhart, G.D., and Johnson A.E. (1993). The signal sequence moves through a ribosomal tunnel into a noncytoplasmic aqueous environment at the ER membrane early in translocation. Cell *73*, 1101–1115.

8. Plath, K., Mothes, W., Wilkinson, B.M., Stirling, C.J., and Rapoport, T.A. (1998). Signal sequence recognition in posttranslational protein transport across the yeast ER membrane. Cell *94*, 795–807.

9. Jungnickel, B., and Rapoport, T.A. (1995). A posttargeting signal sequence recognition event in the endoplasmic reticulum membrane. Cell *82*, 261–270.

10. Shan, S., Schmid, S.L., and Zhang, X. (2009). Signal recognition particle (SRP) and SRP receptor: a new paradigm for multistate regulatory GTPases. Biochemistry *48*, 6696–6704.

11. Halic, M., Blau, M., Becker, T., Mielke, T., Pool, M. R., Wild, K., Sinning, I., and Beckmann, R. (2006). Following the signal sequence from ribosomal tunnel exit to signal recognition particle. Nature *444*, 507–511.

12. Egea, P. F., Stroud, R. M., and Walter, P. (2005). Targeting proteins to membranes: structure of the signal recognition particle. Curr. Opin. Struct. Biol. *15*, 213–220.

13. Song, W., Raden, D., Mandon, E. C., and Gilmore, R. (2000). Role of Sec61α in the regulated transfer of the ribosome-nascent chain complex from the signal recognition particle to the translocation channel. Cell *100*, 333–343.

14. von Heijne, G. (1985). Signal sequences. The limits of variation. J. Mol. Biol. *184*, 99–105.

15. Martoglio, B., and Dobberstein, B. (1998). Signal sequences: more than just greasy peptides. Trends Cell Biol. *8*, 410–415.

16. Sakaguchi, M., Tomiyoshi, R., Kuroiwa, T., Mihara, K., and Omura, T. (1992). Functions of signal and signal-anchor sequences are determined by the balance between the hydrophobic segment and the N-terminal charge. Proc. Natl. Acad. Sci. USA *89*, 16–19.

17. Higy, M., Junne, T., and Spiess, M. (2004). Topogenesis of membrane proteins at the endoplasmic reticulum. Biochemistry *43*, 12716–12722.

18. Janda, C. Y., Li, J., Oubridge, C., Hernández, H., Robinson, C. V., and Nagai, K. (2010). Recognition of a signal peptide by the signal recognition particle. Nature *465*, 507–510.

19. Keenan, R. J., Freymann, D. M., Walter, P., and Stroud, R. M. (1998). Crystal structure of the signal sequence binding subunit of the signal recognition particle. Cell *94*, 181–191.

20. Ng, D. T. W., Brown, J. D., and Walter, P. (1996). Signal sequences specify the targeting route to the endoplasmic reticulum membrane. J. Cell Biol. *134*, 269–278.

21. Rutkowski, D.T., Lingappa, V.R., and Hegde, R.S. (2001). Substrate-specific regulation of the ribosome- translocon junction by N-terminal signal sequences. Proc. Natl. Acad. Sci. USA *98*, 7823–7828.

22. Kim, S.J., Mitra, D., Salerno, J.R., and Hegde, R.S. (2002). Signal sequences control gating of the protein translocation channel in a substrate-specific manner. Dev. Cell *2*, 207–217.

23. Fons, R.D., Bogert, B.A., and Hegde, R.S. (2003). Substrate-specific function of the translocon-associated protein complex during translocation across the ER membrane. J. Cell Biol. *160*, 529–539.

24. Voigt, S., Jungnickel, B., Hartmann, E., and Rapoport, T.A. (1996). Signal sequence-dependent function of the TRAM protein during early phases of protein transport across the endoplasmic reticulum membrane. J. Cell Biol. *134*, 25–35.

25. Kang, S.W., Rane, N.S., Kim, S.J., Garrison, J.L., Taunton, J., and Hedge, R.S. (2006). Substrate-specific translocational attenuation during ER stress defines a pre-emptive quality control pathway. Cell *127*, 999-1013.

26. Mothes, W., Jungnickel, B., Brunner, J., and Rapoport, T.A. (1998). Signal sequence recognition in cotranslational translocation by protein components of the endoplasmic reticulum membrane. J. Cell Biol. *142*, 355–364.

27. Skach, W.R. (2009). Cellular mechanisms of membrane protein folding. Nat. Struct. Mol. Biol. *16*, 606–612.

28. Rapoport, T.A. (2007). Protein translocation across the eukaryotic endoplasmic reticulum and bacterial plasma membranes. Nature *450*, 663–669.

29. Cannon, K.S., Or, E., Clemons, W.M., Jr., Shibata, Y., and Rapoport T.A. (2005). Disulfide bridge formation between SecY and a translocating polypeptide localizes the translocation pore to the center of SecY. J. Cell Biol. *169*, 219–225.

30. Becker, T., Bhushan, S., Jarasch, A., Armache, J.-P., Funes, S., Jossinet, F., Bembart, J., Mielke, T., Berninghausen, O., Schulten, K., et al. (2009). Structure of Monomeric Yeast and Mammalian Sec61 Complexes Interacting with the Translating Ribosome. Science *326*, 1369–1373.

31. Van den Berg, B., Clemons, W.M., Jr., Collinson, I., Modis, Y., Hartmann, E., Harrison, S.C., and Rapoport, T.A. (2004). X-ray structure of a protein-conducting channel. Nature *427*, 36–44.

32. Gumbart, J., and Schulten, K. (2007). Structural determinants of lateral gate opening in the protein translocon. Biochemistry *46*, 11147–11157.

33. Shaw, A.S., Rottier, P.J.M., and Rose, J.K. (1988). Evidence for the loop model of signal-sequence insertion into the endoplasmic reticulum. Proc. Natl. Acad. Sci. *85*, 7592–7596.

34. Liao, S., Lin, J., Do, H., and Johnson, A.E. (1997). Both lumenal and cytosolic gating of the aqueous ER translocon pore are regulated from inside the ribosome during membrane protein integration. Cell *90*, 31–41.

35. Pool, M. (2009). A trans-membrane segment inside the ribosome exit tunnel triggers RAMP4 recruitment to the Sec61p translocase. J. Cell Biol. *185*, 889–902.

36. Gumbart, J., Trabuco, L. G., Schreiner, E., Villa, E., and Schulten, K. (2009). Regulation of the Protein-Conducting Channel by a Bound Ribosome. Structure *17*, 1453–1464.

37. Egea, P.F., and Stroud, R.M. (2010). Lateral opening of a translocon upon entry of protein suggests the mechanism of insertion into membranes. Proc. Natl. Acad. Sci. *107*, 17182–17187.

38. Tsukazaki, T., Mori, H., Fukai, S., Ishitani, R., Mori, T., Dohmae, N., Perederina, A., Sugita, Y., Vassylyev, D.G., Ito, K., et al. (2008). Conformational transition of Sec machinery inferred from bacterial SecYE structures. Nature *455*, 988–991.

39. Zimmer, J., Nam, Y., and Rapoport, T.A. (2008). Structure of a complex of the ATPase SecA and the protein-translocation channel. Nature *455*, 936–943.

40. Hessa, T., Meindl-Beinker, N.M., Bernsel, A., Kim, H., Sato, Y., Lerch-Bader, M., Nilsson, I., White, S.H., and von Heijne, G. (2007). Molecular code for transmembrane-helix recognition by the Sec61 translocon. Nature *450*, 1026–1030.

41. Hessa, T., Kim, H., Bihlmaier, K., Lundin, C., Boekel, J., Andersson, H., Nilsson, I., White, S.H., and von Heijne, G. (2005). Recognition of transmembrane helices by the endoplasmic reticulum translocon. Nature *433*, 377–381.

42. von Heijne, G. (2007). Formation of transmembrane helices in vivo–is hydrophobicity all that matters? J. Gen. Physiol. *129*, 353–356.

43. Sadlish, H., Pitonzo, D., Johnson, A.E., and Skach, W.R. (2005). Sequential triage of transmembrane segments by Sec61α during biogenesis of a native multispanning membrane protein. Nat. Struct. Mol. Biol. *12*, 870–878.

44. McCormick, P.J., Miao, Y., Shao, Y., Lin, J., and Johnson, A.E. (2003). Cotranslational Protein Integration into the ER Membrane Is Mediated by the Binding of Nascent Chains to Translocon Proteins. Mol. Cell *12*, 329–341.

45. Junne, T., Kocik, L., and Spiess, M. (2010). The hydrophobic core of the Sec61 translocon defines the hydrophobicity threshold for membrane integration. Mol. Biol. Cell *21*, 1662–1670.

46. Goder, V., Junne, T., and Spiess, M. (2004). Sec61p contributes to signal sequence orientation according to the positive-inside rule. Mol. Biol. Cell *15*, 1470-1478.

47. Foster, C. A., Dreyfuss, M., Mandak, B., Meingassner, J. G., Naegeli, H. U., Nussbaumer, A., Oberer, L., Scheel, G., and Swoboda, E. M. (1994). Pharmacological modulation of endothelial cell-associated adhesion molecule expression: implications for future treatment of dermatological diseases. J. Dermatol. *21*, 847-854.

48. Chen, Y., Bilban, M., Foster, C. A., and Boger, D. L. (2002). Solution-phase parallel synthesis of a pharmacophore library of HUN-7293 analogues: a general chemical

mutagenesis approach to defining structure-function properties of naturally occurring cyclic (depsi)peptides. J. Am. Chem. Soc. *124*, 5431–5440.

49. Garrison, J.L., Kunkel, E.J., Hegde, R.S., and Taunton, J. (2005). A substrate-specific inhibitor of protein translocation into the endoplasmic reticulum. Nature *436*, 285–289.

50. Besemer, J., Harant, H., Wang, S., Oberhauser, B., Marquardt, K., Foster, C.A., Schreiner, E.P., de Vries, J.E., Dascher-Nadel, C., and Lindley, I.J.D. (2005). Selective inhibition of cotranslational translocation of vascular cell adhesion molecule 1. Nature *436*, 290–293.

51. Harant, H., Lettner, N., Hofer, L, Oberhauser, B, de Vries, J.E., and Lindley, I.J.D. (2006). The translocation inhibitor CAM741 interferes with vascular cell adhesion molecule 1 signal peptide insertion at the translocon. J. Biol. Chem. *281*, 30492–30502.

52. Harant, H., Wolff, B., Schreiner, E.P., Oberhauser, B., Hofer, L., Lettner, N., Maier, S., de Vries, J.E., and Lindley, I.J. (2007). Inhibition of vascular endothelial growth factor cotranslational translocation by the cyclopeptolide CAM741. Mol. Pharmacol. *71*, 1657–1665.

53. Maifeld, S.V., MacKinnon, A.L., Garrison, J.L., Sharma, A., Hegde, R.S., Kunkel, E.J., and Taunton, J. (2011). Secretory protein profiling reveals TNFα inactivation by selective and promiscuous Sec61 modulators. Chem. Biol. *In press.*

54. Zhang, B., and Miller, T.F., III. (2010). Hydrophobically stabilized open state for the lateral gate of the Sec translocon. Proc. Natl. Acad. Sci. *107*, 5399-5404.

Chapter 2: Photo-leucine incorporation reveals the molecular target of cotransins

2.1 Abstract

Identifying the direct molecular target of CT represents a major step toward deciphering its mechanism of action. Since the target was most likely an integral membrane protein of the ER, we reasoned that photo-affinity labeling would be the most appropriate strategy for target identification. Towards this end, we prepared a CT photo-affinity probe where a leucine side chain of HUN-7293 was replaced with a nearly isosteric photo-reactive amino acid analog, known as photo-leucine. Photo-leucine would enable covalent crosslinking between the probe and the target upon activation with light. The photo-affinity probe also contained an alkyne "handle" to enable detection of the crosslinked target following conjugation with a reporter group under click chemistry conditions. The probe retained potent biological activity in cell-based assays and was used to identify Sec61α, the structural core of the Sec61 translocation channel, as the direct molecular target of CT. These results provide a solid foundation on which to pursue more detailed studies on the molecular mechanism by which CT blocks substrate translocation through the Sec61 channel.

2.2 Introduction

Target identification is often the rate-determining step in deciphering the mechanism of action of biologically active small molecules. While genetic and genome-wide approaches can be applied for target identification in bacteria and yeast,[1] target identification in mammalian systems typically requires more direct biochemical approaches. One traditional biochemical approach for small molecule target identification

employs purification of the target by affinity chromatography, followed by identification of the target by mass spectrometry or Edman degradation.[2-4] In this method, a complex protein mixture is passed over a resin matrix that has been covalently modified with the small molecule of interest. The affinity matrix is stringently washed and specifically-bound proteins are eluted, resolved by SDS-PAGE, and identified. The success of this approach requires that the target and small molecule have a sufficiently strong binding affinity (typically in the nM range) to survive the extensive washing steps required to reduce non-specific binding of proteins to the affinity matrix. However, in a recent variation of this technique, less stringent washing conditions coupled with highly sensitive quantitative mass spectrometry were used to identify specific protein targets of inhibitors with μM affinity.[5] The approach works best with soluble protein targets since integral membrane proteins require detergent-solubilization prior to chromatography, which often prevents binding to the affinity matrix.

Photo-affinity labeling (PAL), the focus of this chapter, is another useful biochemical strategy for small molecule target identification. PAL uses an analog of a biologically active small molecule, known as a photo-affinity probe, that bears photo-reactive and reporter functional groups to identify macromolecular binding partners.[6] The photo-affinity probe is designed and synthesized based on SAR (structure-activity relationships) of a parent small molecule having known biological activity. During PAL, the photo-affinity probe is incubated with a protein mixture under native conditions and irradiated with UV light. Irradiation of the photo-reactive group generates a highly reactive chemical species (e.g. carbene, nitrene, or free radical) that covalently crosslinks the

photo-affinity probe to its macromolecular binding partner(s). Photo-crosslinked protein targets are then visualized by the reporter group (e.g. fluorophore, biotin, or radioactive label) (**Figure 2-1**). Covalent bond formation between the probe and target often enables their subsequent purification and identification using techniques such as SDS-PAGE, immunoprecipitation, and biotin-streptavidin affinity purification coupled with mass spectrometry.

PAL has several features that distinguish it from the traditional affinity chromatography approach. First, since photo-activation is performed under native conditions, PAL provides the opportunity for detection and identification of integral membrane protein targets,[7,8] an important class of proteins targeted by a large number of small molecule drugs. PAL can also be used to characterize and map the ligand binding sites of known integral membrane proteins or other targets that lack high resolution structural information.[9,10] Finally, since PAL establishes a stable, covalent bond between the small-molecule probe and the target, the targets of even moderately potent small molecules can, in principle, be identified. PAL therefore represented an appropriate biochemical strategy to identify the direct molecular target of CTs.
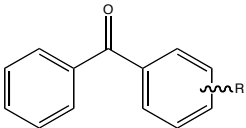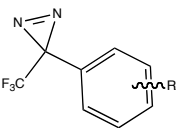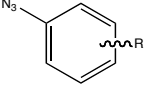
Photo-reactive group	Benefits	Downsides
Benzophenone	Photo-activation at ~350 nm is reversible, leading to high crosslinking yields with proteins. Selective for insertion into C-H σ bonds over bulk solvent.[11] Chemically stable.	Large size. Reported to selectively react with methionine residues in proteins leading to inaccurate determination of probe-binding sites.[12]
3-trifluoromethyl-3-phenyl diazirine	Generates a highly reactive carbene intermediate upon photo-activation at ~350 nm. Photo-insertion of the carbene into proteins can proceed in high (>70%) yield.[13]	Relatively large size. Insertion products may be reversible under some conditions.[14] Can undergo UV light-induced rearrangement to electrophilic diazo isomer[13] leading to non-specific labeling. Challenging to synthesize.
Alkyl diazirine	Small size. Generates highly reactive carbene intermediate upon photo-activation at ~350 nm. Good yield of insertion into protein targets (~25%).[15] Synthesized directly from the ketone precursor.	May undergo UV light-induced rearrangement to electrophilic linear diazo isomer[13] leading to non-specific labeling. Intramolecular rearrangement of the alkyl carbene intermediate may compete with intermolecular insertion into proteins.[16]
Phenyl azide	The singlet nitrene intermediate formed on photo-activation is highly reactive. Photo-activation of nitro-substituted aryl azides occurs at ~340 nm and is therefore not damaging to protein. Perfluoro phenyl azides react primarily via the singlet nitrene intermediate.[13] Easily synthesized.	Un-substituted phenyl azides require activation at short wavelengths (~260 nm) that are damaging to protein. In non-perfluorinated phenyl azides, the singlet nitrene intermediate is prone to ring-expansion to a long-lived electrophilic species,[13] resulting in non-specific labeling. Phenyl azide is chemically less stable than other photo-reactive groups.

Table 2-1. Comparison of commonly used photo-reactive functional groups.

One difficulty with PAL is that the small molecule must retain biological activity after derivatization with a photo-reactive group. While several photo-reactive functional

groups that differ in size, shape, hydrophobicity, photo-physical properties, and ease of chemical synthesis are frequently used in PAL (summarized in **Table 2-1,** and see ref. 6, 11, 13), I will focus here on the alkyl diazirine group, since it holds several unique advantages. First, like most useful photo-affinity groups, the alkyl diazirine (**Figure 2-1**, **(I)**) is activated at a wavelength of light (~355 nm) that is not damaging to protein. Unlike some other photo-reactive groups, however, the alkyl diazirine is extremely compact in size, being nearly isosteric to a methyl group. This allows installation of the diazirine at positions of a small molecule that would not tolerate larger, aryl-based groups such as benzophenone, aryl azide, or 3-trifluoromethyl-3-phenyl-diazirine. Third, the carbene intermediate formed upon photo-activation of the diazirine (**Figure 2-1**, **(II)**) rapidly inserts into X-H bonds (X = N, S, O), as well as C-H bonds, to form stable covalent insertion products (**Figure 2-1**, **(III)**).[13] When not poised for insertion into bonds of the macromolecular target, the alkyl carbene intermediate undergoes rapid quenching by solvent or internal rearrangement to a stable olefin side-product.[16] Fourth, the alkyl diazirine is chemically stable in acidic and basic conditions and in ambient light encountered during routine chemical synthesis. Several improved methods for the synthesis of alkyl diazirines starting from alkyl ketone precursors have also been recently reported.[15,17]
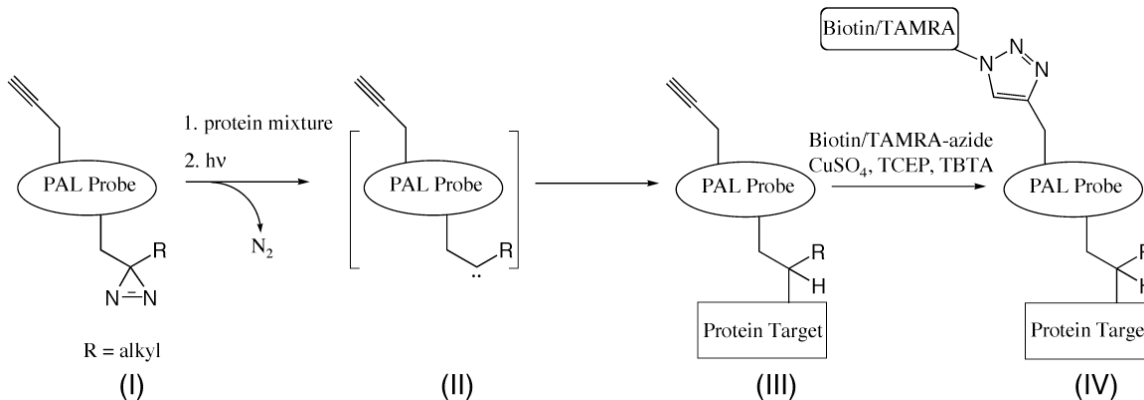
Figure 2-1. Generalized scheme for photo-affinity labeling.
UV irradiation (~350 nm) of the diazirine generates a carbene intermediate (II) that covalently crosslinks to the protein target (III). The adduct is then detected by conjugation with an azide-containing reporter group under click chemistry conditions (IV).

Despite these advantages, there are relatively few examples of the use of alkyl diazirines in PAL studies. One particularly interesting example was the application of two novel diazirine-containing amino acids called photo-leucine and photo-methionine.[18] These photo-reactive amino acids are close mimics of leucine and methionine (**Figure 2-2**). Photo-leucine and photo-methionine have been used to probe protein-protein interactions by PAL after their random biosynthetic incorporation in cells[18] or via site-specific native protein ligation.[19] However, the potential for incorporating these novel amino acids into natural product scaffolds for small molecule target identification has not been explored. Based on the presence of several leucine side chain in the CT scaffold, we reasoned that photo-leucine represented an ideal photo-reactive group that could enable target identification.
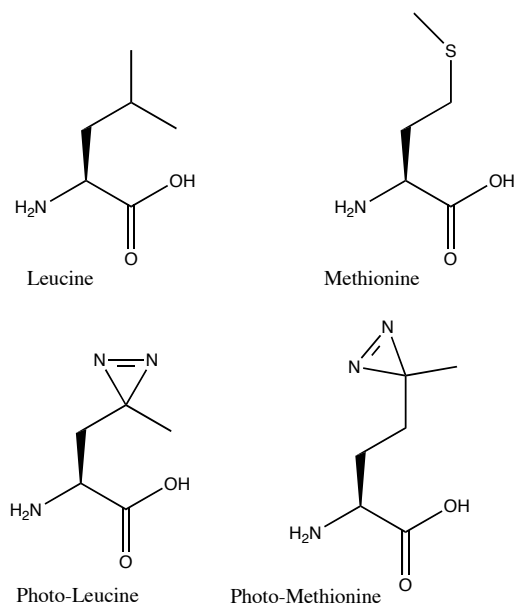
Figure 2-2. Structures of leucine, methionine, photo-leucine, and photo-methionine.

Target identification by PAL also requires a method to detect photo-crosslinked target(s) after formation of the covalent crosslink. Introduction of a radiolabel into the small-molecule probe is a widely used approach to detect probe-modified proteins. While radiolabels are small in size, extremely sensitive, and offer a high signal to noise ratio, radio-labeled probes can be costly to synthesize and radioactive materials require special handling and dedicated equipment. Cu(I)-catalyzed click chemistry provides a non-radioactive alternative which is also highly sensitive, and has the added advantage of coincidently installing a chemical handle (biotin or TAMRA) that can be used to affinity purify and identify probe-modified proteins.[20] In some cases, this method can even afford the precise site of probe modification at the amino acid level.[21-23] During the click reaction, Cu(I) catalyzes a highly selective, 1,3 dipolar cycloaddition reaction between a terminal alkyne and an azide to form a stable triazole product (**Figure 2-1**, **(IV)**). The terminal alkyne is typically present in the small-molecule probe, while the azide is present in a fluorescent or biotinylated reporter group. Alternatively, the azide can be

incorporated into the probe and the alkyne incorporated into the reporter. However, this arrangement has been shown to produce higher background labeling of proteins.[24] Following covalent labeling of protein targets via the photo-reactive moiety within the probe, probe-modified proteins are conjugated to the azide-bearing reporter under click chemistry conditions. The reporter group is thus introduced *after* covalent bond formation between the probe and target protein. This approach thereby avoids directly introducing a bulky reporter into the small-molecule probe, which could perturb the interaction between the probe and the protein target. The terminal alkyne (or azide) is extremely compact and therefore minimally perturbs the structure of the small-molecule, while providing the chemical functionality necessary for detection and affinity purification of targets. A variety of azide- and alkyne-reporters designed for use in bio-conjugate click reactions have been described[21-24] and many are now commercially available.

To summarize, target identification is an extremely challenging, yet essential step in the characterization of biologically active small molecules. Photo-affinity labeling followed by detection of crosslinked targets(s) with click chemistry represents a general strategy for target identification which is well suited for identifying the direct molecular target of CTs. In this chapter, I describe (1) an improved synthesis of photo-leucine, (2) incorporation of photo-leucine and an alkyne click chemistry handle into the CT scaffold, and (3) identification of the target of CT in the ER membrane by photo-affinity labeling.

2.3 Design and synthesis of CT7

To identify the target, we designed a CT photo-affinity probe we named CT7 (**2.2**), in which photo-leucine replaces leucine at position 4 of HUN-7293 (**2.1)** (**Figure 2-3**). We also substituted *N*-methyl-*N'*-methoxy tryptophan at position 5 of HUN-7293 with commercially available *N*-methyl-phenylalanine, previously shown to have a negligible effect on potency.[25] A propargyl substituent was installed at position 1 in CT7 to enable Cu(I)-catalyzed conjugation with a rhodamine-azide reporter (click chemistry) after photo-crosslinking under native conditions (**Figure 2-4**). These conservative modifications were aimed at preserving the biological potency of CT7 while providing the necessary functionality for target identification.
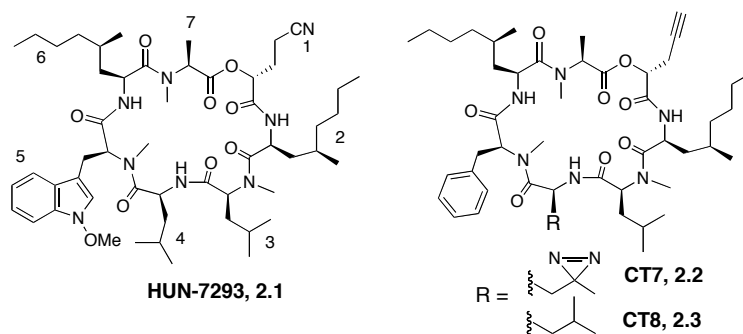
Figure 2-3. Structures of HUN-7293, CT7, and CT8.
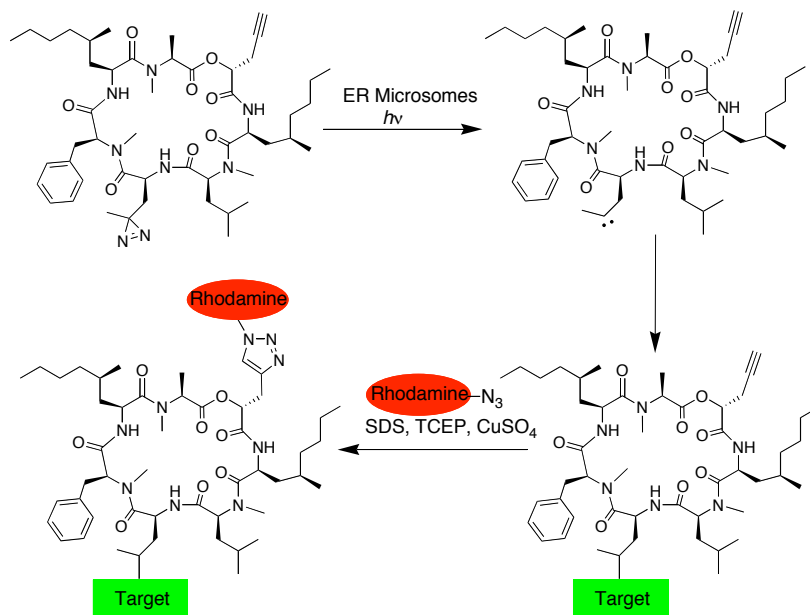
Figure 2-4. Photo-affinity labeling and click chemistry strategy to identify the target of CT7.
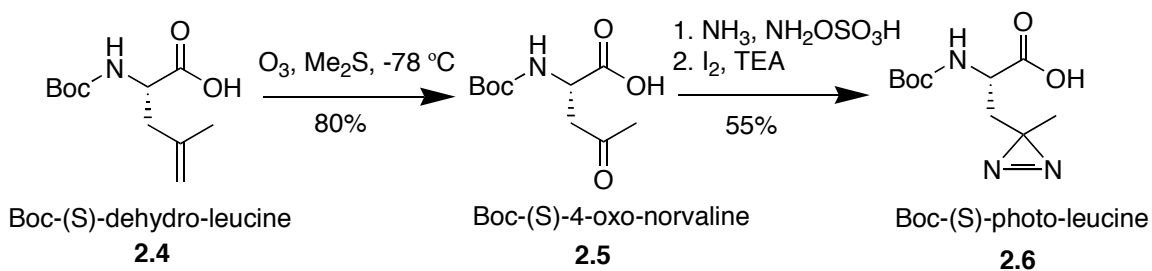
Scheme 2-1. Synthesis of Boc-(S)-photo-leucine.

Synthesis of CT7 required Boc-(*S*)-photo-leucine (**2.6**), which we prepared via ozonolysis of commercially available Boc-(*S*)-dehydro-leucine (**2.3**),[26] followed by formation of the diazirine by the method of Church and Weiss (**Scheme 2-1**).[27] Boc-(*S*)-photo-leucine was efficiently coupled to peptides (EDCI-HOAt) or deprotected (4 N HCl) to give the free amino acid in quantitative yield. This route is a significant improvement over the original

35

six-step synthesis of (*S*)-photo-leucine, which proceeded in low yield and required enzymatic resolution of a racemic intermediate.[18] Synthesis of CT7 followed the solution-phase route developed by Boger and coworkers[25] with slight modifications (**Scheme 2-2**). The diazirine side chain was stable to ambient light and the acidic and basic conditions used to prepare CT7. We also synthesized CT8 (**2.3**) as a photo-stable control compound by an identical route (**Figure 2-3**). Both CT7 and CT8 were equipotent to the natural product HUN-7293 at inhibiting VCAM expression in transfected cells (EC$_{50}$ ~25 nM, **Figure 2-5**).
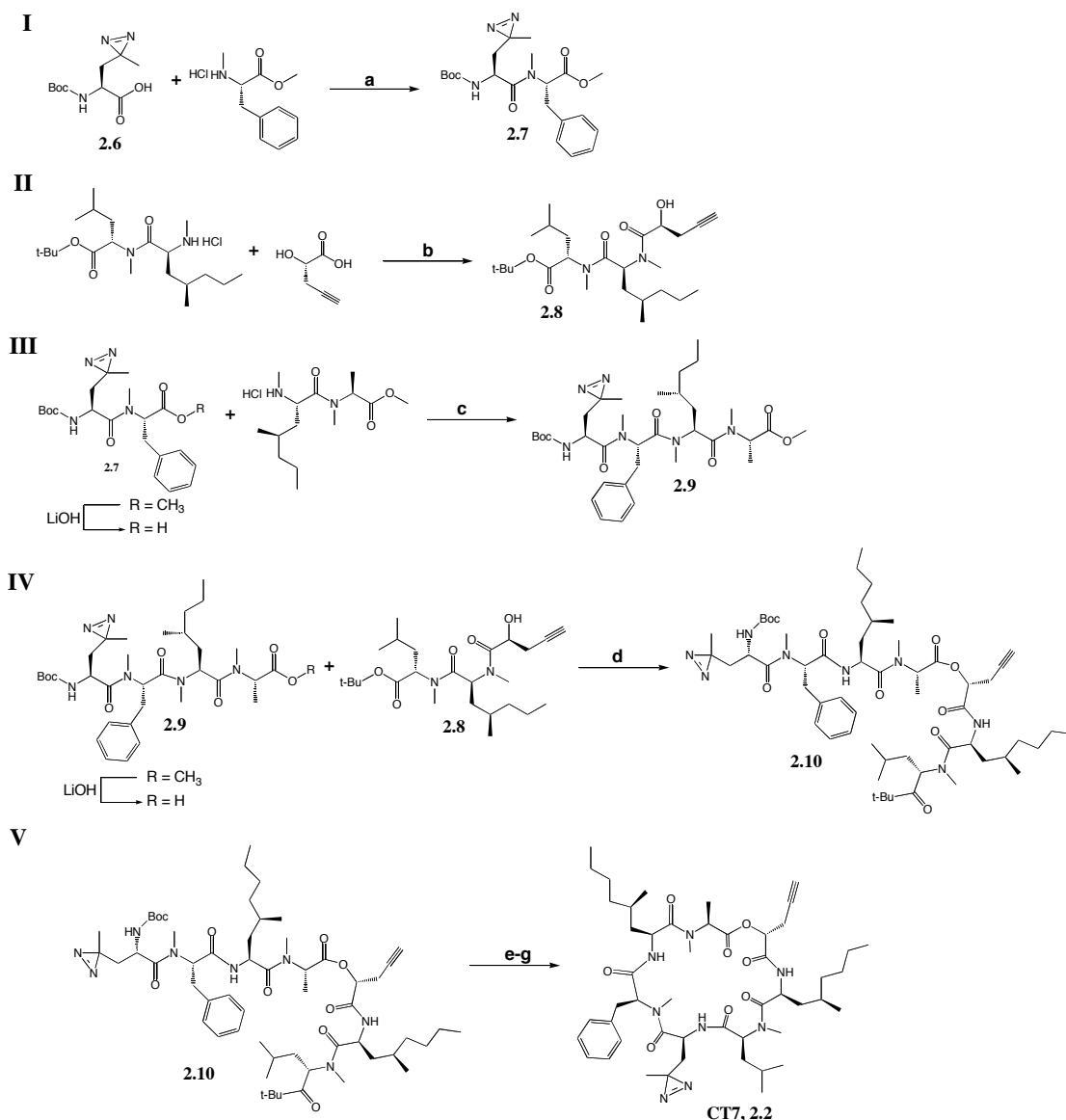
Scheme 2-2. Synthesis of CT7 (compound 2.2).
I. Dipeptide **2.7** was prepared from Boc-photo-leucine (**2.6**) and commercially available N-methyl phenylalanine. **II**. Tripeptide (**2.8**) was prepared from the previously described dipeptide.[25] **III**. Tetrapeptide **2.9** was prepared by coupling dipeptide **2.7** (free acid from saponification of the methyl ester) with the previously described dipeptide.[25] **IV**. The hepta(depsi)peptide **2.10** was prepared by a solid-phase mitsunobu esterification between the tetrapeptide **2.9** (free acid from saponification of the methyl ester) and tripeptide **2.8**. The hepta(depsi)peptide was doubly deprotected and cyclized to yield CT7 (compound **2.2**). Reagents and conditions: **a**, EDC, HOAT, 5:1 DCM/DMF, 0° C (60% yield); **b**, EDC, HOAT, 2,6-lutidine, 5:1 DCM/DMF, 0° C (72% yield); **c**, EDC, HOAT, 2,6-lutidine, 5:1 DCM/DMF, –30 °C, (70% yield); **d**, solid phase-immobilized triphenylphosphine, DIAD, THF, (70% yield); **e**, TFA, anisole; **f**, 4.0 M HCl-dioxane; **g**, DPPA, DIEA, DMF, 0° C (37% yield).
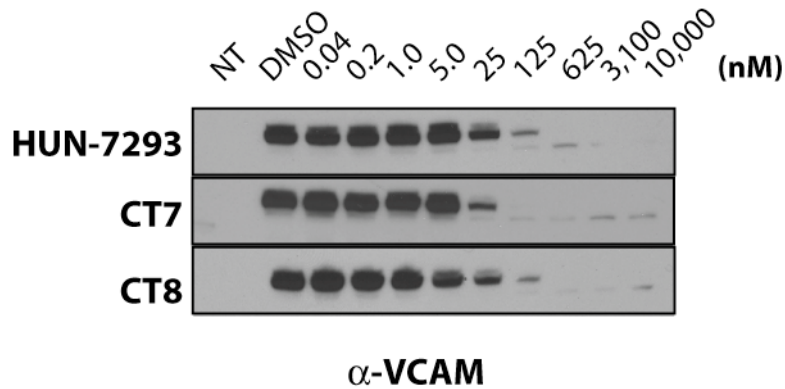
Figure 2-5. Validation of CT7 and CT8 as inhibitors of VCAM expression in transfected cells.
NT (non-transfected control). Total cell lysates were analyzed by Western blot using antibodies against VCAM. Jennifer Garrison acknowledged for the production of data in Figure 2-5.

2.4 Photo-affinity labeling and target identification

We incubated a crude ER microsome fraction with 500 nM CT7 and irradiated the mixture with ~350 nm light for 1 minute. Proteins were then denatured in 1% sodium dodecylsulfate (SDS) and subjected to standard click chemistry conditions using a rhodamine-azide reporter. Following electrophoresis, in-gel fluorescent scanning revealed a major rhodamine-labeled protein with an apparent molecular weight of ~50 kDa (**Figure 2-6**). Labeling of this protein required both UV light and CT7, and was competed by an excess of CT8. Weak labeling of two additional proteins (~60 kDa and ~40 kDa) was not competed by excess CT8 and is likely non-specific. Background labeling by the rhodamine-azide, independent of UV light or CT7, was also observed.
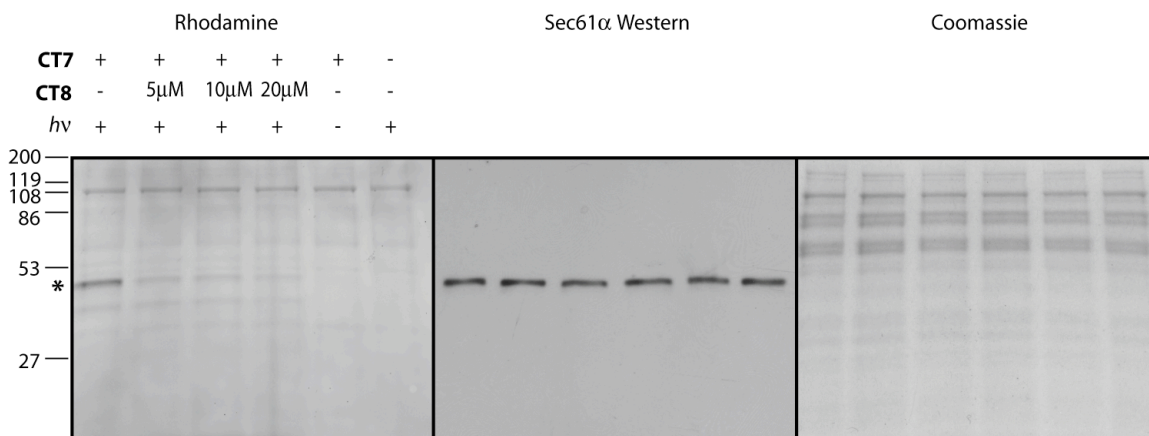
Figure 2-6. Photo-crosslinking of CT7 in the presence of ER microsomes.
An asterisk marks the major photo-crosslinked protein. A portion (30 µL) of each reaction was resolved by SDS-PAGE and analyzed by in-gel fluorescent scanning (left panel) followed by Coomassie staining (right panel). A smaller portion (5 µL) of each reaction was separated by SDS-PAGE, transferred to nitrocellulose and analyzed by Western blot (center panel) with Sec61α antibodies. Note that Sec61α runs at the same relative mobility as the major fluorescent band at ~50 kDa, but does not represent a major Coomassie-stained band.

The major crosslinked protein migrated on SDS gels with the same relative mobility as Sec61α, the largest subunit of the Sec61 complex (**Figure 2-6**). Consistent with Sec61α as the primary target of CT7, the ~50 kDa rhodamine-labeled protein was immunoprecipitated directly from the click reaction mixture with an antibody raised against Sec61α, but not with a control antibody (**Figure 2-7**).
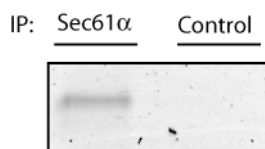
Figure 2-7. IP of click reactions using Sec61α antibodies or control antibodies.

To independently confirm that Sec61α is the photo-crosslinked protein, we prepared proteoliposomes reconstituted from either a detergent extract of ER microsomes, a Sec61-depleted extract, or a depleted extract replenished with purified Sec61 complex.[28]

Depletion of the intact Sec61 complex from the detergent extract using antibodies against Sec61β[29] was ~90% efficient (as judged by immunoblotting for the α and β subunits), whereas other ER proteins were not affected (not shown). Compared to proteoliposomes derived from control extracts, photo-crosslinking of CT7 to the ~50 kDa protein was significantly diminished in Sec61-depleted proteoliposomes and was restored after adding back purified Sec61 complex (**Figure 2-8**). We conclude that Sec61α, known to form the channel through which all proteins transit as they enter the secretory pathway, is the primary target of CT7 in the ER.
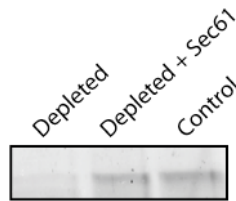
Figure 2-8. Photo-crosslinking of CT7 in the presence of proteoliposomes.
Proteoliposomes were reconstituted from a total detergent extract of ER microsome (control), a Sec61-depleted extract (depleted), or a depleted extract replenished with purified Sec61 complex (depleted + Sec61).

2.5 Photo-cross-linking efficiency

To gauge the general utility of the alkyl diazirine as a photo-reactive functional group in PAL studies, we also estimated the yield of crosslinking between CT7 and Sec61α. To generate a standard curve, a propargylated RSK-1 CTD reference protein (C-terminal kinase domain, amino acids 410-735) was generated by incubating RSK-1 CTD (230 nM) with Fmk-propargylamine (375 nM) in PBS for 1.5 hours at room temperature. These labeling conditions effect quantitative, stoichiometric modification of RSK-1 CTD with the propargylated fluoromethylketone inhibitor as determined by ESI-MS.[30] The propargylated RSK-1 CTD reference protein and a standard photo-crosslinking reaction

were then subjected to the click reaction under standard conditions with Rox-azide. A dilution series of the Rox-labeled RSK-1 CTD was then analyzed by SDS-PAGE and in-gel fluorescence scanning, and the background-corrected mean fluorescence intensities were used to construct the standard curve. Using the mean fluorescence intensity of labeled Sec61α from the photo-crosslinking reaction which contained a known amount of total Sec61, and assuming a 1:1 stoichiometry of CT7:Sec61α, the photo-crosslinking yield was estimated at ~23% (**Figure 2-9**).
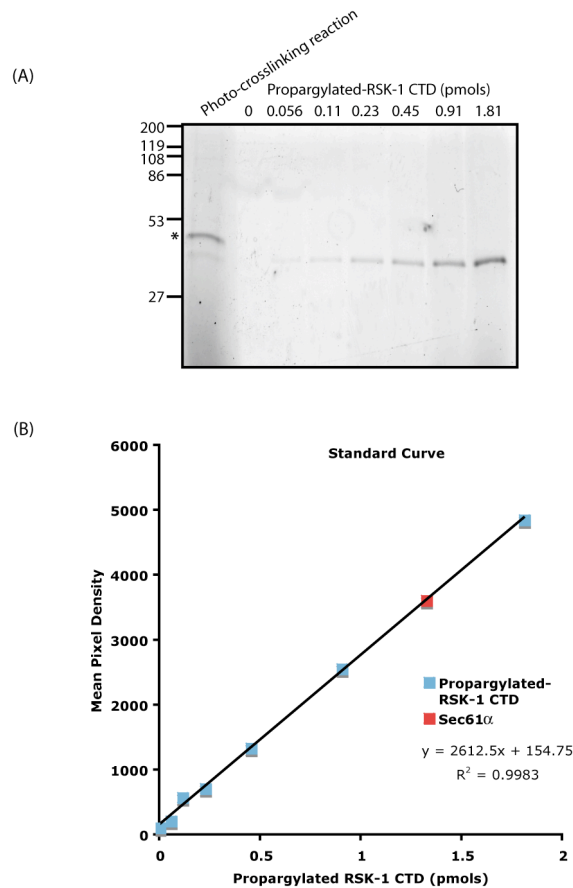
Figure 2-9. Estimated yield of photo-crosslinked Sec61α in ER microsomes.
(A) Photo-crosslinking and click reactions were performed as described. The total amount of Sec61 complex in the photo-crosslinking reaction (5.88 pmols) was calculated based on a previous estimate of 1.7 pmols Sec61 per equivalent microsomes[31] (as defined in Ref. 32). The propargylated RSK-1 standard was constructed as described in the text. Using the mean fluorescence intensity of labeled Sec61α (Lane 1, asterisk) and the linear fitted equation to the standard curve, photo-crosslinked Sec61α was estimated at 1.32 pmols, corresponding to a photo-crosslinking yield of 23%. **(B)** Graphical analysis of gel data shown in **(A).**

2.6 Discussion

Photo-crosslinking of CT7 to Sec61α was remarkably selective given the proteomic complexity of the ER, which contains hundreds of membrane and lumenal proteins;[33] Sec61α is a relatively minor constituent (~0.7% of total ER protein).[34] We attribute this high selectivity to two factors. First, due to its similar size, shape, and hydrophobicity, photo-leucine likely forms intimate contacts with Sec61α in a manner similar to the leucine side chain of HUN-7293. Second, the short lifetime (nanoseconds)[16] of the carbene derived from CT7 (**Figure 2-4**) ensures that molecules not bound to Sec61α are rapidly quenched by intramolecular rearrangement, solvent, or membrane lipids. Despite the short lifetime, the photo-crosslinking yield of CT7 to Sec61α was quite good, estimated at ~23% (**Figure 2-8**). Thus, depending on the specific application, alkyl diazirines may offer advantages over the widely used benzophenone crosslinker.

These results also reveal that CT7 directly bind to Sec61α with high affinity in the absence of a bound ribosome or nascent chain. This suggests that substrate selectivity of CT7 is probably not conferred by direct binding to the signal sequence. These findings therefore present a paradoxical mechanism of action: how does CT *selectively* block substrate translocation by binding to a channel component utilized by *every* translocated protein? With these novel chemical tools in hand, we were poised to address the mechanistic basis of this unprecedented mode of inhibition.

2.7 Experimental procedures

Photo-crosslinking reactions in ER microsomes and reconstituted proteoliposomes

Canine ER microsomes that were stripped of ribosomes (prepared as previously described)[28] were incubated with or without CT7 (500 nM) and CT8 (0–20 μM, final concentration of 4% DMSO in all samples) in physiological salt buffer (PSB, 50 mM Hepes pH 7.4, 150 mM potassium acetate, 5 mM magnesium acetate) containing 250 mM sucrose (37.5 μL reaction volume, 1 mg total protein/mL) for 1 h at room temperature (RT) in the dark. Samples were transferred to a single well of separate 96-well plates and photolyzed at RT. Photolysis was conducted using a Hg(Xe) lamp (Oriel Instruments, model 6295) operated at 1000 W using a filter with a maximum transmittance at 350 nm (#59810, Oriel Instruments) and a filter to absorb heat (#59044, Oriel Instruments). Samples were irradiated 6 cm from the source for 1 min (longer irradiation times did not increase the yield of crosslinking). A control sample was left in the dark. Following photolysis, the concentration of CT8 was equalized in all samples (20 μM) to control for the total concentration of alkyne present in the subsequent click reaction. Samples were then diluted to 50 μL with PSB and sedimented through a sucrose cushion (0.5 M sucrose in PSB, 200 μL) by centrifugation at 100,000 rpm for 45 min at 4 °C in a TLA 100 rotor. The cushion was removed, the membrane pellet was resuspended in 31.5 μL of phosphate buffered saline (PBS, 137 mM NaCl, 10 mM Na_2HPO_4, 2.7 mM KCl, pH 7.4) and the membranes were transferred to a fresh tube for the click reaction (described below). Photo-crosslinking in reconstituted proteoliposomes was conducted as follows: proteoliposomes were incubated with CT7 (250 nM) in PBS (20 μL reaction volume, 0.5 mg total protein/mL) for 1 h at RT in the dark. Samples were photolyzed as described

above and 19.5 μL of each sample was transferred directly to a fresh tube for the click reaction.

Click chemistry

Click reactions were performed essentially as previously described.[24] Tris(benzyltriazolylmethyl) amine (TBTA) was synthesized as previously described.[35] The rhodamine-azide reporter (Rox-N$_3$) was synthesized from 5-(and-6)-carboxy-X-rhodamine succinimidyl ester (Invitrogen) and 3-azido propylamine as previously described.[24] To the photo-crosslinked microsomes (prepared as described above) were added the following reagents in order: 1% SDS (10% stock in H$_2$O), 50 μM Rox-N$_3$ (2.5 mM stock in DMSO), 1 mM tris(carboxyethyl) phosphine (TCEP, 50 mM stock in H$_2$O, pH 7), 100 μM TBTA (1.7 mM stock in 4:1 *tert*-BuOH/H$_2$O), and lastly 1 mM CuSO$_4$ (50 mM stock in H$_2$O). Reactions were mixed gently and incubated at RT for 1 h. Laemmli sample buffer (5×, 7.5 μL) was added and the reactions were resolved by SDS-electrophoresis on 12% acrylamide mini-gels (BioRad). Gels were scanned for fluorescence (610 nm emission) using a Typhoon 9400 phosphorimager (Amersham).

Immunoprecipitation

ER microsomes were incubated with a saturating concentration of CT7 (5 μM) in PSB containing 0.25 M sucrose (25 μL total reaction volume, 2 mg total protein/mL) for 1 h and subjected to photo-crosslinking and click reactions as described above. Following the click reaction, samples (25 μL) were diluted ten-fold with IP buffer (1% Triton X-100, 50 mM Hepes pH 7.4, 100 mM sodium chloride) and incubated with rabbit antiserum

raised against Sec61α[36] or non-immune rabbit serum (Animal Pharm Services) for 2 h at 4 °C. Protein A beads (50 μL of a 50% slurry, Amersham), pre-equilibrated in IP buffer, were added and samples were rotated overnight (18 h) at 4 °C. The beads were sedimented by centrifugation (2000 rpm, 1 min), the supernatants removed, and the beads washed (5×) with ice cold IP buffer (0.5 mL). Proteins were eluted with Laemmli sample buffer (1×, 50 μL) at RT for 1 h and analyzed by SDS-PAGE and in-gel fluorescent scanning.

Cell-based assays

VCAM expression analysis in COS-7 cells was performed as previously described.[36] Briefly, cells were transfected with a VCAM expression plasmid using Lipofectamine 2000 (Invitrogen), or not transfected (NT). 5 h after transfection, the media was changed to include HUN-7293 (a generous gift from Dale Boger, The Scripps Research Institute), CT7, or CT8 at the indicated concentrations. After 24 h, cells were harvested in lysis buffer (1% SDS, 0.1 M Tris-HCl pH 8.0) and equal amounts of total protein were resolved by SDS-PAGE and analyzed by immunoblotting with VCAM antibodies (α-VCAM, Santa Cruz Biotechnology). Under these conditions HUN-7293, CT7, and CT8 had no obvious effect on cell viability.

Proteoliposomes

A detergent extract of ER microsomes was reconstituted directly into proteoliposomes or first immunodepleted of the Sec61 complex using Sec61β antibodies as previously described.[28] The Sec61-depleted extract was either reconstituted directly into

proteoliposomes or first replenished with Sec61 complex (purified from canine pancreatic ER microsomes as previously described[28]). Reconstituted proteoliposomes were analyzed by Coomassie staining and immunoblotting against the following antigens: SRα (SRP receptor α; antibody from ref. 29), RbI (Ribophorin I; antibody was a gift from Reid Gilmore, University of Massachusetts Medical School, Worcester), CNX (Calnexin; antibody from Stressgen Biotechnologies), TRAPα (Translocon-associated protein complex subunit α; antibody from ref. 29), TRAM (Translocating-chain associating membrane protein; antibody was a gift from Peter Walter, University of California, San Francisco), Sec61α (antibody from ref. 36), Sec61β (antibody from ref. 29).

Chemical synthesis

General

Materials obtained from commercial sources were reagent grade and used without further purification. 1-Ethyl-3-(3'-dimethylaminopropyl) carbodiimide (EDCI) and 1-hydroxy-7-azabenzotriazole (HOAt) were from AKSci. All other commercially available reagents were obtained from Sigma-Aldrich unless otherwise noted. (*S*)-2-hydroxypent-4-ynoic acid was prepared by diazotization[37] of (*S*)-propargyl-glycine (Bachem) and was consistent with published data.[38] Anhydrous solvents were obtained from a commercial drying/purification system (Glass Contour, Inc., Laguna Beach, CA).

Air- and water-sensitive reactions were conducted under an inert argon atmosphere in flame-dried glassware. Reactions were monitored by analytical thin layer chromatography (TLC) on silica gel 60 F_{254} glass plates (EM Science, 0.25 mm) and by

LC-ESI-MS using a Waters 2695 Separations Module (Xterra MS C18 column (Waters), flow rate 0.2 mL/min) connected inline to a Waters ZQ mass detector. Preparative reverse phase high performance liquid chromatography (HPLC) was carried out on a Peeke Scientific Combi-A 5 μM preparative C18 column (50 × 22 mm, flow rate 10 mL/min) using a Varian Prostar 210 solvent delivery system equipped with a UV/vis detector (monitoring at 220 and 245 nm). Silica gel chromatography was conducted with 230-400 mesh silica gel (EM Scientific). All ^{1}H and ^{13}C NMR spectra were recorded on a Varian 400 MHz spectrometer. ^{1}H spectra are referenced to TMS at 0.00 ppm, and ^{13}C spectra are referenced to the center of the CDCl$_3$ triplet at 77.16 ppm. High resolution MS data were collected at the UCSF Mass Spectrometry Facility (HR-EI-MS spectra were acquired on a VG70-SE instrument from MicroMass, Manchester, UK; HR-FT-MS spectra were acquired on a Finnigan LTQ-FTICR instrument from Thermoscientific, Waltham, MA).

Solution phase syntheses of CT7 and CT8 were conducted as previously described for the synthesis HUN-7293 and its analogs,[25] with the exception of the linear heptadepsipeptide as described below.

(*S*)-Boc-photo-leucine, **2.6**
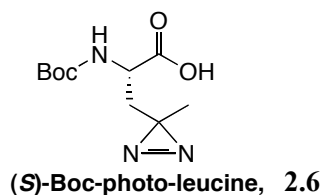
Synthesis of (*S*)-Boc-photo-leucine (2.6):

(*S*)-Boc-4-oxo-norvaline (**2.5**) was synthesized by the method of Cornish *et al.*[26] (*S*)-Boc-4,5-dehydro-leucine (**2.4**, ChemImpex, 1.616 g, 7.05 mmol) was dissolved in DCM (45 mL, 0.16 M) and cooled to −78 °C. O_3/O_2 gas was slowly bubbled through the solution (0.5 L/min, ~0.5 g O_3/h) until a purple color formed (~1.5 h). Nitrogen was then passed through the solution until it returned to a colorless mixture. Dimethylsulfide (1.095 g, 17.62 mmol) was added and the reaction was warmed to RT and stirred overnight (18 h). The solvent and excess dimethylsulfide were removed *in vacuo* and the amber colored residue was chromatographed on silica gel (5% MeOH in DCM, 0.1% AcOH) to yield 1.30 g (80%) of (*S*)-Boc-4-oxo-norvaline (**2.5**) as a transparent oil. ^{1}H and ^{13}C NMR of **5** were consistent with published data.[39]

Diazirine formation followed the general procedure described by Church and Weiss.[27] (*S*)-Boc-4-oxo-norvaline (**2.5**, 0.480 g, 2.08 mmol) was charged into a three-necked flask and azeotroped (3×) with dry toluene. The flask was then fitted with a dry-ice condenser and ammonia (15 mL, 0.14 M) was slowly condensed into the flask. The solution was refluxed for 5 h with stirring, cooled to −78 °C, and a solution of hydroxylamine-*O*-sulfonic acid (HOSA) in MeOH (0.270 g, 2.39 mmol, 1.84 M) was added drop-wise over 20 min. The ice bath was then removed and the mixture was held at reflux temperature for an additional 1 h. Anhydrous MeOH (3 mL) was then added, and the reaction was warmed to RT and stirred overnight. The following day, the slurry was filtered, the filter cake was washed with MeOH (25 mL), and the combined washes were treated with triethylamine (0.210 g, 2.08 mmol) and concentrated to 8 mL. An additional equivalent of triethylamine (0.210 g, 2.08 mmol) was then added, and the solution was cooled to 0

°C and titrated with a solution of I$_2$ in MeOH (0.1 M). When a slight orange color persisted, the solvent was removed, and the residue brought up in dH$_2$O (20 mL) and acidified to pH 2 with 1 M HCl. The aqueous phase was extracted with three portions of EtOAc (20 mL) and the combined organic fractions were washed with saturated NaCl solution (1×), dried over Na$_2$SO$_4$, filtered, and the solvent removed. The resulting orange solid was purified by silica chromatography (gradient elution 0%–2.5% MeOH in DCM, 0.1% AcOH) to yield 0.280 g (55%) of **2.6** as a slightly yellow gum. ^{1}H NMR (400 MHz, CDCl$_3$): δ 5.07 (d, J = 7.4 Hz, 1H), 4.28–4.38 (m, 1H), 2.06 (dd, J = 15.1, 4.1 Hz, 1H), 1.61 (dd, J = 15.1, 8.8 Hz, 1H), 1.48 (s, 9H), 1.10 (s, 3H). ^{13}C NMR (100 MHz, CDCl$_3$): δ 176.2, 155.5, 80.8, 50.4, 37.7, 28.4, 23.9, 19.8. HR-FT-MS m/z 244.1292 ([M+H]$^+$, C$_{10}$H$_{18}$N$_3$O$_4$ requires 244.1297).

2.7
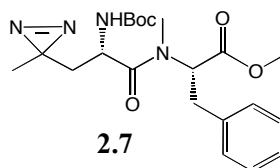
Synthesis of dipeptide 2.7:

To a stirred solution of Boc-(*S*)-photo-leucine (**2.6,** 119.5 mg, 0.491 mmol) and *N*-methyl-L-phenylalanine methyl ester hydrochloride (Bachem) (124.1 mg, 0.540 mmol) in DCM/DMF (5:1, 5 mL, 0.1 M) at 0 °C was added HOAt (73.5 mg, 0.540 mmol), EDCI (188.2 mg, 0.982 mmol) and NaHCO$_3$ (45.4 mg, 0.540 mmol). The ice bath was removed and the reaction was warmed to RT and stirred overnight (18 h). Workup and removal of the solvent as previously described[25] yielded a residue that was chromatographed on silica gel (20% EtOAc in hexanes) to yield 124.3 mg (60%) of **2.7** as a transparent gum that solidified at –20 °C. ^{1}H NMR (400 MHz, CDCl$_3$, major rotamer): δ 7.15–7.38 (m, 5H), 5.31 (dd, J = 10.5, 5.5 Hz, 1H), 4.83 (br d, J = 9.5 Hz, 1H), 4.51–4.57 (m, 1H), 3.73

(s, 3H), 3.39 (dd, J = 14.6, 5.5 Hz, 1H), 3.02 (dd, J = 14.6, 10.5 Hz, 1H), 2.93 (s, 3H),

1.78 (dd, J = 15.0, 5.3 Hz, 1H), 1.44 (s, 9H), 1.32 (dd, J = 15.0, 8.6 Hz, 1H), 1.05 (s, 3H).

^{13}C NMR (100 MHz, CDCl$_3$, major rotamer): δ 171.9, 170.9, 155.0, 136.7, 128.9, 128.6,

127.0, 80.0, 58.6, 52.5, 46.8, 38.5 34.6, 32.7, 28.4, 23.7, 20.0. HR-EI-MS m/z 419.2281

([M+H]$^+$, C$_{21}$H$_{31}$N$_4$O$_5$ requires 419.2294).

2.8
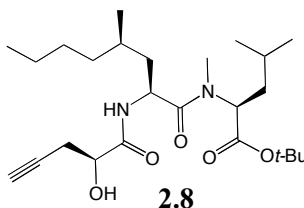
Synthesis of tripeptide 2.8:

To a stirred solution of *N*-[(2S,4R)-2-[*N*-(*tert*-Butoxycarbonyl)amino)-4-methyloctanoyl]-

N-methyl-L-leucine *tert*-butyl ester hydrochloride[25] (138.0 mg 0.351 mmol) and (S)-2-

hydroxypent-4-ynoic acid (40.0 mg, 0.351 mmol) in DCM/DMF (5:1, 3.5 mL, 0.1 M) at

0 °C was added HOAt (52.5 mg, 0.386 mmol), EDCI (134.6 mg, 0.704 mmol), and 2,6-

lutidine (41.0 µL, 0.354 mmol). The solution was warmed to RT and stirred overnight

(18 h). After workup and removal of the solvent as previously described,[25] the residue

was chromatographed on silica gel (30% EtOAc in hexane) to yield 109.5 mg (72%) of

2.8 as a transparent oil. ^{1}H NMR (400 MHz, CDCl$_3$): δ 7.35 (br d, J = 8.8 Hz, 1H), 5.18

(dd, J = 10.5, 5.2 Hz, 1H), 4.98–5.04 (m, 1H), 4.25 (q, J = 5.5 Hz, 1H), 3.85 (d, J = 5.5

Hz, 1H), 2.98 (s, 3H), 2.63–2.78 (m, 2H), 2.06 (t, J = 2.6 Hz, 1H), 1.43–1.76 (m, 6H),

1.44 (s, 9H), 1.14–1.35 (m, 6H), 1.0 (d, J = 6.4 Hz, 3H), 0.93 (d, J = 6.7 Hz, 3H), 0.82–

0.91 (m, 6H). ^{13}C NMR (100 MHz, CDCl$_3$): δ 173.5, 171.8, 170.7, 81.8, 79.8, 71.4, 70.0,

55.4, 47.5, 40.1, 37.5, 37.2, 31.0, 29.5, 29.3, 28.2, 25.3, 25.0, 23.4, 23.0, 21.6, 19.2, 14.2.

HR-EI-MS m/z 452.3250 ([M]$^+$, C$_{25}$H$_{44}$N$_2$O$_5$ requires 452.3250).

2.9
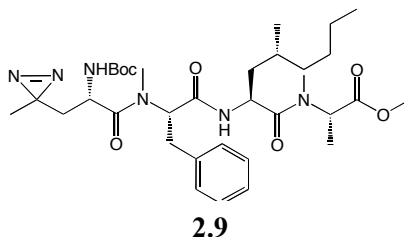
Synthesis of tetrapeptide 2.9:

To a stirred solution of **2.7** (120.0 mg, 0.287 mmol) in *tert*-BuOH/H$_2$O (2:1, 2.8 mL, 0.1 M) at 0 ºC was added LiOH·H$_2$O powder (24.1 mg, 0.573 mmol), and the reaction was stirred until no starting material was detected by TLC (2 h). Workup of the reaction as previously described[25] yielded 110 mg (95%) of the carboxylic acid of **2.7** as a white solid that was used without further purification. To a stirred solution of the carboxylic acid derived from **2.7** (72.6 mg, 0.179 mmol) and *N*-[(2*S*,4*R*)-2-amino-4-methyloctanoyl]-*N*-methyl-L-alanine methyl ester hydrochloride[25] (63.0 mg, 0.204 mmol) in DCM/DMF (5:1, 2 mL, 0.1 M) at −30 °C was added HOAt (29.2 mg, 0.215 mmol), EDCI (68.8 mg, 0.359 mmol), and 2,6-lutidine (23.0 μL, 0.204 mmol). The mixture was stirred at −30 °C for 5 h, warmed to RT, and stirred overnight (18 h). After workup and removal of the solvent as previously described[25] the residue was purified by silica gel chromatography (33% EtOAc in hexane) to yield 82.1 mg (70%) of **2.9** as a transparent gum. ^{1}H NMR (400 MHz, CDCl$_3$, two rotamers): δ 8.13 (d, *J* = 8.5 Hz, 1H), 8.09 (d, *J* = 8.5 Hz, 1H), 7.15–7.42 (m, 10H), 6.70 (d, *J* = 8.8 Hz, 1H), 6.68 (d, *J* = 9.1 Hz, 1H), 5.34–5.46 (m, 2H), 5.18–5.30 (m, 1H), 5.06 (dt, *J* = 8.8, 4.1, 1H), 4.97–5.02 (m, 1H), 4.72–4.90 (m, 2H), 4.42 (q, *J* = 7.4 Hz, 1H), 3.71 (s, 3H), 3.70 (s, 3H), 3.63–3.70 (m, 1H, partially overlapped), 3.30 (dd, *J* = 14.5, 6.5 Hz, 1H), 3.07 (s, 3H), 2.96–3.02 (m, 1H, partially overlapped), 2.98 (s, 3H), 2.96 (s, 3H), 2.89 (s, 3H), 1.91 (br s, 1H), 1.83 (dd, *J*

= 14.6, 6.5 Hz, 1H), 1.55–1.67 (m, 2H), 1.46–1.53 (m, 2H), 1.45 (s, 9H), 1.44 (s, 9H), 1.38–1.43 (m, 10H), 1.12–1.33 (m, 12H), 1.06 (s, 3H), 1.00 (d, J = 5.8 Hz, 3H), 0.94 (d, J = 6.3 Hz, 3H), 0.85–0.91 (m, 6H), 0.76 (s, 3H), −0.07–0.06 (m, 1H). ^{13}C NMR (100 MHz, CDCl$_3$, two rotamers): δ 172.9, 172.8, 172.6, 172.4, 172.2, 172.0, 169.4, 168.9, 156.0, 154.9, 137.7, 136.9, 129.7, 129.5, 129.1, 128.6, 127.1, 126.9, 81.2, 80.2, 62.3, 58.0, 52.4, 52.3, 52.1, 51.9, 47.7, 47.6, 46.8, 45.7, 40.3, 39.6, 38.2, 37.5, 37.3, 36.0, 34.5, 34.5, 34.1, 31.4, 31.1, 31.0, 29.8, 29.6, 29.5, 29.4, 29.3, 28.5, 28.5, 24.0, 23.4, 23.1, 20.2, 19.7, 19.2, 19.1, 14.5, 14.4, 14.2, 14.2. HR-EI-MS m/z 658.4047 ([M]$^+$, C$_{34}$H$_{54}$N$_6$O$_7$ requires 658.4053).

2.10
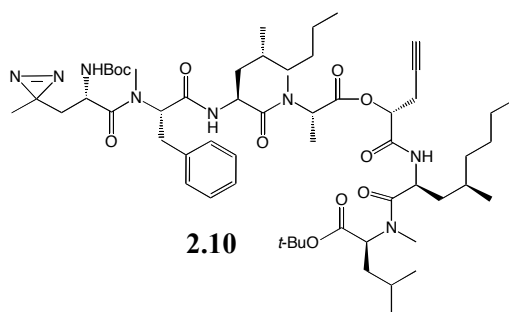
Synthesis of hepta(despi)peptide 2.10:

To a stirred solution of **2.9** (47.0 mg, 73.1 μmol) in *tert*-BuOH/H$_2$O (2:1, 0.75 mL, 0.1 M) at 0 °C was added LiOH·H$_2$O powder (6.0 mg, 143.0 μmol), and the reaction was stirred until no starting material was detected by TLC (1 h). Workup of the reaction as previously described[25] yielded the carboxylic acid of **2.9** as a transparent gum that was used directly in the next step without further purification. Polystyrene-immobilized triphenyl phosphine (Fluka, cat. #93093) was washed alternately (3×) with THF (2 mL) and MeOH (2 mL) followed by two additional washes with THF (2 mL) and was dried under vacuum. The washed beads (104.0 mg, 312 μmol) were then added to a stirred solution of the carboxylic acid derived from **2.9** (46.0 mg, 71.3 μmol) and tripeptide **2.8**

(32.3 mg, 71.3 μmol) in dry THF (1 mL, 0.07 M) and the mixture was stirred at RT for 45 min. Diisopropyl azodicarboxylate (DIAD) (63.0 mg, 312 μmols) was added and the mixture was stirred overnight at RT (18 h). The following day the mixture was filtered, the polystyrene beads were washed with THF (4 mL), and the solvent was removed. The residue was purified by preparative HPLC (MeOH/H_2O, linear gradient elution: 30/70 to 65/35 at 5 min, then 65/35 to 90/10 at 40 min, then 95/5 to 100/0 at 45 min, R_t = 44.4 min) to yield 53.0 mg (70%) of **2.10** as a white solid. ^{1}H NMR (CDCl$_3$, 400 MHz, two rotamers): δ 8.11 (d, J = 8.1 Hz, 1H), 8.07 (d, J = 8.5 Hz, 1H), 7.70 (d, J = 9.2 Hz, 1H), 7.50 (d, J = 9.0 Hz, 1H), 7.10–7.45 (m, 10H), 7.03 (d, J = 7.6 Hz, 1H), 7.00 (d, J = 5.0 Hz, 1H), 5.42–5.51 (m, 1H), 5.17–5.31 (m, 3H), 4.80–5.12 (m, 6H), 4.43–4.56 (m, 2H), 4.20–4.32 (m, 1H), 3.70–3.77 (m, 1H), 3.17–3.32 (m, 2H), 3.14 (s, 3H), 3.12 (s, 3H), 2.99–3.11 (m, 2H, overlapped), 2.98 (s, 3H), 2.96 (s, 3H), 2.94 (s, 3H), 2.89 (s, 3H), 2.73–2.85 (m, 3H), 2.59 (ddd, J = 15.0, 8.2, 2.4 Hz, 1H), 1.95 (t, J = 2.5 Hz, 1H), 1.94 (t, J = 2.7 Hz, 1H), 1.53–1.71 (m, 21H), 1.49 (d, J = 7.3 Hz, 6H), 1.45 (s, 18H), 1.44 (s, 18H), 1.12–1.32 (m, 24H), 1.05 (s, 3H), 0.87–1.03 (m, 36H), 0.76 (s, 3H), 0.11 (d, J = 15.5 Hz, 1H). HR-FT-MS m/z 1079.7141 ([M+H]$^+$, C$_{58}$H$_{95}$N$_8$O$_{11}$ requires 1079.7120).

CT7
2.2
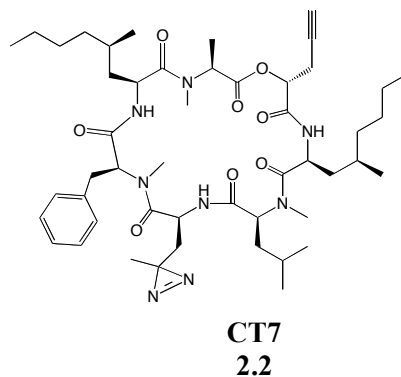
Synthesis of CT7 (compound 2.2):

To a stirred solution of **2.10** (15.0 mg, 13.9 μmol) in DCM (2.3 mL, 6 mM) at 0 °C were added TFA (0.460 mL) and anisole (three drops) and the reaction was stirred at 0 °C until the *N*-Boc and *tert*-butyl ester protecting groups were removed (as determined by LC-ESI-MS) (2 h). The solvent was removed with a stream of argon and the residue was dried under vacuum. The resulting solid was then treated at 0 °C with 4.0 M HCl/EtOAc (3 mL) for 30 sec. The solvent was again removed with a stream of argon and the residue was azeotroped (2×) with toluene. The residue was dissolved in DMF (14 mL, 1 mM), cooled to 0 °C, and treated with DIPEA (4.9 μL, 27.8 μmol) and diphenylphosphorylazide (DPPA) (6.0 μL, 27.8 μmol) and the reaction was stirred at 4 °C for 100 h. After removal of the solvent by rotary evaporation, the residue was purified by preparative HPLC (MeOH/H_2O linear gradient elution: 30/70 to 70/30 at 5 min, then 70/30 to 90/10 at 40 min, then 90/10 to 100/0 at 50 min. R_t = 34.5 min) to yield 4.7 mg (37%) of CT7 (compound **2.2**) as a white solid. ^{1}H NMR (CDCl$_3$, 400 MHz, major rotamer): δ 8.44 (d, J = 10.0 Hz, 1H), 7.81 (d, J = 9.7 Hz 1H), 7.09–7.27 (m, 5H), 6.03 (d, J = 5.9 Hz, 1H), 5.21–5.27 (m, 1H), 5.13 (dd, J = 11.8, 3.2 Hz, 1H), 4.95–5.07 (m, 2H), 4.79–4.93 (m, 2H), 4.55 (dd, J = 7.1, 4.0 Hz, 1H), 3.58–3.80 (m, 2H), 3.20 (s, 3H), 2.91–3.09 (m, 2H), 2.88 (s, 3H), 2.51 (s, 3H), 2.10 (t, J = 2.4 Hz, 1H), 1.74–1.91 (m, 3H), 1.58 (d, J = 7.0 Hz, 3H), 1.45–1.55 (m, 7H, overlapped), 1.14–1.37 (m, 12H), 1.11 (d, J = 6.3 Hz, 3H), 1.02 (d, J = 6.6 Hz, 3H), 0.92–0.99 (m, 6H), 0.86–0.91 (m, 6H), 0.78 (s, 3H), 0.19 (dd, J = 15.7, 2.9 Hz, 1H). HR-FT-MS *m/z* 905.5884 ([M+H]$^+$, C$_{49}$H$_{77}$N$_8$O$_8$ requires 905.5864).

2.11
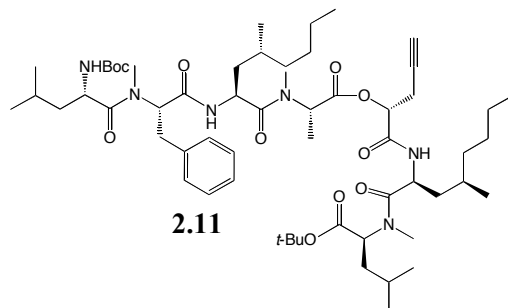
Synthesis of hepta(depsi)peptide 2.11:

To a stirred solution of *N*-[(2*S*,4*R*)-2-[*N*-[*N*-(*tert*-Butoxycarbonyl)-L-leucinyl]-*N*-methyl-L-phenylalanyl]amino-4-methyloctanoyl]-L-alanine methyl ester[25] (106.0 mg, 164.0 μmol) in *tert*-BuOH/H$_2$O (2:1, 1.7 mL, 0.1 M) at 0 °C was added LiOH·H$_2$O powder (14.0 mg, 328 μmol) and the reaction was stirred until no starting material was detected by TLC (2 h). Workup of the reaction as previously described[25] yielded the carboxylic acid that was used directly without further purification. To a stirred solution of the crude carboxylic acid (95.0 mg, 150 μmol) and tripeptide **2.8** (68.0 mg, 150 μmol) in toluene (3 mL, 0.05 M) was added pre-washed polystyrene-immobilized triphenyl phosphine (350.0 mg, 1.05 mmol, washing done as described above) and the reaction was stirred at RT for 45 min. Diisopropyl azodicarboxylate (DIAD) (212.3 mg, 1.05 mmol) was then added and the mixture was stirred overnight at RT (18 h). The following day the mixture was filtered, the polystrene beads were washed with toluene and the solvent was removed. The residue was purified by preparative HPLC (MeOH/H$_2$O linear gradient elution: 60/40 to 100/0 over 23 min, R$_t$ = 18.5 min) to yield 69.0 mg (43%) of **2.11** as an off-white solid. ^{1}H NMR (400 MHz, CDCl$_3$ two rotamers): δ 8.58 (d, *J* = 9.5 Hz, 1H), 8.21 (d, *J* = 8.3 Hz, 1H), 7.85 (d, *J* = 8.6 Hz, 1H), 7.43 (d, *J* = 8.2 Hz, 1H), 7.03–7.38 (m, 10H), 6.67 (d, *J* = 6.6 Hz, 1H), 6.65 (d, *J* = 7.5 Hz, 1H), 5.37–5.48 (m, 1H), 5.09–5.32

(m, 4H), 5.32–4.74 (m, 6H), 4.37–4.59 (m, 2H), 4.03–4.19 (m, 1H), 3.24 (s, 3H), 3.13–

3.30 (m, 4H, partially overlapped), 3.11 (s, 3H), 2.99 (s, 3H), 2.98 (s, 3H), 2.95 (s, 3H),

2.94 (s, 3H), 2.74–2.93 (m, 3H), 2.56 (ddd, J = 17.4, 8.2, 2.5 Hz, 1H), 1.94 (t, J = 2.5 Hz,

1H), 1.90 (t, J = 2.1 Hz, 1H), 1.23–1.77 (m, 23H, partially overlapped), 1.50 (d, J = 7.1

Hz, 3H), 1.47 (d, J = 7.3, 3H), 1.45 (s, 18H), 1.41 (s, 18H), 1.18–1.26 (m, 24H), 0.83–

1.03 (m, 36H), 0.78 (d, J = 6.3 Hz, 6H), 0.66 (d, J = 6.6 Hz, 3H), 0.62 (d, J = 6.5 Hz,

3H), −0.31– −0.17 (m, 1H). HR-FT-MS m/z 1067.7371 ([M+1]$^+$, $C_{59}H_{99}N_6O_{11}$ requires

1067.7371).

CT8
2.3
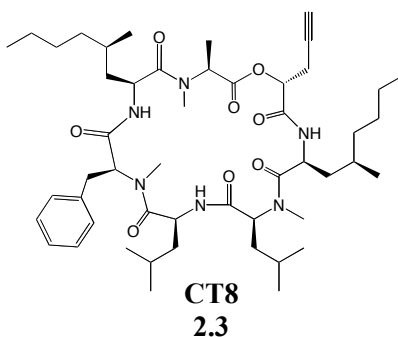
Synthesis of CT8 (compound 2.3):

To a stirred solution of **2.11** (28.8 mg, 27.0 μmol) in DCM (4.2 mL, 6 mM) at 0 ˚C were

added TFA (0.833 mL) and anisole (three drops) and the reaction was stirred until the *N*-

Boc and *tert*-butyl ester protecting groups were removed (as determined by LC-ESI-MS)

(2 h). The solvent was removed with a stream of argon, the residue was dried under

vacuum and then brought up in 4.0 M HCl/EtOAc (1 mL) for 30 sec. The solvent was

again removed with a stream of argon and the residue azeotroped (2×) with toluene. The

residue was then dissolved in DMF (25 mL, 1 mM), cooled to 0 ºC, and treated with

DIPEA (28.2 μL, 162 μmol) and diphenylphosphorylazide (DPPA) (17.4 μL, 81.0 μmol)

and the reaction was stirred at 4 °C for 190 h. After removal of the solvent by rotary

evaporation, the residue was purified by preparative HPLC (MeOH/H$_2$O linear gradient elution: 50/50 to 100/0 over 30 minutes, R$_t$ = 21.8 min) to yield 8.9 mg (37%) of **2.3** as a white solid. ^{1}H NMR (400 MHz, CDCl$_3$, major rotamer): δ 8.53 (d, J = 10.3 Hz, 1H), 7.81 (d, 9.5 Hz, 1H), 7.07–7.38 (m, 5H), 6.07 (d, J = 6.3 Hz, 1H), 5.12 (dd, J = 11.6, 2.9 Hz, 1H), 4.93–5.03 (m, 2H), 4.83–4.92 (m, 2H), 4.54 (dd, J = 11.0, 3.7 Hz, 1H), 4.22–4.32 (m, 1H), 3.71–3.78 (m, 1H), 3.55–3.63 (m, 1H), 3.07–3.17 (m, 2H), 3.06 (s, 3H), 2.91 (s, 3H), 2.54 (s, 3H), 2.01 (t, J = 2.5 Hz, 1H), 1.79–1.90 (m, 4H), 1.55 (d, J = 6.9 Hz, 3H), 1.37–1.65 (m, 7H), 1.16–1.37 (m, 12H), 1.07 (d, J = 6.5 Hz, 3H), 1.00 (d, J = 6.7 Hz, 3H), 0.97 (d, J = 6.3 Hz, 3H), 0.85–0.95 (m, 9H), 0.77 (d, J = 6.3 Hz, 3H), 0.64 (d, J = 6.4 Hz, 3H), 0.03–0.09 (m, 1H). HR-FT-MS m/z 893.6132 ([M+H]$^+$, C$_{50}$H$_{81}$N$_6$O$_8$ requires 893.6116).

2.8 References

1. Lokey, R.S. (2001). Forward chemical genetics: progress and obstacles on the path to a new pharmacopoeia. Curr. Opin. in Chem. Biol. *7*, 91–96.

2. Ding, S., Wu, T.Y.H., Brinker, A., Peters, E.C., Hur, W., Gray, N.S., and Schultz, P.G. (2004). Synthetic small molecules that control stem cell fate. Proc. Natl. Acad. Sci USA. *100*, 856–861.

3. Taunton, J., Hassig, C.A., and Schreiber, S.L. (1996). A mammalian histone deacetylase related to the yeast transcriptional regulator Rpd3p. Science *272*, 408–411.

4. Harding, M.W., Galat, A., Uehling, D.E., and Schreiber, S.L. (1989). A receptor for the immuno-suppressant FK506 is a *cis-trans* peptidyl-prolyl isomerase. Nature *341*, 758–760.

5. Ong, S., Schenone, M., Margolin, A.A., Li, X., Do, K., Doud, M.K., Mani, D.R., Kuai, L., Wang, X., Wood, J.L., Tolliday N.J., Koehler A.N., Marcaurelle L.A., Golub, T.R., Gould, R.J., Schreiber, S.L., and Carr, S.A. (2009). Identifying the proteins to which small-molecule probes and drugs bind in cells. Proc. Natl. Acad. Sci. USA *106*, 4617–4622.

6. Sadakane, Y., and Hatanaka Y. (2006). Photochemical fishing approaches for identifying target proteins and elucidating the structure of a ligand-binding region using carbene-generating photoreactive probes. Anal. Sci. *22*, 209–218.

7. Colca, J.R., McDonald, W.G., Waldon, D.J., Leone, J.W., Lull, J.M., Bannow, C.A., Lund, E.T., and Mathews, W.R. (2004). Identification of a novel mitochondrial protein ("mitoNEET") cross-linked specifically by a thiazolidinedione photoprobe. Am. J. Physiol. Endocrinol. Metab. *286*, E252–E260.

8. Saghatelian, A., Jessani, N., Joseph, A., Humphrey, M., and Cravatt, B.F. (2004). Activity-based probes for the proteomic profiling of metaloproteases. Proc. Natl. Acad. Sci. USA. *101*, 1000–1005.

9. Al-Mawsawi, L.Q., Fikkert, V., Dayam, R., Witvrouw, M., Burke, T.R. Jr., Borchers, C.H., and Neamati, N. (2006). Discovery of a small-molecule HIV-1 integrase inhibitor-binding site. Proc. Natl. Acad. Sci. USA *103*, 10080–10085.

10. Xi, J., Liu, R., Rossi, M.J., Yang, J., Loll, P.J., Dailey, W.P., and Eckenhoff, R.G. (2006). Photoactive analogues of the haloether anesthetics provide high-resolution features from low-affinity interactions. ACS Chem. Biol. *1*, 377–384.

11. Dormán, G., and Prestwich G.D. (1994). Benzophenone photophores in biochemistry. Biochemistry *33*, 5661–5673.

12. Wittelsberger, A., Thomas, B.E., Mierke, D.F., and Rosenblatt, M. (2006). Methionine acts as a "magnet" in photoaffinity crosslinking experiments. FEBS Lett. *580*, 1872–1876.

13. Brunner, J. (1993). New photolabeling and crosslinking methods. Annu. Rev. Biochem. *62*, 483–514.

14. Platz, M., Admasu, A.S., Kwiatkowski, S., Crocker, P.J., Imai, N., and Watt, D.S. (1991). Photolysis of 3-aryl-3-(trifluoromethyl) diazirines: a caveat regarding their use in photoaffinity probes. Bioconjug. Chem. *2*, 337–341.

15. MacKinnon, A.L., Garrison J.L., Hegde, R.S., and Taunton, J. (2007). Photo-leucine incorporation reveals the target of a cyclodepsipeptide inhibitor of cotranslational translocation. J. Am. Chem. Soc. *129*, 14560–14561.

16. Ford, F., Yuzawa, T., Platz, M. S., Matzinger, S., and Fulscher, M. (1998). Rearrangement of dimethylcarbene to propene: study by laser flash photolysis and *ab initio* molecular orbital theory. J. Am. Chem. Soc. *120*, 4430–4438.

17. Bond, M.R., Zhang, H., Vu, P.D., and Kohler J.J. (2009). Photocrosslinking of glycoconjugates using metabolically incorporated diazirine-containing sugars. Nat. Protoc. *4*, 1044–1063.

18. Suchanek, M., Radzikowska, A., and Thiele, C. (2005). Photo-leucine and photo-methionine allow identification of protein-protein interactions in living cells. Nat. Methods. *2*, 261–268.

19. Vila-Perelló, M., Pratt, M. R., Tulin, R., and Muir T.A. (2007). Covalent capture of phospho-dependent protein oligomerization by site-specific incorporation of a diazirine photo-cross-linker. J. Am. Chem. Soc. *129*, 8068–8069.

20. Best, M.D. (2009). Click chemistry and bioorthogonal reactions: unprecedented selectivity in the labeling of biological molecules. Biochemistry *48*, 6571–6584.

21. Weerapana, E., Speers, A.E., and Cravatt, B.F. (2007). Tandem orthogonal proteolysis-activity-based protein profiling (TOP-ABPP)– a general method for mapping sites of probe modification in proteomes. Nat. Protoc. *2*, 1414–1425.

22. Speers, A.E., and Cravatt, B.F. (2005). A tandem orthogonal proteolysis strategy for high-content chemical proteomics. J. Am. Chem. Soc. *127*, 10018–10019.

23. Adam, G.C., Burbaum, J., Kozarich, J.W., Patricelli, M.P., and Cravatt, B.F. (2004). Mapping enzyme active sites in complex proteomes. J. Am. Chem. Soc. *126*, 1363–1368.

24. Speers, A.E., Cravatt, B.F. (2004). Profiling enzyme activities in vivo using click chemistry methods. Chem. Biol. *11*, 535–546.

25. Chen, Y., Bilban, M., Foster, C. A., and Boger, D. L. (2002). Solution-phase parallel synthesis of a pharmacophore library of HUN-7293 analogues: a general chemical mutagenesis approach to defining structure-function properties of naturally occurring cyclic (depsi)peptides. J. Am. Chem. Soc. *124*, 5431–5440.

26. Cornish, V. W., Hahn, K. M., and Shultz, P. G. (1996). Site-specific protein modification using a ketone handle. J. Am. Chem. Soc. *118*, 8150–8151.

27. Church, R. F. R., and Weiss, M. J. (1970). Diazirines. II. Synthesis and properties of small functionalized diazirine molecules. Observations on the reaction of a diaziridine with the iodine-iodide ion system. J. Org. Chem. *35*, 2465–2471.

28. Görlich, D., and Rapoport, T.A. (1993). Protein translocation into proteoliposomes reconstituted from purified components of the endoplasmic reticulum membrane. Cell *75*, 615–630.

29. Fons, R.D., Bogert, B.A., and Hegde, R.S. (2003). Substrate-specific function of the translocon-associated protein complex during translocation across the ER membrane. J. Cell Biol. *160*, 529–539.

30. Cohen, M. S., Hadjivassiliou, H., and Taunton, J. (2007). A clickable inhibitor reveals context-dependent autoactivation of p90 RSK. Nat. Chem. Biol. *3*, 156–160.

31. Hanein, D., Matlack, K. E. S., Jungnickel, B., Plath, K., Kalies, K., Miller, K. R., Rapoport, T.A., and Akey, C. W. (1996). Oligomeric rings of the Sec61p complex induced by ligands required for protein translocation. Cell *87*, 721–732.

32. Walter, P., Ibrahimi, I., and Blobel, G. (1981). Translocation of proteins across the endoplasmic reticulum. I. Signal recognition protein (SRP) binds to in-vitro-assembled polysomes synthesizing secretory protein. J. Cell Biol. *91*, 545–550.

33. Gilchrist, A., Au, C. E., Hiding, J., Bell, A. W., Fernandez-Rodriguez, J., Lesimple, S., Nagaya, H., Roy, L., Gosline, S. J. C., Hallett, M., Paiement, J., Kearney, R. E., Nilsson, T., and Bergeron, J. J. M. (2006). Quantitative proteomics analysis of the secretory pathway. Cell *127*, 1265–1281.

34. Guth, S., Volzing, C., Muller, A., Jung, M., and Zimmermann, R. (2004). Protein transport into canine pancreatic microsomes: a quantitative approach. Eur. J. Biochem. *271*, 3200–3207.

35. Chan, T. R., Hilgraf, R., Sharpless, K. B., and Fokin, V. V. (2004). Polytriazoles as copper(I)-stabilizing ligands in catalysis. *Org. Lett. 17*, 2853–2855.

36. Garrison, J.L., Kunkel, E.J., Hegde, R.S., and Taunton, J. (2005). A substrate-specific inhibitor of protein translocation into the endoplasmic reticulum. Nature *436*, 285–289.

37. Deechongkit, S., You, S., and Kelly J. W. (2004). Synthesis of all nineteen appropriately protected chiral alpha-hydroxy acid equivalents of the alpha-amino acids for Boc solid-phase depsi-peptide synthesis. Org. Lett. *6*, 497–500.

38. Cavelier, F., Jacquier, R., Mercadier, J., Verducci, J., Traris, M., and Vey, A. (1997). Destruxin analogs: variations of the alpha-hydroxy acid side chain. J. Pep. Res. *50*, 94–101.

39. Xu, T., Werner, M., Lee, K., Fettinger, J. C., Davis, J. T., and Coward, J. K. Synthesis and evaluation of tripeptides containing asparagine analogues as potential substrates or inhibitors of oligosaccharyltransferase. J. Org. Chem. *63*, 4767–4778.

Chapter 3: Cotransins reveals the mechanism of Sec61-mediated transmembrane domain integration

3.1 Abstract

Membrane protein integration relies on the movement of hydrophobic transmembrane domains (TMDs) from the aqueous pore of the Sec61 channel into the surrounding lipid bilayer. Molecular insight into this reaction has been hampered by the challenge of stabilizing an intrinsically dynamic process. Here, we utilize cotransin to dissect the mechanism of TMD integration. We demonstrate that cotransin impedes progression of a TMD through the integration reaction, thereby permitting analysis of a stabilized pre-integrated intermediate. Extensive site-specific crosslinking studies of this intermediate revealed an α-helical TMD docked near the cytosolic face of the lateral gate in Sec61α. Progression through this cotransin-stabilized stage was strongly influenced by α-helical propensity and hydrophobicity of the TMD. Thus, direct contacts between a TMD and the lateral gate precede TMD transfer into the membrane, a dynamic step amenable to modulation by cotransin.

3.2 Introduction

Most eukaryotic membrane proteins are cotranslationally integrated into the endoplasmic reticulum (ER) membrane.[1] This process begins when the first hydrophobic domain of a nascent membrane protein, often a transmembrane domain (TMD), emerges from a translating ribosome and is recognized by the signal recognition particle (SRP). The SRP system targets the ribosome-nascent polypeptide complex (RNC) to the ER membrane[2] and transfers it to a translocation channel formed by the heterotrimeric Sec61 complex.[3] Sec61 binds near the polypeptide exit tunnel on the ribosome and mediates both co-translational translocation and TMD integration. This suggests that the Sec61 channel not

only opens towards the ER lumen but also laterally towards the lipid bilayer. While lateral TMD release through Sec61 was proposed long ago,[4-6] the precise mechanism of this crucial step in membrane protein biogenesis has been unclear.

During integration into the membrane, TMDs must move from the aqueous pore of the Sec61 channel into the surrounding lipid bilayer. At least two different models have been proposed to explain this reaction. In one model, the TMD is proposed to thermodynamically equilibrate between the aqueous Sec61 channel and the lipid bilayer.[7-9] This partitioning would be facilitated by an intrinsically dynamic "lateral gate" in Sec61 that allows the polypeptide segment inside the channel to constantly sample the membrane environment. Support for this model comes from experiments in which an extensive set of model TMDs was analyzed for integration efficiency. The strong correlation between net insertion efficiency and the summed hydrophobicities of individual residues along the TMD was interpreted to indicate a simple thermodynamic partitioning event. While this correlative analysis has provided considerable insight into the features of a TMD that determine its final stability in the lipid bilayer, the issue of precisely how it moves into the bilayer was not examined in these endpoint assays, and hence remains unresolved.

An alternative model proposes that lateral integration of TMDs is a kinetically controlled event that depends on specific interactions between the TMD and Sec61. This conclusion is based on the analysis of stalled RNCs of membrane proteins at different lengths. Not only do the TMDs of such stalled RNCs crosslink to Sec61, but they also appear to be

oriented in a specific manner as judged by asymmetric crosslinks seen from adjacent residues.[10,11] Furthermore, RNCs of successive lengths seem to make a series of stereotyped interactions with Sec61 and other channel proteins before eventual contact with lipids. These observations have been interpreted as illustrating direct TMD-Sec61 interactions (as opposed to simply being in the vicinity of Sec61 during integration), implying an active role for the TMD in mediating its integration.

Conceptualizing the mechanistic basis of TMD integration has been aided by structural studies of the Sec61 complex. The crystal structure of the archeal complex revealed that SecY (homologous to Sec61α, the largest subunit and structural core of complex) is comprised of a compact bundle of 10 α-helical transmembrane domains (TMDs 1–10). These TMDs are arranged in a pseudo-two-fold symmetric structure with TMDs 1–5 and 6–10 forming the two halves of a "clamshell". The interior of the clamshell forms an hourglass–shaped pore in the membrane,[12] the center of which is occluded by a short α-helix termed the plug. The backside of the clamshell is braced by SecE (Sec61γ in metazoans), while the front of the clamshell forms the so-called lateral gate. This gate is formed at the interface of TMDs 2b/3 and TMDs 7/8 and represents a seam in the channel that when opened, could provide direct access to the lipid bilayer from the central pore.

Translocation across the membrane is proposed to occur when a TMD (or signal sequence) of an RNC binds at the lateral gate of Sec61α. Intercalation of a TMD into this site would destabilize the plug,[13] position the nascent polypeptide within the channel,[14] and provide the TMD direct access to the lipid bilayer. This idea is supported by the

observation that a signal sequence can be crosslinked to lateral gate TMDs 2 and 7,[15] and that mutations in the lateral gate can influence TMD integration and translocation.[16] Various structures of Sec61 have also revealed the lateral gate in a continuum of partially open states,[17-19] implicating the lateral gate as a potential site of TMD exit into the lipid bilayer. However, the functional significance of these structural changes and the role of the lateral gate during TMD integration remain speculative. A major obstacle to understanding TMD integration is the challenge of stabilizing what is presumably an intrinsically dynamic process. Thus, tools that can selectively modulate the integration reaction would be valuable in studying this process.

We and others previously described cotransin (CT), a cyclodepsipeptide that blocks translocation through Sec61 in a signal sequence-dependent manner.[20,21] CT binds directly to the Sec61α subunit of the channel[22] and blocks translocation through Sec61 at a step after RNC targeting. CT can also potently block TMD integration into the ER membrane[23] and may therefore represent a unique chemical tool to probe the poorly understood process of TMD integration. Here, we have investigated the mechanism underlying CT inhibition of TMD integration. Our analysis reveals a previously unappreciated intermediate during membrane integration and suggests that direct interactions between the TMD and the lateral gate of Sec61 play an essential role in TMD integration.

3.3 Experimental strategy

To dissect the mechanism of TMD integration, we used a reconstituted translocation system comprised of a translation extract supplemented with microsomal ER

69

membranes.[24] When programmed with a truncated mRNA transcript that lacks a stop codon, ribosomes in the extract translate to the end of the transcript and "stall", creating a synchronized population of ribosome nascent chain complexes (RNCs) that functionally engage the Sec61 machinery.[25] Systematically varying the length of the truncated mRNA and hence the length of the nascent chain produces RNC-Sec61 complexes that represent discrete stages along the integration pathway. We used this approach to prepare integration intermediates of the membrane protein TNFα, whose integration into the ER is potently blocked by CT8.[23] TNFα is a type II membrane protein that contains a single TMD, also called a signal anchor domain, which mediates both RNC targeting to Sec61 and stable integration of TNFα into the lipid bilayer (**Figure 3-1**).
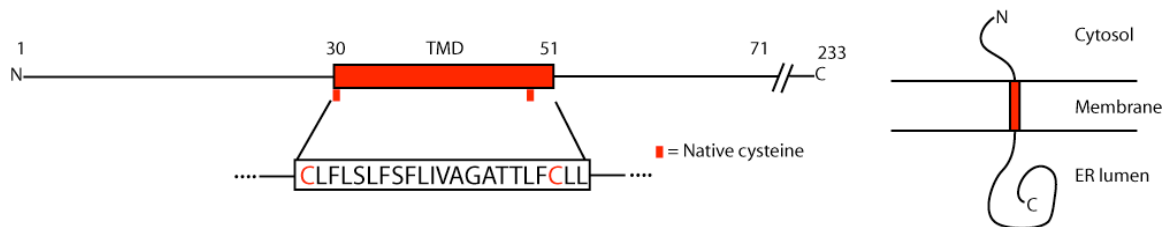
Figure 3-1. Schematic diagram of the type II membrane protein TNFα.
Left, primary structure of TNFα highlighting the transmembrane domain (TMD). *Right*, type II topology of TNFα.

3.4 CT8 blocks TMD integration after RNC targeting to Sec61

The mechanism by which hydrophobic TMDs pass from Sec61 into the membrane is not known. We sought to use CT8 as a chemical tool to dissect this process. We first tested if CT8 blocks TMD integration for translationally stalled integration intermediates. Since the TMD of TNFα extends from residue 30 to 51 (**Figure 3-1**), nascent chains of 126 amino acids (a.a., 126mers) are predicted to be sufficiently long to mediate both targeting

70

to Sec61 and integration into the membrane.[4] As expected, digestion of 126mers with

protease resulted in formation of a more mobile protease-protected fragment that

corresponded in size to the TMD and C-terminal domain of TNFα (**Figure 3-2**). These

regions of the nascent chain are most likely protected from the action of the protease by

Sec61 and the ER membrane, consistent with an integrated conformation of the TMD. By

contrast, a reduced amount of the protease-protected fragment was observed when

126mers were assembled in the presence of CT8, suggesting CT8 blocked TMD
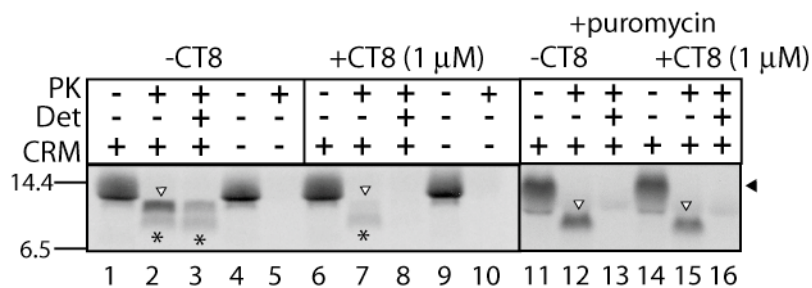
integration into the membrane.

Figure 3-2. Protease K protection of TNFα 126mers.
Translation reactions were performed in the presence or absence of canine rough microsomes (CRM) and CT8, and then digested with Protease K (PK) in the presence or absence of TX-100 (Det). For some experiments, puromycin was brought to 2 mM after the translation, and samples were incubated at 37°C prior to digestion with PK. The positions of the undigested nascent chain and protease-protected fragment are indicated (closed and open triangle, respectively). The weak band marked by an asterisk was only observed in some experiments; its identity is not known.

To provide more direct evidence that CT8 blocks TMD integration, we probed the

solvent accessibility of the TMD using a two-step thiol labeling protocol, adapted from

Sakaguchi and coworkers.[26] In this assay, intact integration intermediates are first treated

with N-ethyl-maleimide (NEM) to alkylate solvent-accessible cysteines in the TMD. In a

second step, cysteines that were inaccessible to NEM in the intact intermediate are

exposed by denaturation in SDS and then modified with PEG-maleimide (PEG-Mal),

71

causing a shift in the mobility of the nascent chain by SDS-PAGE. Using this assay, we found that a TMD containing a cysteine at position 49 (hereafter referred to as the C49 construct) was more efficiently alkylated with NEM in the presence versus the absence of CT8 (**Figure 3-3**). Since alkylation requires an aqueous environment, this result directly demonstrates that CT8 promotes exposure of the TMD to the aqueous phase and blocks its transition into an NEM-inaccessible environment, which is most likely identical to the hydrophobic lipid membrane.
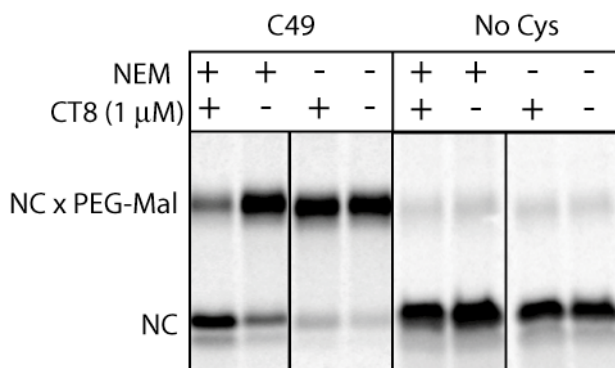

Figure 3-3. NEM-accessibility of C49 126mers.
126mer intermediates containing a single cysteine present in the TMD (C49) were prepared in the presence or absence of CT8 and then alkylated with N-ethyl-maleimide (NEM). Samples were then denatured in SDS and reacted with 5 kDa PEG-Maleimide (Peg-Mal), followed by analysis of the reactions by SDS-PAGE and autoradiography. A control construct lacked all cysteines (No Cys).

We next tested if CT8 perturbed RNC targeting to Sec61. When 126mers were treated with puromycin prior to digestion with protease, nearly equivalent amounts of the protease-protected fragment were observed in the presence or absence of CT8 (**Figure 3-2**). Puromycin releases the nascent chain from the ribosome and drives membrane integration of partially integrated intermediates.[5] Since puromycin promoted integration of 126mers even in the presence of CT8, the nascent chains were most likely properly targeted to Sec61 and on a productive integration pathway. Consistent with this idea,

when RNCs bearing N-terminally 3x-Flag tagged nascent chains were prepared in the presence or absence of CT7, solubilized with 1% Deoxy BigChap (DBC), and immunopurified, identical amounts of Sec61 were found in the eluent (**Figure 3-4**). HA-tagged intermediates served as a control. CT7 remained tightly bound to the RNC-Sec61 complex throughout the purification. These results indicate that CT7, Sec61, and the RNC form a stable complex in detergent solution, and that TMD integration is therefore blocked after formation of a targeted intermediate.
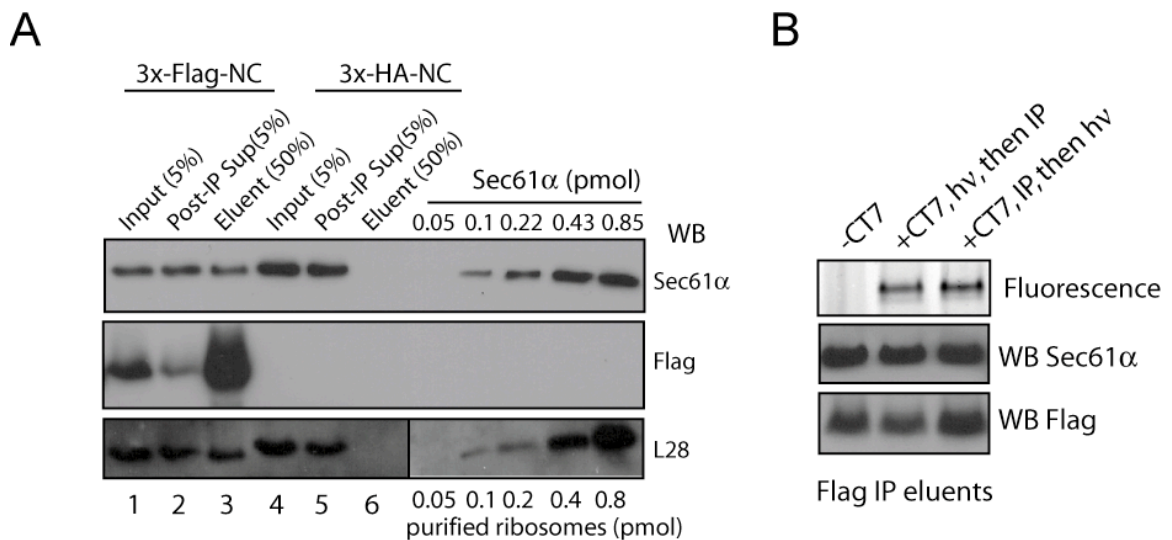
Figure 3-4. Co-immunopurification of Sec61-RNC complexes.
(A) 126mers containing a 3x-Flag or 3x-HA tag at the N-terminus were solubilized in 1% Deoxy BigChap (DBC) and immunopurified (IP) with anti-Flag affinity resin. The eluents were analyzed by SDS-PAGE and Western blotting (WB) next to Sec61 or ribosome (L28) standards. (B) Same as in (A) but 126mers were prepared in the presence or absence of the photo-affinity probe CT7 and photolyzed (hν) either before (lane 2) or after immunopurification (lane 3). Covalently bound CT7 was detected by click chemistry with TAMRA-azide followed by SDS-PAGE and in-gel fluorescence scanning.

3.5 CT8 stabilizes a pre-integrated translocation intermediate

It is currently unknown if discrete intermediates exist between RNC targeting to Sec61 and insertion of the TMD into the membrane. Since our data indicated that CT8 blocked

TMD integration after targeting, we sought to determine where in Sec61α the TMD was located. Towards this end, we used chemical crosslinking with bis-maleimido-hexane (BMH) to probe the environment of C49 in the TMD for a series of TNFα integration intermediates of different lengths prepared in the presence and absence of CT8. BMH can covalently crosslink two solvent-accessible cysteines residues that lie within ~13 Å of each other. Using this approach, we found that in the absence of CT8, BMH crosslinks first appeared between the 80mer and Sec61β, which contains a single cysteine in a flexible cytosolic tail (**Figure 3-5**). Thus, the 80mer was properly targeted to the Sec61 channel, but C49 of the TMD was exposed to the cytosolic tail of Sec61β and therefore on the cytosolic side of the membrane. Strong crosslinks to S61β persisted as the nascent chain was extended to 96 a.a., at which point crosslinks to Sec61α were also detected (**Figure 3-5**). This suggested the TMD had inserted into the channel pore, as previously reported for signal sequences,[27] but remained accessible to the soluble crosslinking reagent. Control experiments indicated that the observed crosslinks were derived exclusively from RNC complexes, were cysteine-dependent, and were strongly influenced by the position of the cysteine in the TMD (**Figure 3-6**). As the nascent chain was further extended beyond 96 a.a., crosslinks to both Sec61α and Sec61β disappeared. Crosslinks were undetectable by 116 a.a. suggesting the TMD had passed into the lipid membrane. This conclusion was further supported by experiments that measured accessibility of the TMD to NEM (**Figure 3-7**) or to protease (**Figure 3-8**). The loss of BMH crosslinking of the TMD to Sec61 therefore most likely corresponds to TMD movement into the lipid membrane. These experiments also revealed that TMD integration is tightly coupled to nascent chain elongation and proceeds through an

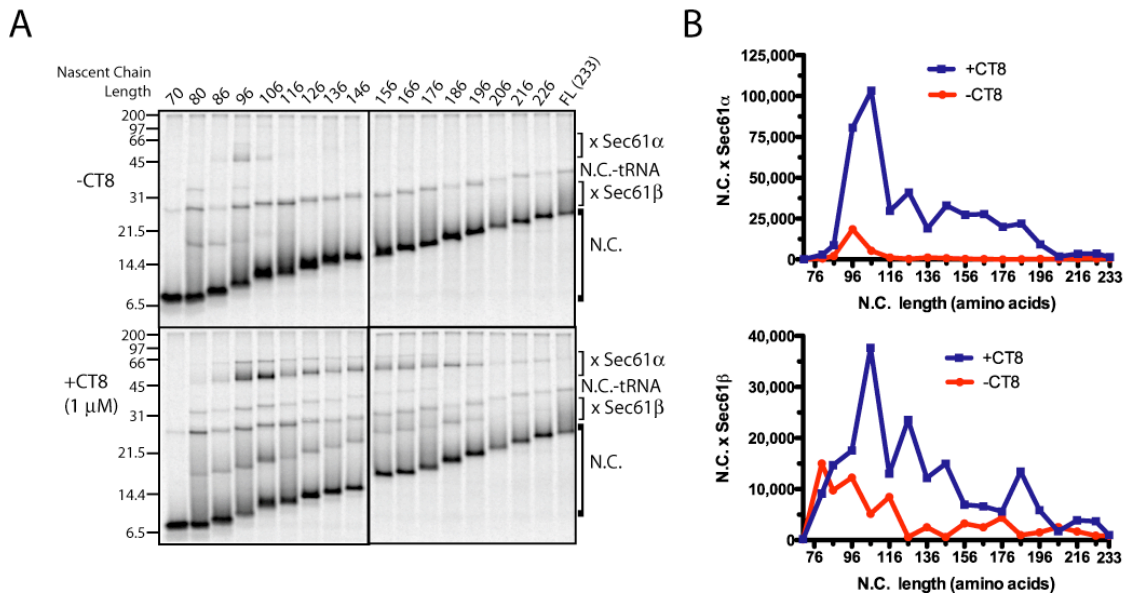intermediate where C49 in the TMD resides within ~13 Å of a solvent-accessible cysteine in Sec61α.

Figure 3-5. BMH crosslinking reactions for a truncated series of C49 intermediates.
(A) All nascent chains contained a single cysteine at position 49 of the TMD (C49). Positions on the gel corresponding to the nascent chain (N.C.), nascent chain-tRNA (N.C.-tRNA), and BMH crosslinks of the N.C. to Sec61α (× Sec61α) and Sec61β (× Sec61β) are indicated. Crosslinks of the N.C-tRNA to Sec61α and Sec61β are also visible on the gel (see also Figure 3-6). (B) Quantitation of the intensity of crosslinks between the nascent chain and Sec61α (top) and Sec61β (bottom) from the experiment shown in (A) was performed by phosphorimaging.

A strikingly different crosslinking profile was observed when truncated intermediates were assembled in the presence of CT8 (**Figure 3-5**). Early intermediates of 80 and 86 a.a. crosslinked to Sec61β with an efficiency similar to those assembled in the absence of CT8, further demonstrating that CT8 did not perturb RNC targeting to Sec61. However, at the 96mer intermediate, CT8 strongly enhanced crosslinks of the TMD to Sec61α by ~4–5-fold. Crosslinks to Sec61β were also enhanced. These strong crosslinks then persisted as the nascent chain was extended past 96 a.a., the point at which crosslinks to

Sec61 disappeared in the absence of CT8. Taken together, these data indicate that CT8 stabilizes an intermediate that occurs only transiently during normal TMD integration. The TMD in this stabilized intermediate is in a solvent-accessible environment and in close proximity to Sec61α. These conclusions were further supported in NEM-accessibility experiments where CT8 blocked movement of the TMD into a solvent-inaccessible environment (**Figure 3-7**).
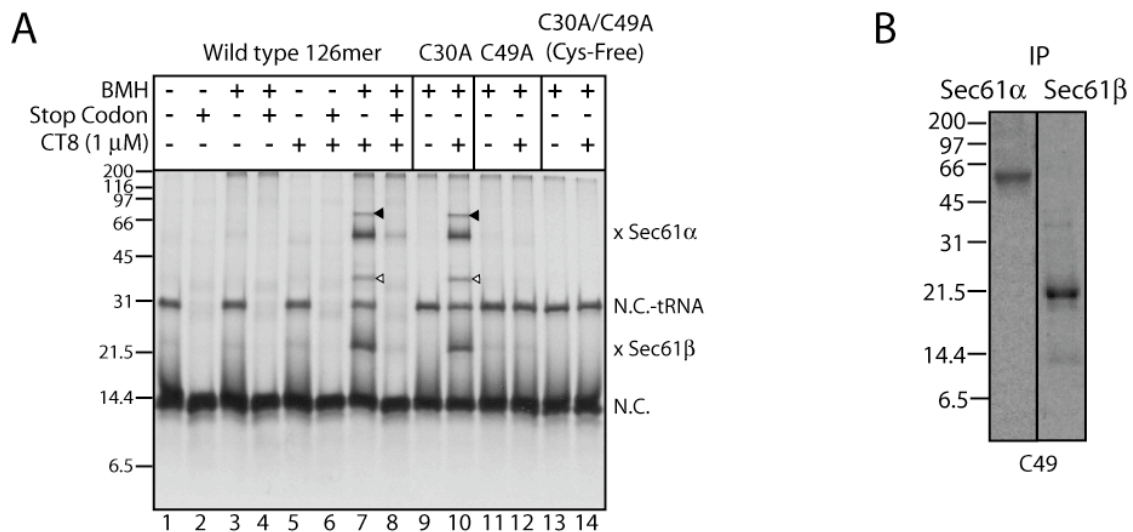
Figure 3-6. BMH crosslinking reactions of TNFα 126mers.
(A) Translocation intermediates were assembled in the presence or absence of CT8, isolated by sedimentation, and reacted with BMH. Translationally terminated nascent chains (+stop codon) served as a control. Positions on the gel corresponding to the nascent chain (N.C.), nascent chain-tRNA (N.C.-tRNA), and BMH crosslinks of the N.C. to Sec61α (× Sec61α) and Sec61β (× Sec61β) are indicated. Crosslinks of the N.C-tRNA to Sec61α and Sec61β are also indicated (closed and open triangle, respectively). The residual tRNA adducts result from incomplete hydrolysis of peptidyl-tRNA during electrophoresis. (B) Denaturing immunoprecipitation (IP) of BMH crosslinking reactions. C49 126mers were prepared in the presence of CT8 and crosslinked with BMH. Reactions were then quenched, denatured in SDS and immunoprecipitated against the indicated proteins. Eluents were analyzed by SDS-PAGE and autoradiography.

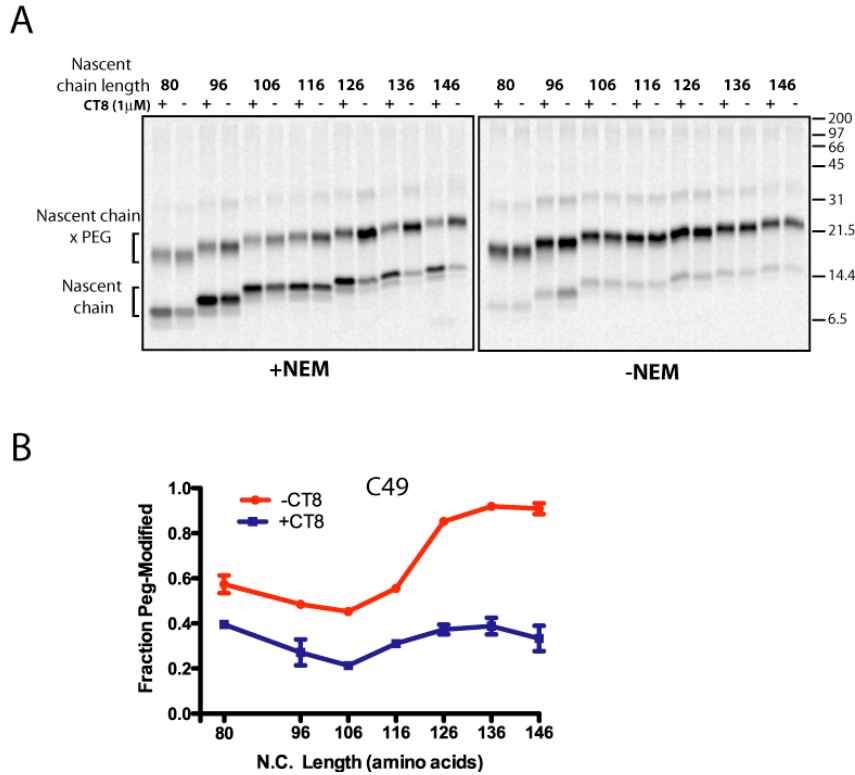**Figure 3-7. NEM-accessibility of a truncated series of C49 intermediates.**
(A) Truncated TNFα translocation intermediates containing a single cysteine at position 49 of the TMD were treated with NEM to alkylate solvent-exposed cysteines, then denatured in SDS and treated with PEG-Mal to alkylate cysteines that were buried in the intact intermediate. (B) Quantified data from gels shown in (A) from two independent experiments.
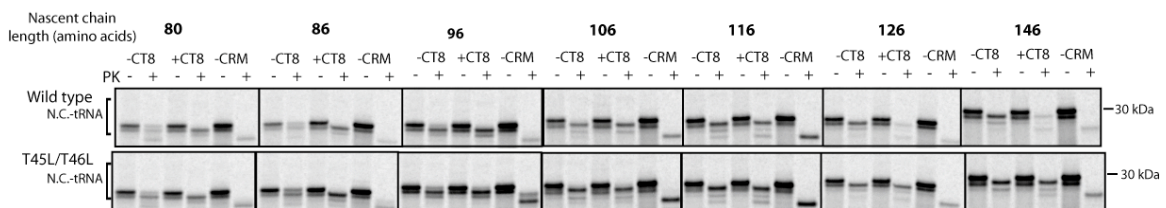
Figure 3-8. Protease K (PK) accessibility of truncated intermediates.
Protease protection assays of truncated wild type or T45L/T46L TNFα translocation intermediates were done in the presence or absence of CT8 (1 μM) and canine rough microsomes (CRM). We focused our analysis on the nascent chain-tRNA species (N.C.-tRNA), which must necessarily contain an intact C-terminus. Thus, any change in mobility of the N.C-tRNA after PK digestion represents proteolysis at the N-terminus of the nascent chain. To preserve the hydrolytically labile peptidyl-tRNA bond for this purpose, reactions were quenched under neutral conditions and resolved on neutral NuPAGE gels.

3.6 TMD integration is irreversible

We found by order of addition experiments that integration of the TMD into the membrane was irreversible once the nascent chain reached a critical length. When 106mer intermediates were first assembled, isolated, and then incubated post-translationally with CT8, enhanced crosslinks of the TMD to Sec61α were observed (**Figure 3-9**). By contrast, when longer 126mer intermediates were first assembled and then incubated post-translationally with CT8, no enhanced crosslinking of the TMD to Sec61 was observed, indicating the position of the integrated TMD could not be "reversed" by CT8 (**Figure 3-9**). These data suggest that at the 126mer stage of translocation, the TMD does not dynamically equilibrate between the membrane and Sec61 environments, and that CT8 therefore blocks a decisive step in TNFα biogenesis.
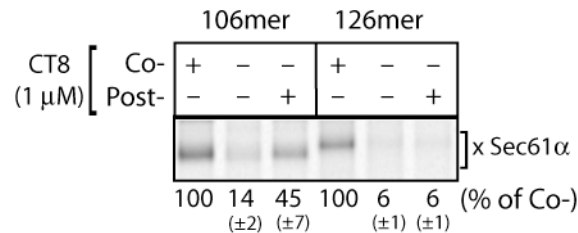
Figure 3-9. The TMD reaches a "point of no return".
Translocation intermediates of the indicated length were either cotranslationally assembled with CT8 (Co-), or were first assembled in the absence of CT8, isolated by sedimentation, and incubated post-translationally with CT8 (Post-), followed by BMH crosslinking. The intensity of crosslinks between the nascent chain and Sec61α ($\times$ Sec61α) were quantified by phosphorimaging and normalized to the Co- sample. Quantified data represent the mean +/- standard deviation of three independent experiments.

3.7 The pre-integrated TMD docks to Sec61α as an α-helix

The prolonged crosslinks between the TMD and Sec61 suggested CT8 may stabilize a structured intermediate. To test this possibility, and to probe the architecture of this

intermediate, we analyzed BMH crosslinking reactions of engineered TNFα constructs containing single cysteine residues at multiple positions of the TMD and flanking regions (**Figure 3-10**). For comparison, the same experiment was performed in the absence of CT8. Notably, no single mutation significantly affected sensitivity to CT8 (**Table 2-1**). In the absence of CT8, the TMD of 126mers showed no crosslinks to Sec61, consistent with a membrane-integrated conformation (**Figure 3-10 B** and **C**). By contrast, in the presence of CT8, the TMD showed crosslinks to Sec61α at a.a. positions 35, 38, 42, 45, and 49, which were separated by three to four positions of weaker crosslinking. This periodic (i – i+4) crosslinking profile suggests the TMD adopts an α-helical structure. Consistent with this notion, the positions of peak crosslinking closely mapped to a single face of an α-helical model of the TMD (**Figure 3-10 C, inset**). Furthermore, introduction of a proline mutation in the center of the TMD (V41P), which is predicted to destabilize α-helical structure, abolished the periodic pattern without significantly affecting RNC targeting to the membrane (as evidenced by robust TMD crosslinks to Sec61β, **Figure 3-11** and data not shown). The periodic crosslinking pattern occurred nearly independent of nascent chain length for chains 96 a.a. or longer (**Figure 3-11**), suggesting the TMD stably docks to Sec61α in an α-helical conformation shortly after RNC targeting. Interestingly, the periodic crosslinking pattern was not present at any chain length in the absence of CT8 (data not shown), which may reflect the intrinsically dynamic nature of the TMD integration reaction.
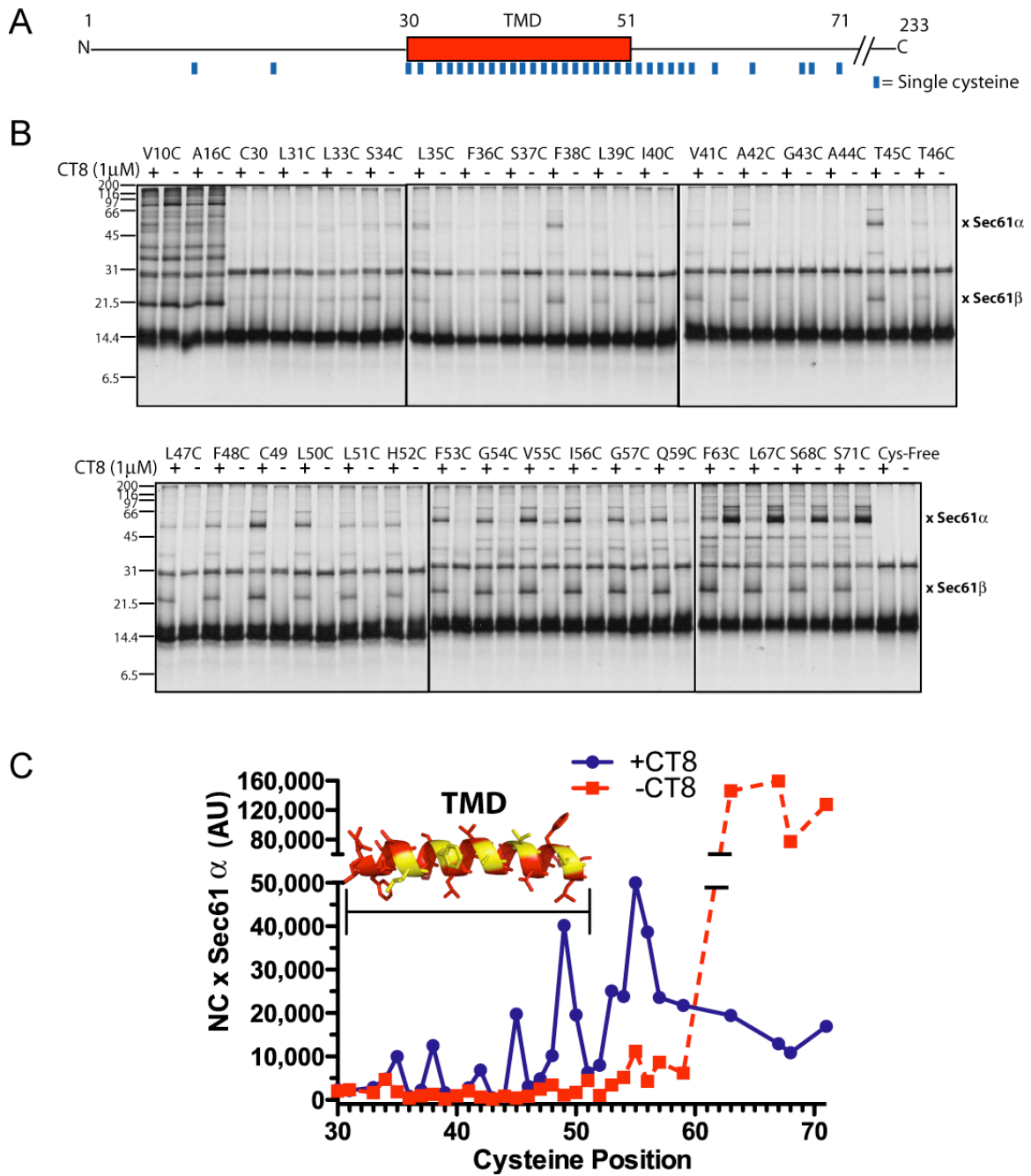
Figure 3-10. The pre-integrated TMD docks to Sec61α as an α-helix.
(A) Primary structure of TNFα and the positions of single cysteine mutations (blue dashes). (B) BMH crosslinking of 126mers containing single cysteines at the positions indicated in part (A). (C) Crosslinking profiles of 126mers. Crosslinks were quantitated by phosphorimaging from gels shown in (B). The inset shows an α-helical model of the TMD (red) with positions of peak crosslinks to Sec61α (× Sec61α) colored in yellow.

TNFα construct	% protected at 1 μM CT8
Wild type	12%
C49A	16%
C30A	28%
C49A/C30A (Cysteine-Free)	25%
C30A/T45L/T46L	90%
L33C/C49A/C30A	25%
S34C/C49A/C30A	61%
L35C/C49A/C30A	23%
F36C/C49A/C30A	26%
S37C/C49A/C30A	55%
F38C/C49A/C30A	22%
L39C/C49A/C30A	34%
I40C/C49A/C30A	30%
V41C/C49A/C30A	31%
A42C/C49A/C30A	32%
G43C/C49A/C30A	56%
A44C/C49A/C30A	29%
T45C/C49A/C30A	39%
T46C/C49A/C30A	63%
L47C/C49A/C30A	41%
F48C/C49A/C30A	18%

Table 3-1. CT8-sensitivity of full-length single cysteine TNFα mutants measured in the PK-protection assay at a single dose of CT8.

BMH crosslinking also revealed the orientation the nascent chain with respect to the membrane. In both the presence and absence of CT8, cysteines at positions 10 or 16 crosslinked many proteins including Sec61β (**Figure 3-10 B**), indicating the N-terminus is exposed to the tail of Sec61β and is therefore localized on the cytosolic side of the membrane. This result strongly suggests that the TMD does not adopt an inverted orientation (i.e. N_{lumen}/C_{cyto}) in the presence of CT8. For cysteines C-terminal to the TMD, strong crosslinks to Sec61α were observed in the absence of CT8, without concomitant crosslinks to Sec61β (**Figure 3-10**). These cysteines most likely lie in the aqueous pore of Sec61α but are shielded from crosslinking with Sec61β by the RNC-

Sec61 junction.[28,29] Conversely, these same cysteines showed strong crosslinks to Sec61β and weak crosslinks to Sec61α in the presence of CT8. Thus, the C-terminus of TNFα is blocked from insertion into the ER lumen and is instead exposed to the cytosol, as depicted in the cartoon model (**Figure 3-12**). Taken together, these data strongly suggest that the TMD stably docks to Sec61α in an on-pathway conformation in the presence of CT8. This docked conformation may represent a kinetic intermediate that occurs during the normal TMD integration reaction.
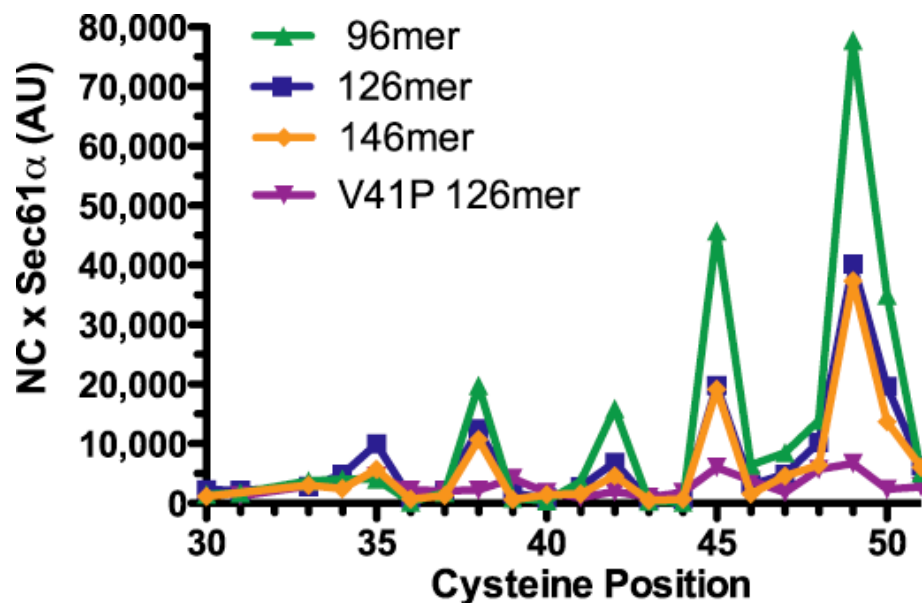
Figure 3-11. BMH crosslinking profile overlay.
TNFα 96mer, 126mer, 146mer, or 126mers containing the V41P mutation in the TMD were analyzed by BMH crosslinking as in Figure 3-10. Quantified data represents the intensity of the crosslink between the nascent chain and Sec61α in the presence of CT8. A control construct (C49 126mer) was included in each experiment to allow direct comparison of crosslinking intensities between different experiments.
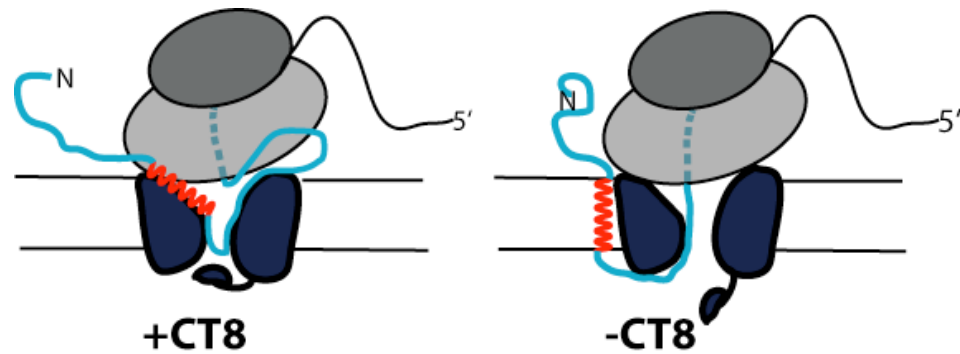
Figure 3-12. Cartoon model of the CT8-stabilized and uninhibited TNFα 126mer intermediates.

3.8 The TMD docks near the cytosolic face of the lateral gate

We next sought to map the position of the docked TMD in Sec61α using bis-maleimide crosslinking. Toward this end, we set up a heterologous expression system for preparation of recombinant Sec61α that contained cysteines at defined positions. This work was performed with the assistance of Dr. Ville Paavilainen. Sec61α and Sec61γ were co-expressed in Sf21 insect cells and found to be functional in several independent lines of experimentation. First, both Sec61α and Sec61γ were purified in a microsomal fraction. Second, Sec61α and Sec61γ were efficiently co-immunoprecipitated from a detergent extract, indicating they form a stable complex (**Figure 3-13**). Third, Sec61α was properly folded as evidenced by crosslinking with the photo-affinity probe CT7 (**Figure 3-14**), which was ~35–50 % as efficient as crosslinking to native Sec61α (data not shown). Lastly, we observed CT8-dependent BMH crosslinks between TNFα RNCs and Sec61α (**Figure 3-15**). Thus the Sec61α/γ complex was properly folded and functional in RNC targeting. We did note that integration of the TMD was deficient with the recombinant complex (data not shown), possibly due to the absence of Sec61β, which was expressed at sub-stoichiometric levels in preliminary experiments, and was

previously shown to improve the efficiency of cotranslational translocation *in vitro*.[30]

Despite this defect, the recombinant Sec61α/γ complex was a tractable system to map the

location of the docked TMD.
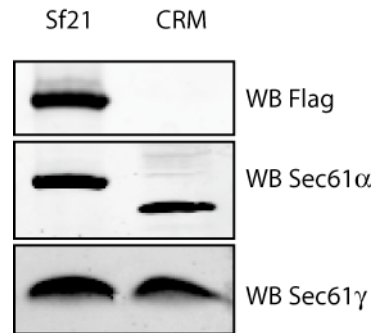
Figure 3-13. Recombinant Sec61α and Sec61γ form a stable complex in detergent.
Sf21 microsomes containing wild-type 3x-Flag S61α/γ complexes were solubilized with 1% Deoxy BigChap (DBC) for 3.5 hr at 4°C. The reaction was then centrifuged at 50,000 rpm in a TLA100 rotor at 4°C for 10 min to remove insoluble material. The supernatant was diluted with IP Buffer (50 mM Hepes, 100 mM NaCl, 0.2% DBC, pH 7.8) and subjected to immunoprecipitation using anti-Flag affinity matrix. Samples (Sf21) were analyzed by Western blotting (WB) next to a sample of canine microsomal ER membranes (CRM).

Figure 3-14. Photo-affinity labeling of recombinant Sec61 complex.
Left, Sf21 microsomal membranes containing 3x-Flag Sec61α/Sec61γ were incubated with CT7 (50 nM) in the presence or absence of CT9 (10 μM, a photo-stable competitor), photolyzed (hν) and subjected to click

chemistry and in-gel fluorescent scanning. *Right,* photo-crosslinking reaction were immunoprecipitated (IP) under denaturing conditions with anti-Flag affinity matrix or anti-HA affinity matrix and analyzed by in-gel fluorescent scanning and Western blotting (WB).
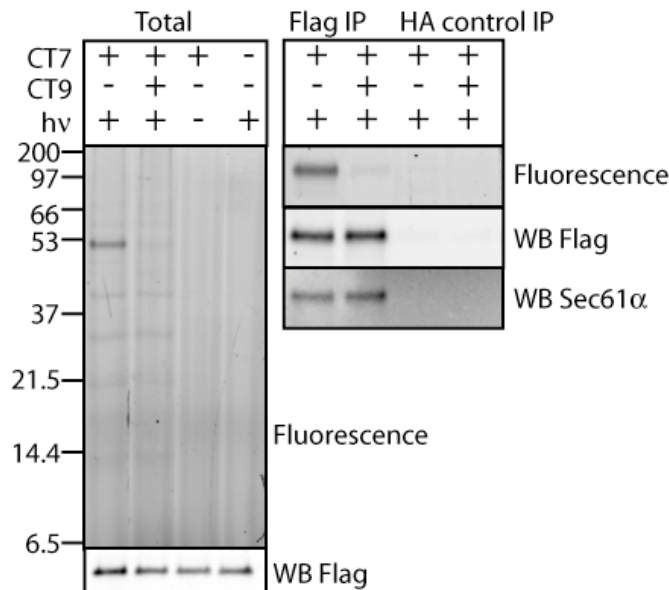
To determine which of the eight native cysteines in Sec61α crosslinked to the TMD, we individually mutated each cysteine to an alanine or serine. All mutants expressed at levels similar to the wild type and were properly folded in the membrane as evidenced by crosslinking to CT7 (**Figure 3-15 A**). Strikingly, a single point mutation (C13A) in Sec61α completely abolished crosslinks to C49 in the TMD in the presence of CT8 (**Figure 3-15 B**). C13 is predicted to lie near the N-terminus of Sec61α in a short α-helix that lies parallel to the cytosolic face of the ER membrane (**Figure 3-16**).
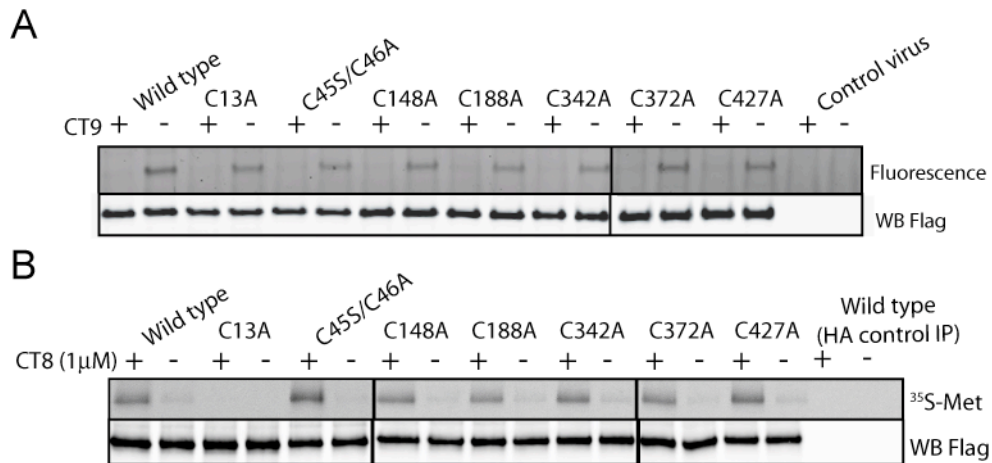
Figure 3-15. C13 of Sec61α crosslinks the TMD in the presence of CT8.
(A) Photo-affinity labeling with different Sec61α mutants was performed as in Figure 3-14. Control virus lacked the Sec61 genes. (B) Wild-type or mutant Sec61α/γ complexes were assembled with C49 126mers and crosslinked with BMH. Sec61α was enriched by Flag IP and analyzed by autoradiography (^{35}S-Met) and Western blotting (WB). A control IP used anti HA-affinity resin.

To further refine the location of the docked TMD, we next mutated non-conserved residues throughout the cytoplasmic vestibule of Sec61α to cysteine in the background of the C13A mutation. To achieve greater spatial resolution in mapping, we used bis-

maleimido-ethane (BMOE), the shortest available bis-maleimide crosslinker (8 Å crosslinker length), instead of the longer BMH reagent (13 Å crosslinker length). Compared to the longer BMH crosslinker, BMOE produced weak, nearly undetectable crosslinks to C13 of wild type Sec61α (**Figure 3-16 A**) indicating crosslinks were strongly dependent on the length of the crosslinker. Most cysteine mutants displayed weak to undetectable crosslinks to the TMD. However, strong crosslinks were observed for cysteine substituted at G88, M91, A95, and S383 (**Figure 3-16**). Three of these mutations (G88C, M91C, A95C) lie on TMD 2b, proposed to constitute part of the lateral gate of Sec61α. S383C lies at the cytosolic tip of TMD 8, which is also proposed to be part of the lateral gate (**Figure 3-16**). Thus, these data indicate that the TMD of TNFα docks near the cytosolic face of the lateral gate in the presence of CT8. These data also provide the first direct experimental evidence that a TMD of a nascent membrane protein can dock to the lateral gate in Sec61, presumably just prior to integrating into the membrane.
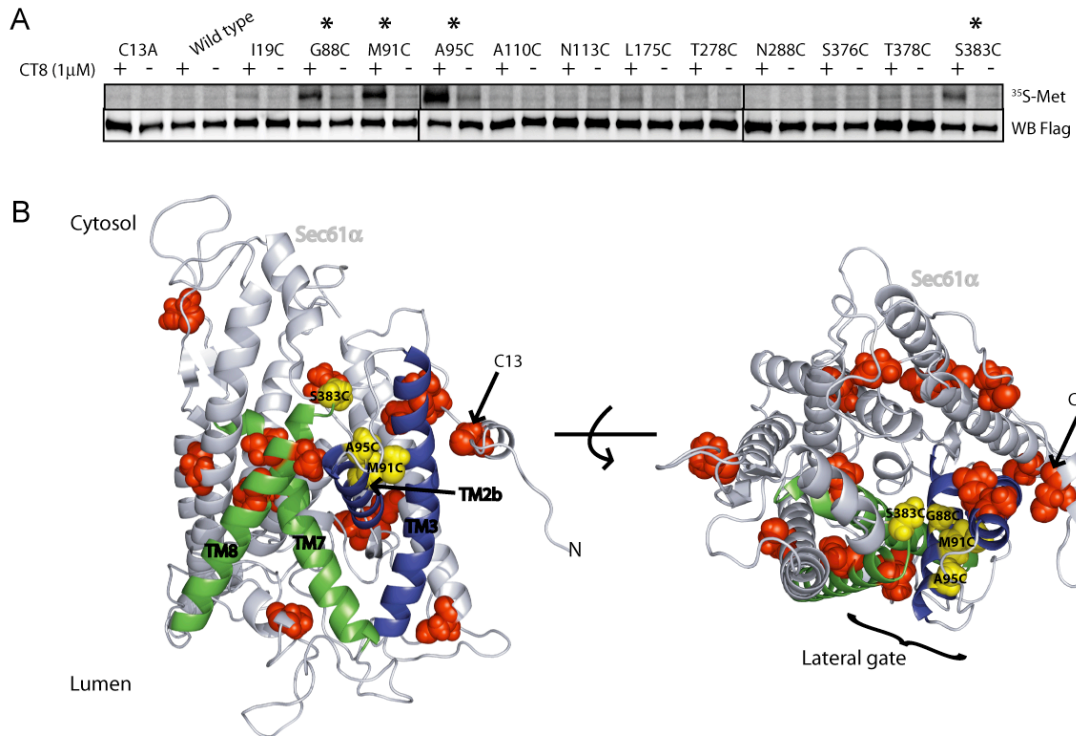
Figure 3-16. The TMD docks near the cytosolic face of the lateral gate.
(A) Wild type or mutant Sec61α/γ complexes were assembled with C49 126mers and treated with BMOE. Reactions were analyzed as in Figure 3-15. Mutants showing strong crosslinks to the TMD are marked with an asterisk (*). (B) Homology model of mammalian Sec61α (adapted from ref. 31). Transmembrane domains that constitute the lateral gate are highlighted blue (TMD 2b and TMD 3) and green (TMD 7 and TMD 8). Mutated residues are displayed in space-filling mode; those showing strong crosslinks to the TMD (* in part A) are colored yellow, while others are colored red.

3.9 α-helical propensity of the TMD influences sensitivity to CT8

CTs were previously shown to block translocation through Sec61 in a substrate-selective manner based on the amino acid composition of the signal sequence.[20,21] By analogy, mutations in the TMD might also modulate sensitivity to CT8. We reasoned that identification of such mutants could yield insight into how the primary sequence of the TMD influences its progression into the membrane. Since the TMD was recognized in an α-helical conformation, we suspected that biophysical features of the α-helix such as its shape, stability, or flexibility might influence its interactions with Sec61 and thereby

influence its integration efficiency. Proline strongly influences the structure and stability of an α-helix when placed in the central or C-terminal region.[32] Therefore, to test the hypothesis that secondary structure of the TMD influences sensitivity to CT8, we scanned a proline residue from the N- to C-terminus of the TMD and measured the sensitivity of each mutant toward CT8 using a protease protection assay with full-length TNFα constructs.

Interestingly, mutants that contained a proline near the N-terminus of the TMD were ~2–3 fold more resistant to CT8 compared with wild-type TNFα (**Figure 3-17**). By contrast, as the proline residue was positioned progressively closer to the middle of the TMD, mutants became progressively more sensitive to CT8. The most CT8-sensitive mutant contained the proline in the center of the TMD at position V41, where the proline was predicted to most strongly destabilize the α-helix. As the proline was then moved toward the C-terminal boundary of the TMD, mutants became progressively more resistant to CT8 and eventually appeared similar to wild type. These position-specific effects of proline on CT8 IC_{50} strongly suggests that the secondary structure of the TMD at least partially controls integration efficiency in the presence of CT8. Notably, the BMH crosslinking profile of the V41P mutant lacked the strong helical periodicity observed for the more resistant wild-type construct (**Figure 3-11**), indicating this mutation also crippled a stable interaction between the TMD and Sec61α. Therefore, these data also imply that stable TMD docking to Sec61α is necessary but not sufficient for membrane integration.
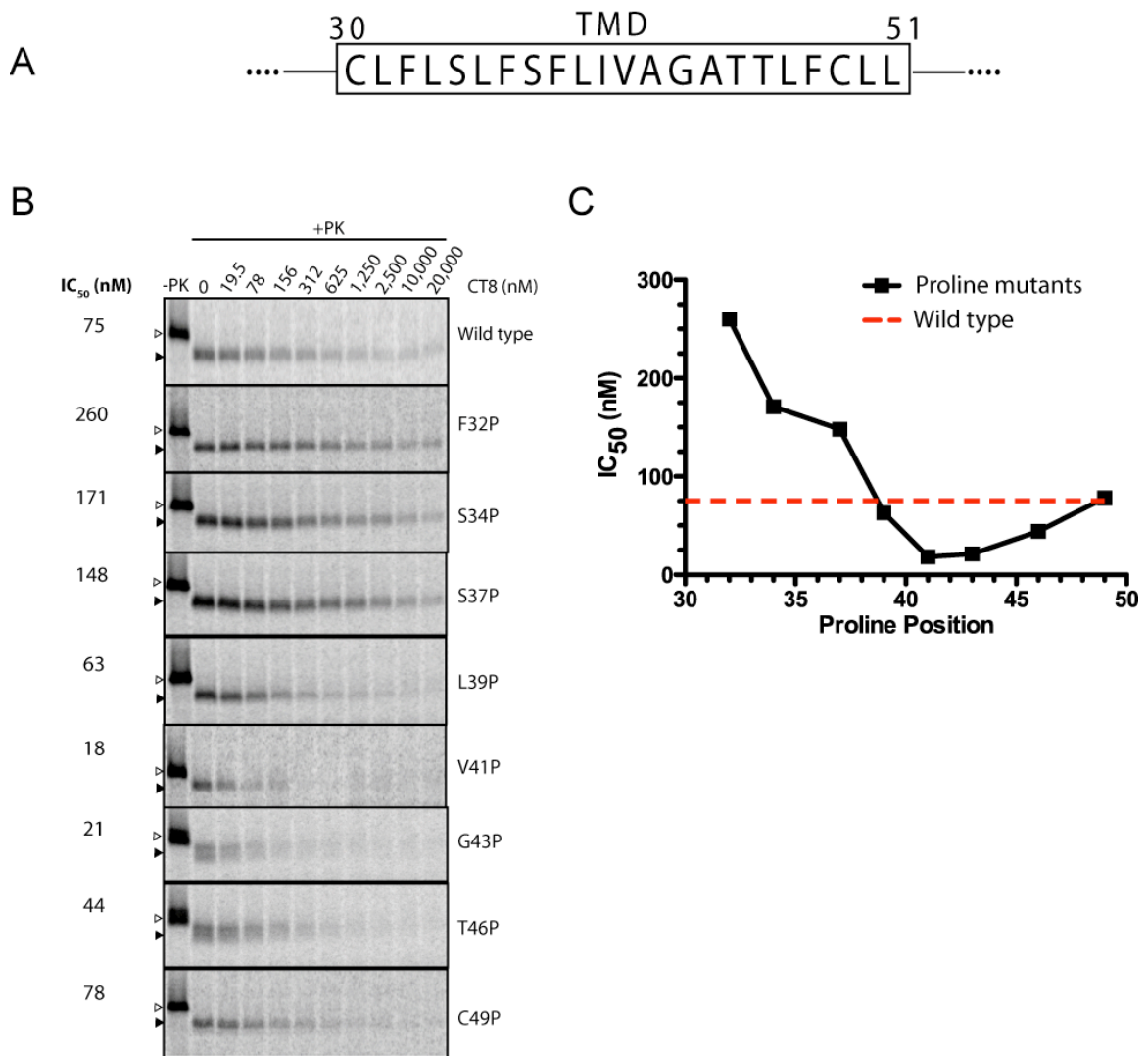
Figure 3-17. The α-helical stability of the TMD influences sensitivity to CT8.
(A) Primary sequence of the TMD in TNFα. (B) Protease K (PK) protection assays of wild-type TNFα and mutants containing proline mutations in the TMD. Full-length TNFα and the protected fragment are indicated as open and closed triangles, respectively. The IC_{50} was determined by quantifying the intensity of the protected fragment (after normalizing to the DMSO control) and fitting the dose-response to a three parameter equation. (C) IC_{50} data from (B) were plotted against the position of the proline mutation in the TMD.

3.10 TMD hydrophobicity loosely correlates with CT8-sensitivity

Previously, it was shown that the integration efficiency of model TMDs quantitatively correlated with their overall hydrophobicity.[8] This correlation was interpreted to mean that interactions between the TMD and membrane lipids provides the primary driving

force for TMD integration. We therefore next tested if the hydrophobicity of the TMD in TNFα correlated with sensitivity to CT8. Strikingly, double mutation of T45 and T46 in the TMD to leucine (T45L/T46L) resulted in a >10-fold increase in resistance to CT8, while each single mutant had a smaller effect (**Figure 3-18 A**, and **Table 3-2**). Likewise, double mutation of S34 and S37 to leucine (S34L/S37L) also increased resistance, albeit only 3–4-fold (**Figure 3-18**). In this case, however, either mutation alone had a similar effect on CT8-sensitivity (**Table 3-2**). Combination of all four mutations (T45L/T46L/S34L/S37L) yielded a hyper-resistant mutant where the measured IC_{50} approached the resolution limit of the assay. These data indicate that TMD integration in the presence of CT8 is strongly favored by the presence of hydrophobic amino acids in the TMD, just as hydrophobicity of the TMD was previously shown to favor TMD integration.[8,9]
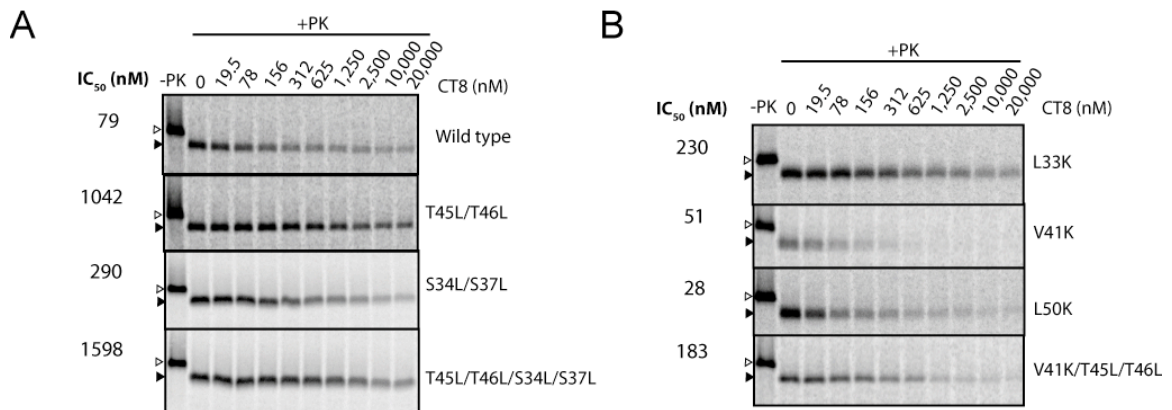

Figure 3-18. Hydrophobicity of the TMD influences CT8-sensitivity.
(A) PK protection assays of TNFα mutants where polar residues in the TMD were mutated to leucine. The positions of the full length and protease-protected fragment are indicated (open and closed triangles, respectively). (B) PK protection assays of TNFα mutants where nonpolar residues of the TMD were mutated to lysine.

Based on these observations, we predicted that introduction of a charged lysine residue into the TMD would inhibit the integration reaction in the presence of CT8. While this held true for several mutants (V41K, L50K), other lysine mutants (L31K, L33K) were unexpectedly less sensitive to CT8 than wild-type TNFα (**Figure 3-18**), implying a more complex relationship between TMD hydrophobicity and integration efficiency than first suspected. Consistent with this idea, when the calculated hydrophobicities (ΔG_{pred}) of a 30-member collection of TNFα mutants were plotted against the natural logarithm (LN) of the measured IC_{50} for each mutant, only a weak correlation was observed (**Figure 3-19**). These data indicate that while hydrophobicity plays a significant role in determining sensitivity to CT8, other factors such as α-helical stability, the presence of charged residues near the N-terminus, and most likely other biophysical features of the TMD appear to also be important.
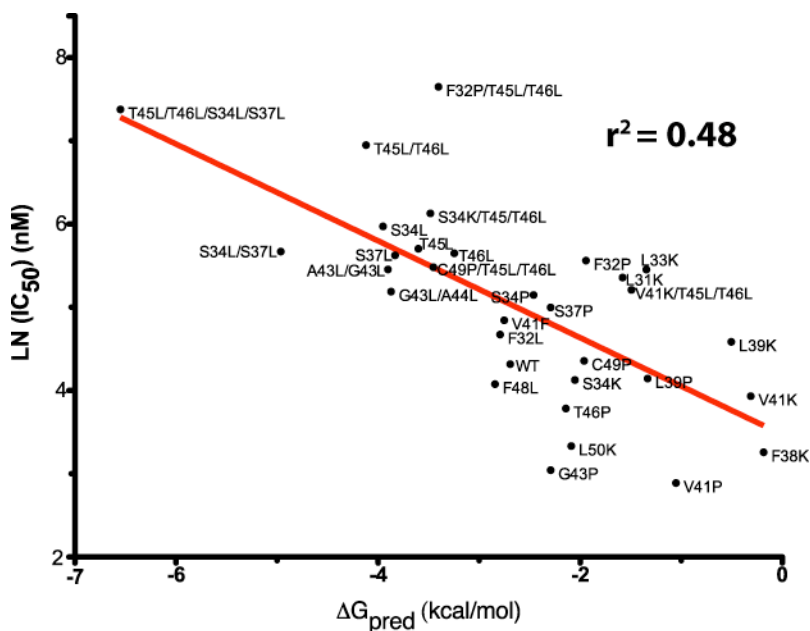

Figure 3-19. Correlation between the predicted free energy of TMD integration and CT8-sensitivity. The calculated hydrophobicity of the TMD (ΔG_{pred}) was based on the model from ref 8. Data were fitted to a straight line.

TNFα construct	ΔG_{pred}	IC$_{50}$ (nM)	Ln(IC$_{50}$)
Wild type	-2.69	75	4.32
S34L	-3.95	392	5.97
S37L	-3.83	277	5.62
G43L/A44L	-3.87	179	5.19
A43L/G43L	-3.90	234	5.46
V41K	-0.31	51	3.93
S34K	-2.05	62	4.13
F32L	-2.79	107	4.67
V41F	-2.75	127	4.84
F48L	-2.84	59	4.08
V41P	-1.05	18	2.89
C49P	-1.96	78	4.36
T45L/T46L	-4.12	1042	6.95
F32P/T45L/T46L	-3.40	2096	7.65
C49P/T45L/T46L	-3.45	240	5.48
V41P/T45L/T46L	-2.46	172	5.15
F32P	-1.94	260	5.56
V41K/T45L/T46L	-1.49	183	5.21
S34K/T45/T46L	-3.48	459	6.13
L31K	-1.58	212	5.36
L33K	-1.34	230	5.44
F38K	-0.18	26	3.26
L39K	-0.50	98	4.58
S34P	-2.35	171	5.14
S37P	-2.29	148	5.00
L39P	-1.33	69	4.14
G43P	-2.29	21	3.04
T46P	-2.14	44	3.78
T45L	-3.60	300	5.70
T46L	-3.24	284	5.65
S34L/S37L	-4.96	290	5.67
T45L/T46L/S34L/S37L	-6.55	1598	7.38
L50K	-2.09	28	3.33

Table 3-2. CT8-sensitivity of full-length TNFα constructs measured in PK protection assays.

3.11 The T45L/T46L mutant passes through the CT8-stabilized pre-integration intermediate

It remained to be tested if CT8-resistant TMDs passed through the same pre-integrated intermediate that was stabilized for wild-type TNFα. To test this possibility, we probed the environment of C49 in the TMD of the T45L/T46L mutant, which was >10-fold more resistant to CT8 than wild-type TNFα. Crosslinks between the mutant TMD and Sec61α were observed at a nascent chain length of 96 a.a., which then disappeared as the nascent chain was further extended, indicating a step-wise integration pathway in the absence of CT8 that was similar to the wild-type TMD (**Figure 3-20**). Also similar to wild type, the TMD of the T45L/T46L mutant docked as an α-helix to Sec61α in the presence of CT8 for nascent chains of 96 a.a. (**Figure 3-21**). However, upon further chain elongation, the mutant TMD efficiently progressed through the CT8-stabilized intermediate and integrated into the membrane (**Figure 3-20** and **Figure 3-22**). These data indicate that both CT8-sensitive and CT8-resistant TMDs can pass through a similar pre-integrated intermediate where the TMD is bound to Sec61α as an α-helix. This indicates that direct contacts between the TMD and the lateral gate of Sec61α precede TMD transfer into the membrane.
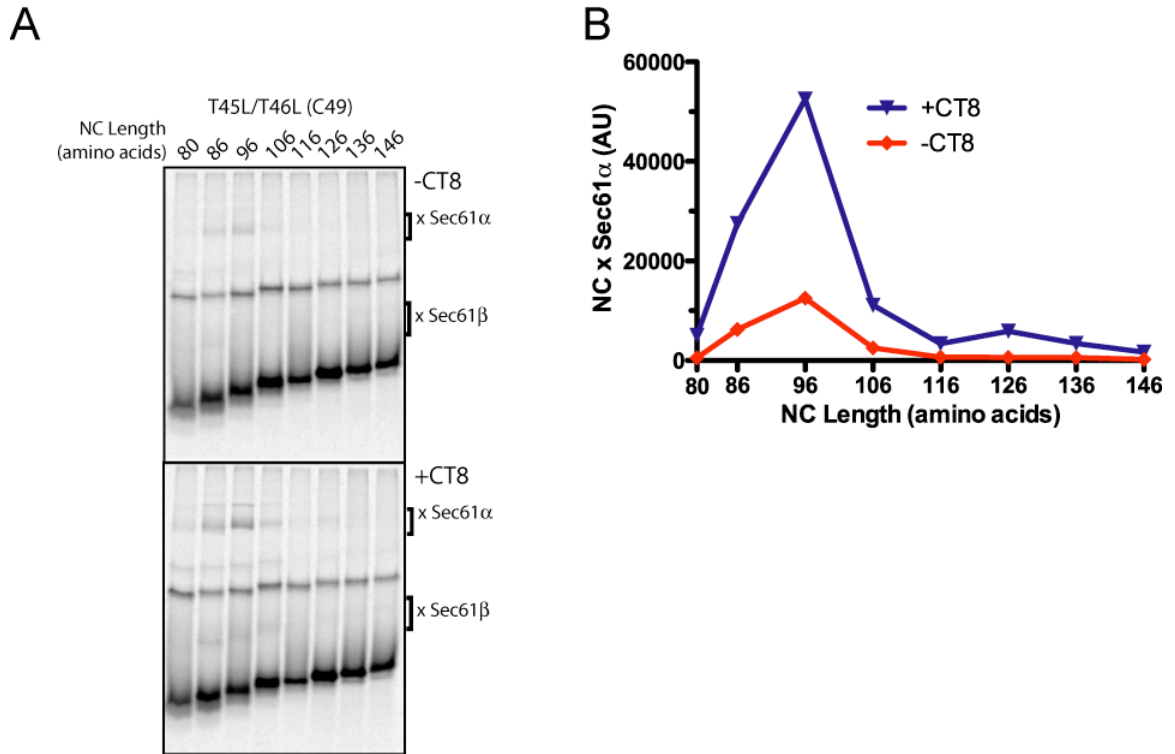
Figure 3-20. The T45L/T46L TMD passed through the CT8-stabilized intermediate.
(A) BMH crosslinking of a truncated series of T45L/T46L intermediates containing a single cysteine at position 49 of the TMD. (B) Quantitation of the data from (A) was performed by phosphorimaging.

94
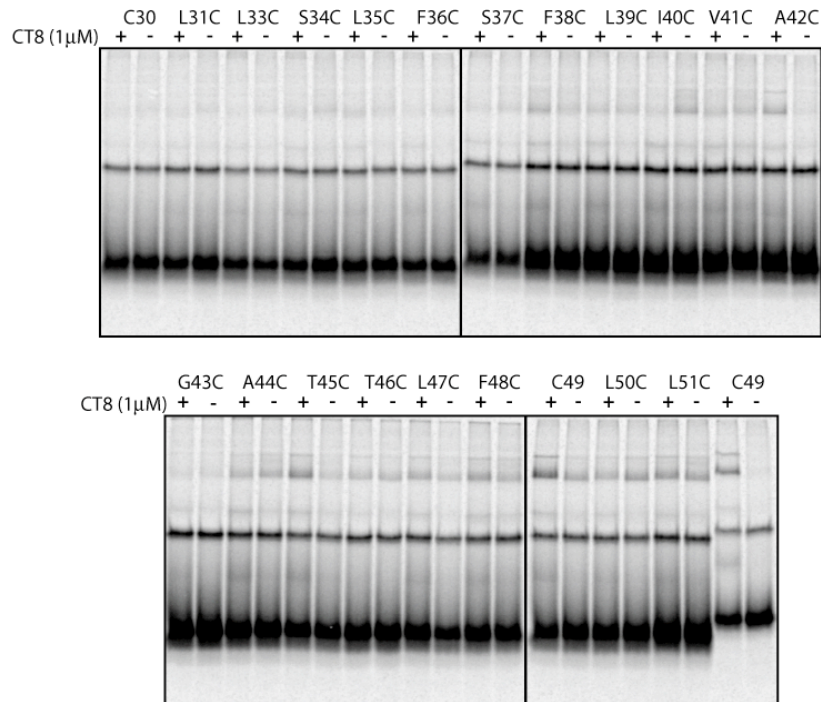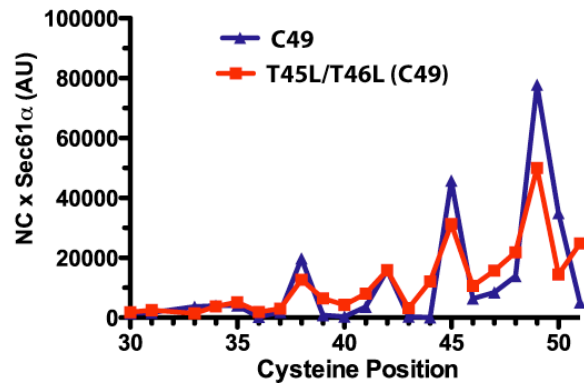
Figure 3-21. The T45L/T46L TMD docks as an α-helix to Sec61α.
(A) BMH crosslinking reactions of T45L/T46L 96mers in the presence and absence of CT8. (B) Overlay of the BMH crosslinking profiles from cysteine scan experiments with wild type (C49) and T45L/T46L 96mers in the presence of CT8.
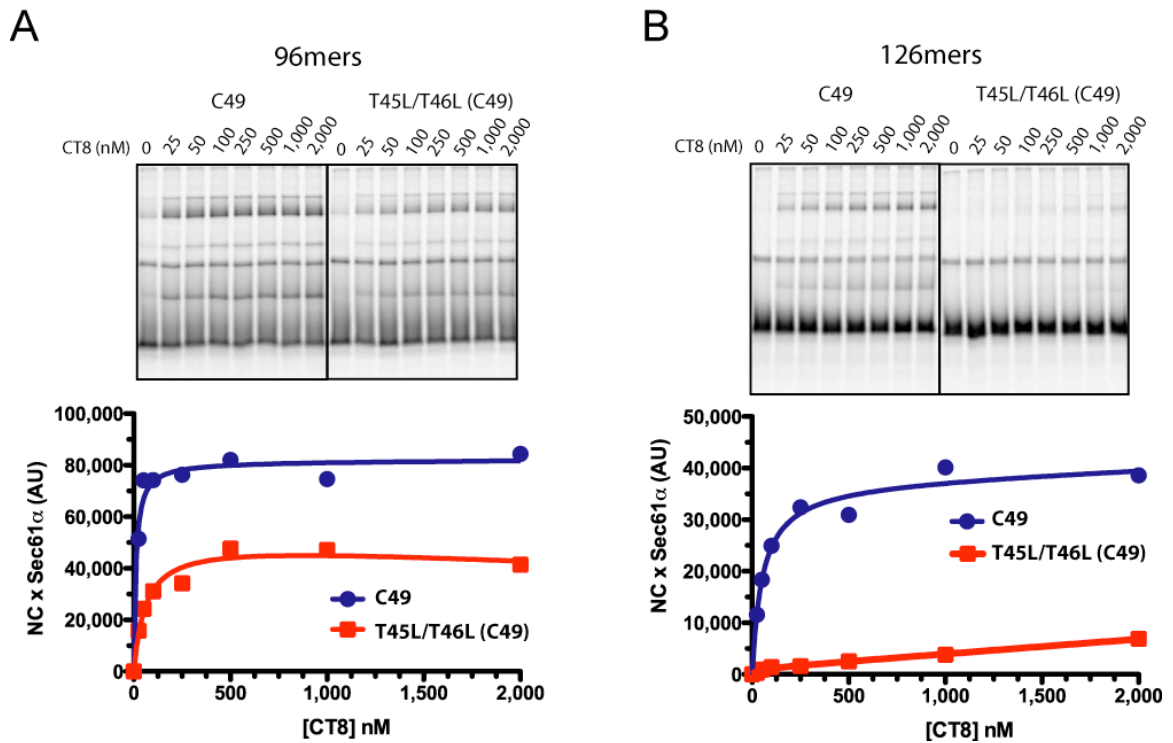
Figure 3-22. Nascent chain elongation provides a driving force for TMD integration.
(A) *Top,* BMH crosslinking reactions of wild-type or T45L/T46L 96mers in the presence of increasing concentrations of CT8. *Bottom,* quantitation of the data normalized to the DMSO control. (B) Same as in (A) but with 126mers.

3.12 Discussion

In this study, we exploited CT8, a substrate-selective inhibitor of membrane protein biogenesis, to dissect the mechanism of Sec61-mediated TMD integration. We found that CT8 stabilized a pre-integrated intermediate, providing a unique opportunity to analyze the mechanism by which the TMD transitions from the Sec61 channel into the membrane. The CT8-stabilized TMD adopted an α-helix that docked to Sec61α near the cytosolic side of the lateral gate, apparently poised for integration into the membrane. The α-helical propensity and hydrophobicity of the TMD, as well as positive charges flanking the N-terminus of the TMD, influenced its ability progress through this

96

stabilized intermediate and integrate into the membrane. These results indicate that TMD integration relies on critical interactions between the TMD and the lateral gate of Sec61α.

One critical issue raised in this study is whether the pre-integrated intermediate observed in the presence of CT8 also occurs during normal TMD integration in the absence of CT8. We believe this is most likely the case, based on several lines of evidence. First, we observed a crosslink between the TMD and Sec61α in the absence of CT8 for 96mers (**Figure 3-5**), which was a hallmark of the CT8-stabilized intermediate. Second, we found that a CT8-resistant TMD (T45L/T46L) also formed an α-helix that docked to Sec61α in the presence of CT8 as a 96mer (**Figure 3-21**), yet efficiently integrated into the membrane once it had elongated to a 126mer, indicating that TMD docking can occur along a productive integration pathway. Finally, we found that the TMD docked in close proximity to the lateral gate of Sec61α (**Figure 3-16**), previously proposed to be a possible site of TMD passage from Sec61 into the membrane.[12] The CT8-stabilized pre-integrated intermediate therefore represents an on-pathway intermediate which may also occur during normal TMD integration.

Unexpectedly, we did not observe a periodic crosslinking pattern of the TMD in the absence of CT8 (data not shown), which was characteristic of the CT8-stabilized pre-integrated intermediate. This may reflect the conformational flexibility of the TMD and Sec61 in the absence of CT8. CT8 appears to stabilize an intrinsically unstable docked conformation of the TMD which may occur as a transient kinetic intermediate during normal TMD integration.

It is not entirely clear how CT8 stabilizes this intermediate. We previously showed that the photo-affinity probe CT7 binds to Sec61α in the absence of an RNC,[22] suggesting it does not directly interact with the signal sequence or TMD. Consistent with this idea, highly divergent signal sequences were shown to be similarly sensitive to the action of CT8.[21] Based on these observation, we suspect that CT8 stabilizes a closed conformation of Sec61 by binding to a lipid-exposed region of the lateral gate, the plug domain, or both, and thereby blocks a TMD-dependent conformational change of Sec61α. This conformational change is most likely identical to "lateral gating" and involves separation of the helices in Sec61α which form the lateral gate to allow direct access of the TMD to the lipid bilayer.

Given the substrate-selectivity of CT8,[23] this model of TMD-directed lateral gating implies that different TMDs are intrinsically better or worse at carrying out this process. Consistent with this idea, N-terminal signal sequences were previously shown to vary greatly in the ability to initiate transport across the membrane after RNC targeting to Sec61.[29,33] Given that the TMD and Sec61α form a tight complex in the presence of CT8, we propose that direct interactions between amino acid side chains of the TMD and Sec61α mediate the lateral gating step of integration (**Figure 3-23**). The efficiency of the TMD/Sec61α interactions may therefore directly control the efficiency of TMD integration. For example, a rigid α-helical conformation may be required for the TMD to effectively dock against the helices of the lateral gate prior to gating and progression into the membrane. This model is supported by our observation that a helix-breaking proline

mutation (V41P) strongly inhibited TMD integration (**Figure 3-17**) and prevented stable TMD docking (**Figure 3-11**).
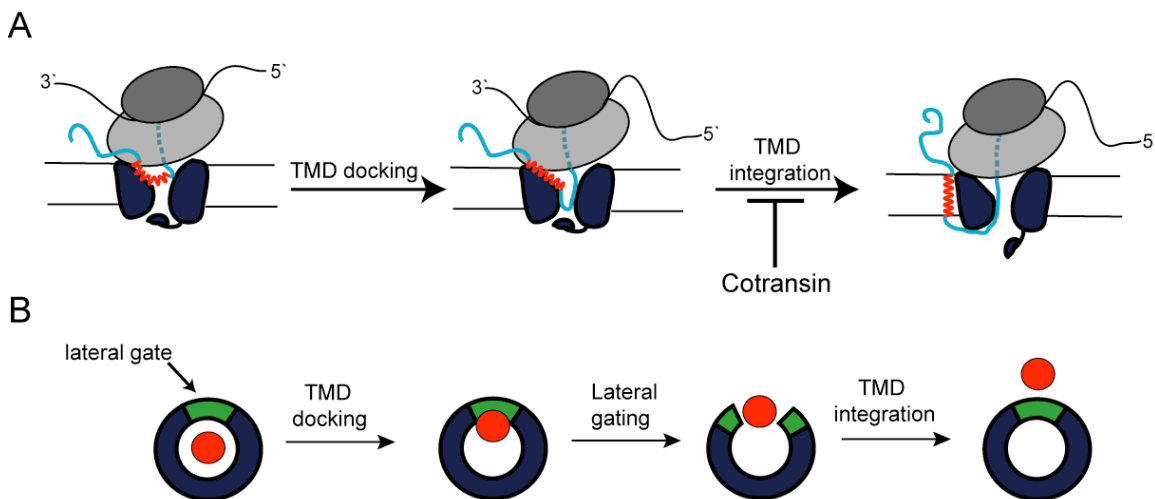

Figure 3-23. Proposed mechanism of TMD integration via Sec61.
The TMD integration reaction viewed from within the plane of the membrane (A) and from the cytosol (B). Following targeting to Sec61, the TMD docks to the lateral gate of Sec61α. Upon further nascent chain elongation, the TMD mediates "lateral gating", or the opening of the lateral gate toward the lipid membrane, followed by insertion of the TMD into the lipid bilayer. Different TMDs appear to differ in their ability to carry out the lateral gating step.

TMD-directed lateral gating (**Figure 3-23**) differs from previous models proposed for integration of TMDs. In these models, the lateral gate was proposed to fluctuate between open and closed states, allowing the TMD to thermodynamically equilibrate between the aqueous pore of Sec61 and the hydrophobic lipid bilayer. This model accounts for the strong correlation observed between hydrophobicity and integration efficiency of model TMDs.[8,9] However, we found that integration of the TNFα TMD was an irreversible event (**Figure 3-9**), since addition of CT8 after a critical nascent chain length could not trap the TMD in the cytosolic binding site. Furthermore, while hydrophobic amino acids favored TMD integration in the presence of CT8 (**Figure 3-18**), the relationship between hydrophobicity and CT8-sensitivity was not strictly correlated (**Figure 3-19**). Thus, our

data suggest that substrate-specific contacts between the TMD and Sec61α may, in addition to TMD/lipid interactions, control the efficiency of TMD integration.

We also found that positive charges near the N-terminus of the TMD improved integration efficiency in the presence of CT8 (**Figure 3-18**). N-terminal charges have been previously shown to promote the type II orientation of TMDs.[34] Lysines positioned near the N-terminus of the TMD may improve the initial insertion of the TMD in a looped conformation into the Sec61 channel as previously proposed,[14] which may lead to further parting of the helices of the lateral gate and eventual TMD integration. In this view, hydrophobic amino acids may promote TMD integration after initial docking by stabilizing a partially open lateral gate that exposes the TMD to the lipid bilayer, as recently suggested from computational studies.[35] This would also be consistent with the fact that there is no obvious hydrophobic binding site in the cytoplasmic vestibule of the closed channel.[12]

To summarize, our results suggest that TMD integration relies on a step-wise process that involves direct contacts between the TMD and the lateral gate of Sec61α. Future studies will seek to more completely formulate the molecular "code" for integration of the TMD in the presence of CT8. Future studies will also seek to determine if CT8 blocks integration of internal TMDs or TMDs that adopt the type I orientation, and thereby provide a general tool for analyzing Sec61-mediated TMD integration. Based on its ability to stabilize the pre-integrated state, CT8 may also be a useful tool for structural

studies, which will ultimately be required to completely characterize the process of TMD integration.

3.13 Experimental procedures

Antibodies, proteins, and reagents: The following commercially available primary antibodies and antibody resins were used: anti-Flag M2 antibody and affinity matrix (Sigma), anti-HA affinity matrix (Roche), anti-ribosomal protein L28 (Santa Cruz Biotechnology), anti-Sec61γ (Proteintech Group), anti-Sec61α (Novus Biologics). The antibody directed against Sec61β was previously described.[36] Secondary antibodies were conjugated with HRP (Santa Cruz Biotechnology) or with infrared-dyes (LI-COR Biosciences). Preparations of rabbit reticulocyte lysate[24] and canine rough microsomes[37] have been previously described. Purified Sec61 complex and purified ribosomes were prepared as previously described.[38] CT7 and CT8 were prepared as previously described.[22] CT9 was prepared as previously described.[23] The sources of other reagents are noted as they are first described and were used without further purification.

Plasmid and DNA construction: Site-directed mutagenesis was performed using the Quickchange method (Stratagene) and all constructs were verified by DNA sequencing. The plasmid encoding human TNFα was previously described.[23] DNA templates encoding truncated TNFα constructs were prepared by PCR using a forward primer that contained a T7 promoter (bold) and a Kozak consensus sequence (underlined) followed by a region complementary to the 5' end of TNFα (5'-**GCCTAATACGACTCACTATAGG**<u>GAGACCATG</u>AGCACTGAAAGCATGATCCG

101

G-3'). The reverse primer annealed to various regions of the TNFα coding region and introduced three additional methionines at the C-terminus to improve detection of translated products by autoradiography. The indicated length of the nascent chain includes the three terminal methionines. A similar strategy was used for production of full-length TNFα DNA templates except the reverse primer included a stop codon. DNA templates encoding N-terminally tagged TNFα constructs were prepared by PCR using forward primers encoding either the 3x-Flag or 3x-HA epitopes immediately upstream of the TNFα start site. All PCR products were gel-purified (Qiagen) prior to *in vitro* transcription reactions.

Construction of the MultiBac baculovirus expression vector followed the strategic guidelines provided in Fitzgerald, et al., 2006.[39] Briefly, human Sec61α and Sec61γ genes were amplified by PCR using templates kindly provided by Professor Tom Rapoport (Harvard Medical School), with introduction of a 3x-Flag tag into the N-terminus of Sec61α. The Sec61α subunit was then cloned into the MCS-1 of vector pUCDM by In-Fusion cloning according to manufacturers instructions (Clontech). The Sec61γ subunit was cloned into SacI/HindIII sites (MCS-2) of vector pKL. The two vectors were then fused by Cre-recombination yielding a "master plasmid", which was used to transform DH10α MultiBac cells for preparation of the MultiBac expression vector. Site-directed mutagenesis to create Sec61α mutants was performed on the master plasmid. All constructs were verified by DNA sequencing.

SDS-PAGE, autoradiography and Western blotting: Unless otherwise noted, SDS-PAGE was performed with 12% Tris/Tricine polyacrylamide gels. Prior to autoradiography, gels were stained with Coomassie Brilliant Blue to confirm equal protein loading and dried under vacuum with a gel drier. For quantitative autoradiography, dried gels were exposed to a storage phosphorous screen (GE Healthcare), and imaged on a Typhoon 9400 phosphorimager (Amersham). The images were quantified using ImageJ software (NIH). Dose-response data were normalized to the DMSO control and fitted with a three-parameter equation using GraphPad Prism (GraphPad Software). For qualitative autoradiography, dried gels were exposed to Biomax MR film (Kodak).

For Western blotting, proteins were transferred to nitrocellulose membranes after SDS-PAGE. After blocking membranes with 5% milk in TBST, membranes were incubated with the appropriate primary antibodies at the following dilutions: 1:10,0000 (anti-Sec61α), 1:20,000 (anti-Sec61β), 1:500 (anti-Sec61γ), 1:20,000 (anti-Flag), 1:500 (anti-L28). Blotting for Sec61γ and L28 typically required overnight incubation at 4°C with the primary antibody. Following incubation with primary antibodies, membranes were washed and incubated with the appropriate HRP-conjugated secondary antibodies followed by chemiluminescent detection (GE Healthcare). Alternatively, blots were incubated with the appropriate infrared dye-conjugated secondary antibodies followed by imaging on an Odyssey infrared fluorescent scanner (LI-COR Biosciences).

Cell-free translation/translocation assays: Cell-free transcription, translation, translocation, and protease protection assays were done as previously described.[24] Briefly, DNA templates encoding full-length or truncated TNFα constructs were transcribed with T7 Polymerase (New England Biolabs) for 1 hr at 37°C and used immediately in the subsequent translation/translocation reactions. Translocation reactions were assembled at 0°C in the presence of CTs (added from a 100× stock in DMSO) or an equivalent volume of DMSO and initiated by transfer to a 32°C waterbath for 30 min. Unless otherwise indicated, reactions included ^{35}S-Methionine (Perkin Elmer, 2 μCi per 10 μL translation), and either canine pancreatic microsomes (CRM, 1 "equivalent" per 10 μL translation, as defined in Walter and Blobel, 1983)[37] or microsomal membranes derived from Sf21 insect cells that contained an equivalent amount of recombinant Sec61 complex. Following the translation, reactions were moved to ice for further processing.

To isolate ER-targeted integration intermediates, reactions were diluted with an equal volume of ice-cold high salt buffer (1M KAc, 10 mM Mg(Ac)$_2$, 50 mM Hepes, pH 7.8) and sedimented through a high salt sucrose cushion (0.5 M KAc, 0.5 M sucrose, 5 mM Mg(Ac)$_2$, 50 mM Hepes, pH 7.8) at 4°C in a TLA100 rotor (Beckman) for 10 min at 50,000 rpm. The membrane pellet was resuspended to the original volume in membrane buffer (100 mM KAc, 250 mM sucrose, 2 mM Mg(Ac)$_2$, 50 mM Hepes, pH 7.8) supplemented with 100 μM TCEP to prevent cysteine oxidation.

For puromycin release of nascent chains, puromycin was added to 2 mM, and samples were incubated at 37°C for 20 min. The puromycin stock solution (20 mM in water) was adjusted to pH ~7 before use.

For analysis of tRNA-associated nascent chains after protease protection, reactions were quenched as previously described[24] except dilution was into 10 volumes of boiling 1% SDS, 0.1 M Tris, pH 6.8, and samples were resolved on 4–12% NuPAGE Bis/Tris gels (Invitrogen) which run at neutral pH, thereby preserving the labile peptidyl-tRNA bond.

Bis-maleimide crosslinking: Targeted integration intermediates were isolated as described above and treated with 50 μM bis-maleimido-hexane (BMH, Pierce) or bis-maleimido-ethane (BMOE, Pierce) for 30 min at 0°C. To analyze total crosslinked products, reactions were quenched by addition of an equal volume of 1× Laemmli sample buffer (which contains a large molar excess of DTT), heated for 1 min at 95°C, and analyzed by SDS-PAGE and autoradiography. To immunoprecipitate (IP) proteins from the reactions, samples were quenched with 1 mM DTT for 10 min at 0°C, denatured with 1% SDS at 95°C for 1 min, and diluted 10-fold with IP buffer (1% Triton-X 100, 100 mM NaCl, 50 mM Hepes, pH 7.8). Anti-Flag affinity resin, anti-HA affinity resin, or protein A sepharose (GE Healthcare), along with the appropriate primary antibodies, were added and samples were rotated overnight (~12–16 hr) at 4°C. The resin was washed four times with IP buffer supplemented with 0.1% SDS, and bound proteins were eluted with 1× Laemmli sample buffer at 95°C for 1 min. Eluted material was analyzed by SDS-PAGE and autoradiography.

NEM-accessibility: Targeted integration intermediates from 20 μL translation reactions were divided into two equal portions (10 μL each) and incubated with either 200 μM N-ethyl-maleimide (NEM, Sigma-Aldrich) or an equal volume of DMSO for 1 hr at 0°C. NEM was quenched with 100 μL of quench buffer (5 mM DTT, 100 mM NaCl, 2 mM Mg(Ac)$_2$, 50 mM Hepes, pH 7.8) for 10 min at 0°C, followed by isolation of membranes by centrifugation at 4°C in a TLA100 rotor (Beckman) for 10 min at 70,000 rpm. The membrane pellet was then solubilized in a detergent-containing buffer (1% SDS, 250 μM TCEP, 50 mM Hepes, pH 7.8) and treated with an equal volume (10 μL) of 16 mM 5 kDa PEG-maleimide (Nektar), prepared in 50 mM Hepes (pH 7.8). Reactions were incubated at 32°C for 1 hr and quenched with 20 mM DTT for 20 min at 32°C. To completely hydrolyze the nascent chain-tRNA bond prior to SDS-PAGE, samples were treated with 100 μL of 200 mM Na$_2$CO$_3$ (pH 12) for 30 min at room temperature, followed by dilution with 1 mL of IP buffer (1% TX-100, 100 mM NaCl, 50 mM Hepes, pH 7.8) and precipitation with 10% trichloroacetic acid (TCA). Precipitated proteins were washed twice with ice-cold acetone, dissolved in 1× Laemmli sample buffer and resolved by SDS-PAGE. The quantities of unmodified and Peg-modified nascent chains were determined by phosphorimaging, and the fraction of total chains that were modified with PEG were normalized to the fraction modified in a control reaction that contained no NEM.

Photo-affinity labeling: Sf21 microsomes containing 50 nM Sec61 were treated with either 10 μM CT9[23] or DMSO for 30 min at 0°C, followed by incubation with 50 nM

CT7 for an additional 30 min at 0°C. Samples were photolyzed, and crosslinked proteins were detected by click chemistry, SDS-PAGE, and in-gel fluorescent scanning, as previously described.[22]

Insect cell culture, protein expression, and purification of Sf21 microsomes: Sf21 insect cells were grown and maintained in SF-900(II) serum free media (Gibco) at 27°C following standard protocols.[39] Cells were transfected with the MultiBac vector using Fugene HD transfection reagent according to the manufacturer instructions (Roche), and virus was propagated following published methods.[39] For expression of Sec61α/γ complexes, a 100 mL culture of cells at 0.5×10^6 cells/mL was infected with 2 mL of first generation virus (V_1), which results in immediate arrest of cell growth. Cells were harvested 48 hr after growth-arrest by sedimentation at $800 \times g$ for 5 min. The cell pellets were swelled in 20 mL hypotonic buffer (20 mM Hepes, pH 7.8) at 0°C for 20 min, and lysed with a microfluidizer (Emulsiflex-C5) at 15,000 psi for 10 min. The lysate was immediately adjusted to 100 mM KAc, 5 mM Mg(Ac)$_2$, 1 mM EDTA, and 1× EDTA-free protease inhibitor cocktail (Roche) and then clarified by centrifugation at $1000 \times g$ for 10 min. To isolate microsomal membranes, the clarified lysate was then centrifuged at 45,000 rpm in a type 70 Ti rotor (Beckman) for 1 hr at 4°C, and the microsomal pellet was resuspended with a glass dounce in 400 μL of buffer (50 mM Hepes, 250 mM sucrose, 1 mM CaCl$_2$, pH 7.8). To remove endogenous RNA, the microsomes were treated with micrococcal nuclease (New England Biolabs, 150 units/mL final concentration) at 25°C for 10 min. The nuclease activity was then quenched by adjustment to 2 mM EGTA. Microsomes containing various Sec61 mutants were

normalized for total protein by BCA protein assay (Pierce) and equivalent amounts of total protein resolved by SDS-PAGE next to a serial dilution of canine rough microsomes (CRM) containing a known concentration of the Sec61 complex. Proteins were then transferred to nitrocellulose and Western blotted for the Flag epitope, Sec61α, or Sec61γ. Following this standardized protocol, the expression level between different Sec61α mutants was found to be very similar, and the concentration of recombinant Sec61 in the final microsomal preparation was similar to the concentration of Sec61 in CRM.

Immunopurification of RNC-Sec61 complexes: Translation reactions (100 μL) were programmed with mRNA templates encoding for the first 126 a.a. of TNFα plus an N-terminal 3x-Flag-tag, or as a control, a 3x-HA-tag. Targeted integration intermediates were isolated as described above except the membrane pellet was brought up in two volumes of membrane buffer (100 mM KAc, 250 mM sucrose, 2 mM Mg(Ac)$_2$, 50 mM Hepes, pH 7.8) supplemented with 1% Deoxy BigChap (DBC, Anatrace). The membranes were solubilized for 10 min at 0°C and insoluble material removed by centrifugation at 50,000 rpm in a TLA100 rotor at 4°C for 10 min. The supernatant was then incubated with anti-Flag affinity resin (20 μL of a 50% slurry) at 4°C for 2.5 hr with rotation, at which time the resin was sedimented (600 × g, 3 min, 4°C) and washed four times with 1 mL of membrane buffer containing 0.3% DBC. After the final wash, bound proteins were eluted with 250 μg/mL of 3x-Flag peptide (Sigma) in membrane buffer containing 0.3% DBC. The eluted material was either analyzed directly by SDS-PAGE and semi-quantitative Western blotting, or first photolyzed, subjected to click chemistry and analyzed by SDS-PAGE and in-gel fluorescent scanning, as previously described.[22]

Typically, ~0.3 pmol of purified RNC-Sec61 complexes were obtained from a 100 µL translation reaction.

3.14 References

1. Shao, S., and Hegde, R.S. (2011). Membrane protein insertion at the endoplasmic reticulum. Annu. Rev. Cell Dev. Biol. *27*, 21.1–21.32.

2. Egea, P. F., Stroud, R. M., and Walter, P. (2005). Targeting proteins to membranes: structure of the signal recognition particle. Curr. Opin. Struct. Biol. *15*, 213–220.

3. Osborne A.R., Rapoport, T.A., and van den Berg, B. (2005). Protein translocation by the Sec6/SecY channel. Annu. Rev. Cell Dev. Biol. *21*, 529–550.

4. Martoglio B., Hofmann, M.W., Brunner, J., and Dobberstein, B. (1995). The protein-conducting channel in the membrane of the endoplasmic reticulum is open laterally toward the lipid bilayer. Cell *81*, 207–214.

5. Do, H., Falcone, D., Lin, J., Andrews, D.W., and Johnson, A.E. (1996). The cotranslational integration of membrane proteins into the phospholipid bilayer is a multistep process. Cell *85*, 369–378.

6. Mothes, W., Heinrich, S.U., Graf, R., Nilsson, I., von Heijne, G., Brunner, J., and Rapoport, T.A. (1997). Molecular mechanism of membrane protein integration into the endoplasmic reticulum. Cell *89*, 523-533.

7. Heinrich, S.U., Mothes, W., Brunner, J., and Rapoport, T.A. (2000). The Sec61p complex mediates the integration of a membrane protein by allowing lipid partitioning of the transmembrane domain. Cell *102*, 233–244.

8. Hessa, T., Meindl-Beinker, N.M., Bernsel, A., Kim, H., Sato, Y., Lerch-Bader, M., Nilsson, I., White, S.H., and von Heijne, G. (2007). Molecular code for transmembrane-helix recognition by the Sec61 translocon. Nature *450*, 1026–1030.

9. Ojemalm, K., Higuchi, T., Jiang, Y., Langel, U., Nilsson, I., White, S.H., Suga, H., and von Heijne, G. (2011). Apolar surface area determines the efficiency of translocon-mediated membrane-protein integration into the endoplasmic reticulum. Proc. Natl. Acad. Sci. E-publication.

10. McCormick, P.J., Miao, Y., Shao, Y., Lin, J., and Johnson, A.E. (2003). Cotranslational Protein Integration into the ER Membrane Is Mediated by the Binding of Nascent Chains to Translocon Proteins. Mol. Cell *12*, 329–341.

11. Sadlish, H., Pitonzo, D., Johnson, A.E., and Skach, W.R. (2005). Sequential triage of transmembrane segments by Sec61α during biogenesis of a native multispanning membrane protein. Nat. Struct. Mol. Biol. *12*, 870–878.

12. Van den Berg, B., Clemons, W.M., Jr., Collinson, I., Modis, Y., Hartmann, E., Harrison, S.C., and Rapoport, T.A. (2004). X-ray structure of a protein-conducting channel. Nature *427*, 36–44.

13. Gumbart, J., and Schulten, K. (2007). Structural determinants of lateral gate opening in the protein translocon. Biochemistry *46*, 11147–11157.

14. Cannon, K.S., Or, E., Clemons, W.M., Jr., Shibata, Y., and Rapoport T.A. (2005). Disulfide bridge formation between SecY and a translocating polypeptide localizes the translocation pore to the center of SecY. J. Cell Biol. *169*, 219–225.

15. Plath, K., Mothes, W., Wilkinson, B.M., Stirling, C.J., and Rapoport, T.A. (1998). Signal sequence recognition in posttranslational protein transport across the yeast ER membrane. Cell *94*, 795–807.

16. Junne, T., Kocik, L., and Spiess, M. (2010). The hydrophobic core of the Sec61 translocon defines the hydrophobicity threshold for membrane integration. Mol. Biol. Cell *21*, 1662–1670.

17. Egea, P.F., and Stroud, R.M. (2010). Lateral opening of a translocon upon entry of protein suggests the mechanism of insertion into membranes. Proc. Natl. Acad. Sci. *107*, 17182–17187.

18. Tsukazaki, T., Mori, H., Fukai, S., Ishitani, R., Mori, T., Dohmae, N., Perederina, A., Sugita, Y., Vassylyev, D.G., Ito, K., et al. (2008). Conformational transition of Sec machinery inferred from bacterial SecYE structures. Nature *455*, 988–991.

19. Zimmer, J., Nam, Y., and Rapoport, T.A. (2008). Structure of a complex of the ATPase SecA and the protein-translocation channel. Nature *455*, 936–943.

20. Besemer, J., Harant, H., Wang, S., Oberhauser, B., Marquardt, K., Foster, C.A., Schreiner, E.P., de Vries, J.E., Dascher-Nadel, C., and Lindley, I.J.D. (2005). Selective inhibition of cotranslational translocation of vascular cell adhesion molecule 1. Nature *436*, 290–293.

21. Garrison, J.L., Kunkel, E.J., Hegde, R.S., and Taunton, J. (2005). A substrate-specific inhibitor of protein translocation into the endoplasmic reticulum. Nature *436*, 285–289.

22. MacKinnon, A.L., Garrison, J.L., Hegde, R.S., and Taunton, J. (2007). Photo-leucine incorporation reveals the target of a cyclodepsipeptide inhibitor of cotranslational translocation. J. Am. Chem. Soc. *129*, 14560–14561.

23. Maifeld, S.V., MacKinnon, A.L., Garrison, J.L., Sharma, A., Hegde, R.S., Kunkel, E.J., and Taunton, J. (2011). Secretory protein profiling reveals TNFα inactivation by selective and promiscuous Sec61 modulators. Chem. Biol. *18*, 1082–1088.

24. Sharma, A. Mariappan, M., Appathurai, S., and Hedge, R.S. (2010). In vitro dissection of protein translocation into the mammalian endoplasmic reticulum. Methods Mol. Biol. *619*, 339–363.

25. Gilmore, R., Collins, P., Johnson, J., Kellaris, K., and Rapiejko, P. (1991). Transcription of full-length and truncated mRNA transcripts to study protein translocation across the endoplasmic reticulum. Meth. Cell Biol. *34,* 223–239.

26. Kida, Y., Kume, C., Hirano, M., and Sakaguchi, M. (2011). Environmental transitions of signal-anchor sequences during membrane insertion via the endoplasmic reticulum translocon. Mol. Bio. Cell *21,*, 418–429.

27. Jungnickel, B., and Rapoport, T.A. (1995). A posttargeting signal sequence recognition event in the endoplasmic reticulum membrane. Cell *82*, 261–270.

28. Crowley, K.S., Reinhart, G.D., and Johnson A.E. (1993). The signal sequence moves through a ribosomal tunnel into a noncytoplasmic aqueous environment at the ER membrane early in translocation. Cell *73*, 1101–1115.

29. Rutkowski, D.T., Lingappa, V.R., and Hegde, R.S. (2001). Substrate-specific regulation of the ribosome- translocon junction by N-terminal signal sequences. Proc. Natl. Acad. Sci. USA *98*, 7823–7828.

30. Kalies, K.U., Rapoport, T.A., and Hartmann, E. (1998). The beta subunit of the Sec61 complex facilitates cotranslational protein transport and interacts with the signal peptidase during translocation. J. Cell Biol. *141*, 887–894.

31. Erdmann, F., Jung, M., Eyrisch, S., Lang, S., Helms, V., Wagner, R., and Zimmermann, R. (2009). Lanthanus ions inhibit the mamalian Sec61 complex in its channel dynamics and protein transport activity. FEBS Let. *583*, 2359–2364.

32. Richardson, J.S., and Richardson, D.C. (1988). Amino acid preferences for specific locations at the ends of α-helices. Science *240*,1648–1652.

33. Kim, S.J., Mitra, D., Salerno, J.R., and Hegde, R.S. (2002). Signal sequences control gating of the protein translocation channel in a substrate-specific manner. Dev. Cell *2*, 207–217.

34. Higy, M., Junne, T., and Spiess, M. (2004). Topogenesis of membrane proteins at the endoplasmic reticulum. Biochemistry *43*, 12716–12722.

35. Zhang, B., and Miller, T.F., III. (2010). Hydrophobically stabilized open state for the lateral gate of the Sec translocon. Proc. Natl. Acad. Sci. *107*, 5399-5404.

36. Fons, R.D., Bogert, B.A., and Hegde, R.S. (2003). Substrate-specific function of the translocon-associated protein complex during translocation across the ER membrane. J. Cell Biol. *160*, 529–539.

37. Walter, P., and Blobel., G. (1983). Preparation of microsomal membranes for cotranslational protein translocation. Methods Enzymol *96*, 84–93.

38. Gorlich, D., and Rapoport, T.A. (1993). Protein translocation into proteoliposomes reconstituted from purified components of the endoplasmic reticulum membrnae. Cell *75*, 615–630.

39. Fitzgerald, D.J., Berger, P., Schaffitzell, C., Yamada, K., Richmond, T.J., and Berger, I. (2006). Protein complex expression by using multigene baculoviral vectors. Nat. Meth. *3*, 1021–1032.

Chapter 4: Conclusions and perspectives

Since the advent of modern medicine, there has existed great interest in the discovery of new chemical compounds that block the function of proteins that drive human disease. Developing such compounds into potent and selective drugs can be greatly aided by an understanding of their mode of action. This includes identification of the compound's cellular target, knowledge of how the target protein's function in inhibited, and the cellular consequences of target inhibition.

In this dissertation, I have provided a more complete description of the mode of action of cotransins, a class of compounds previously shown to inhibit the expression of several therapeutically relevant proteins. I showed that cotransins block the expression these proteins by directly binding to the Sec61 channel, thereby preventing their translocation through Sec61 and leading to their degradation in the cytosol. This discovery highlights Sec61 as a potentially novel therapeutic target. Future structural studies may help guide the design and development of additional cotransin-like molecules.

In our efforts to understand *how* cotransins act at Sec61 to selectively block substrate translocation, we also uncovered new features of Sec61 function. For example, we found that the lateral gate in Sec61α plays a direct role in mediated the partitioning of hydrophobic transmembrane domains into the lipid membrane. This work illustrates a tenet of the field of chemical biology which posits that small molecule inhibitors can often be useful tools to discover new biological functions, even if they lack drug-like properties.
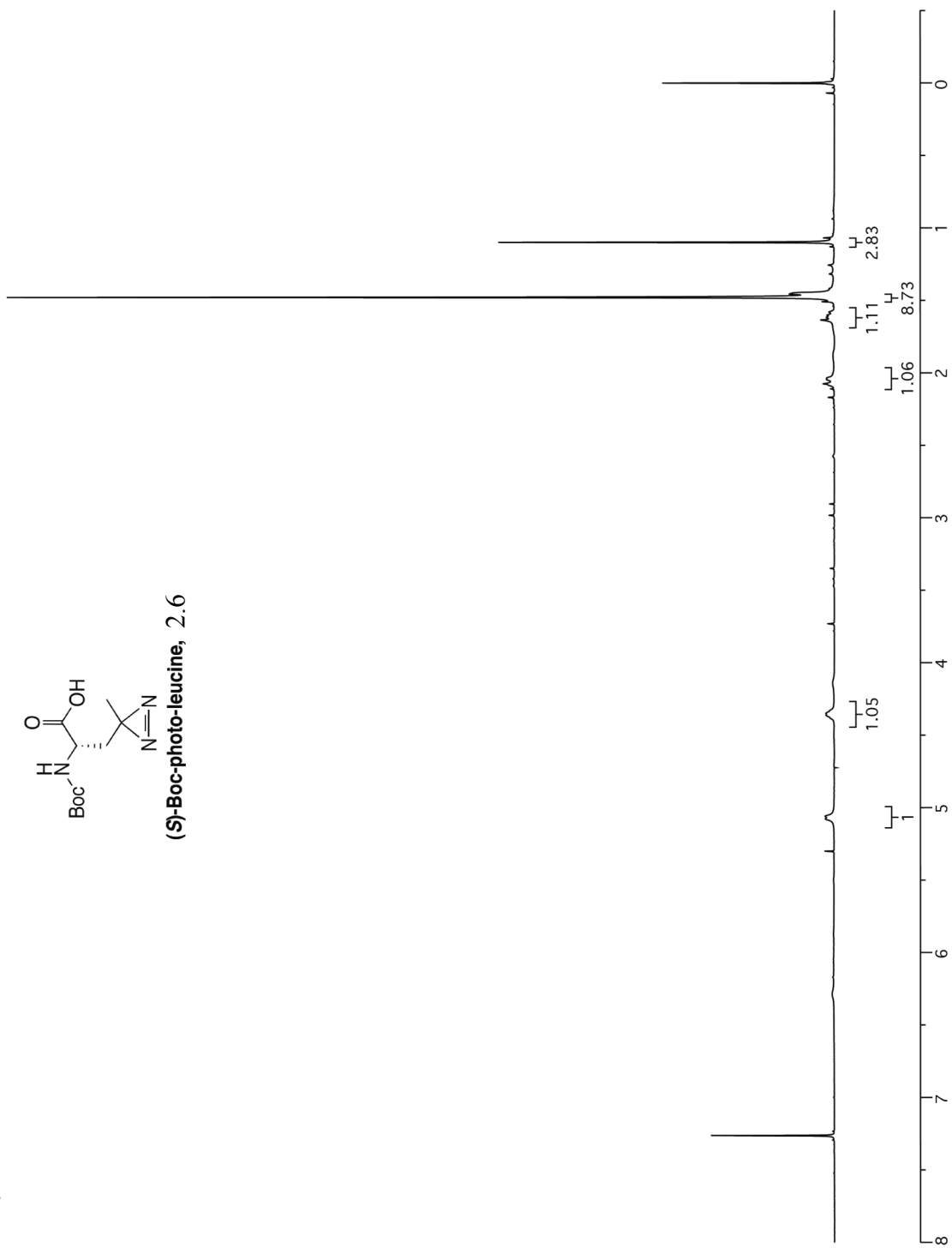
Will cotransins ever be useful therapeutic agents? The answer to this question partially lies in elucidating the full subset of human proteins whose expression is inhibited by cotransins. If cotransins broadly inhibit a large fraction of the secreted proteome across may cell types, they may display undesirable secondary or side effects in animals or people. Presently, we cannot accurately predict whether a given protein (such as one that may drive a particular disease state) will be sensitive or resistant to cotransins. Finally, issues of cotransin stability and distribution in living organisms remain unexplored. Nevertheless, drug discovery and development is often an empirical process (as opposed to a strictly rational process) and evaluation of cotransins' efficacy in cellular or animal models of human disease, especially those diseases involving increased expression of secretory or cell surface receptors, represents an important future goal.
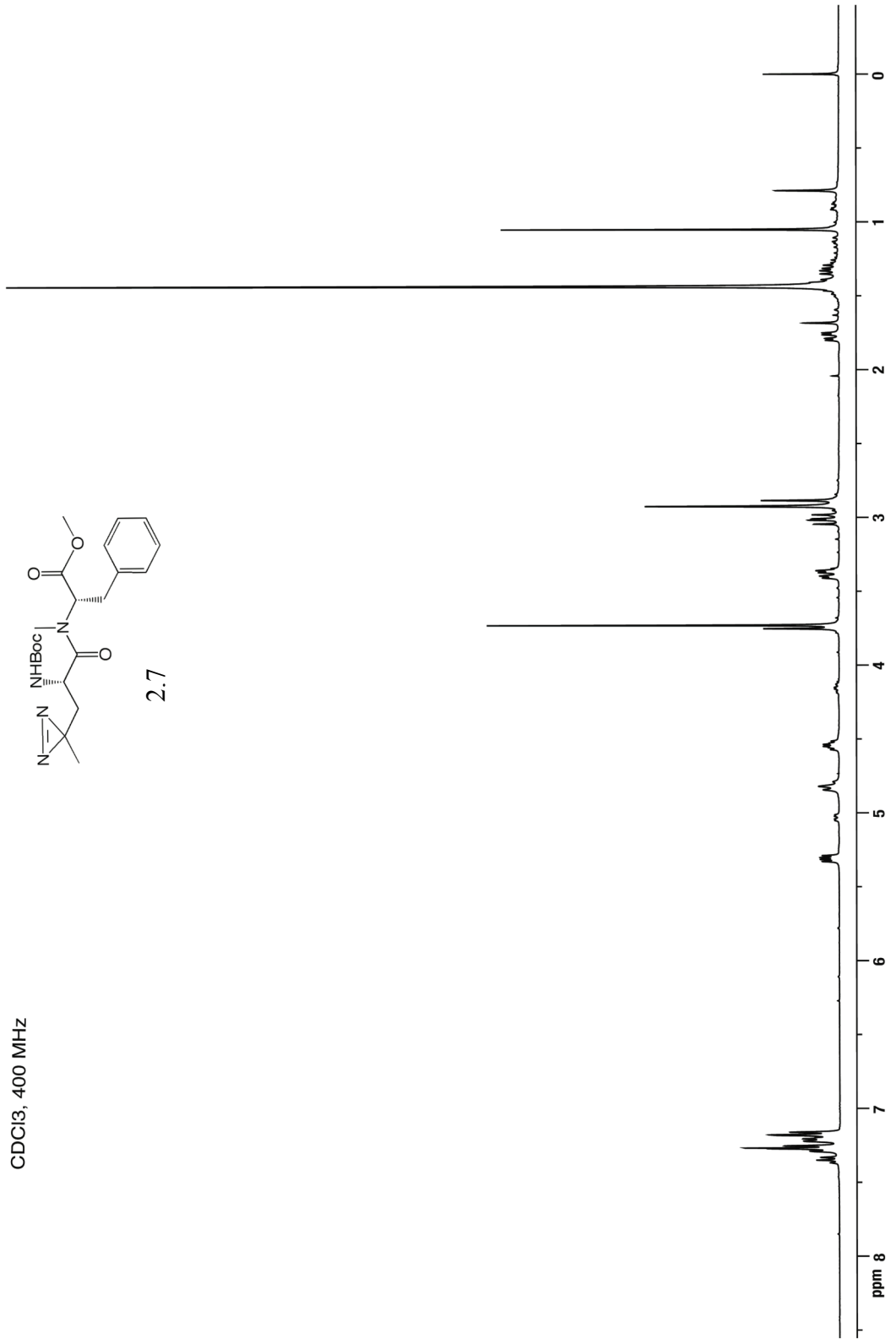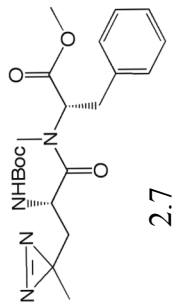
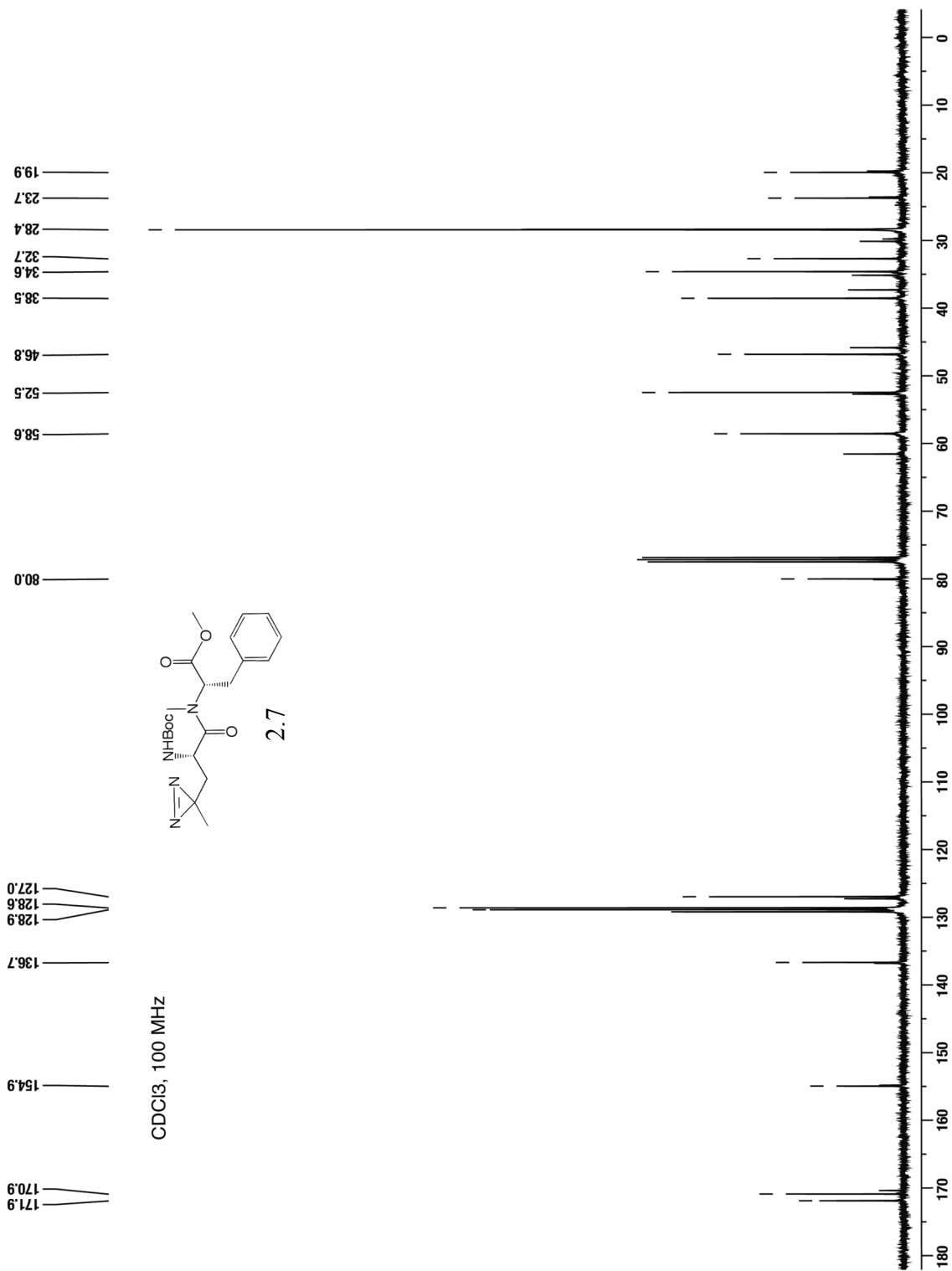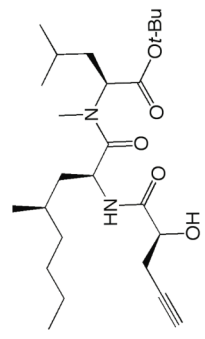# Appendix A: ^{1}H and ^{13}C NMR spectra
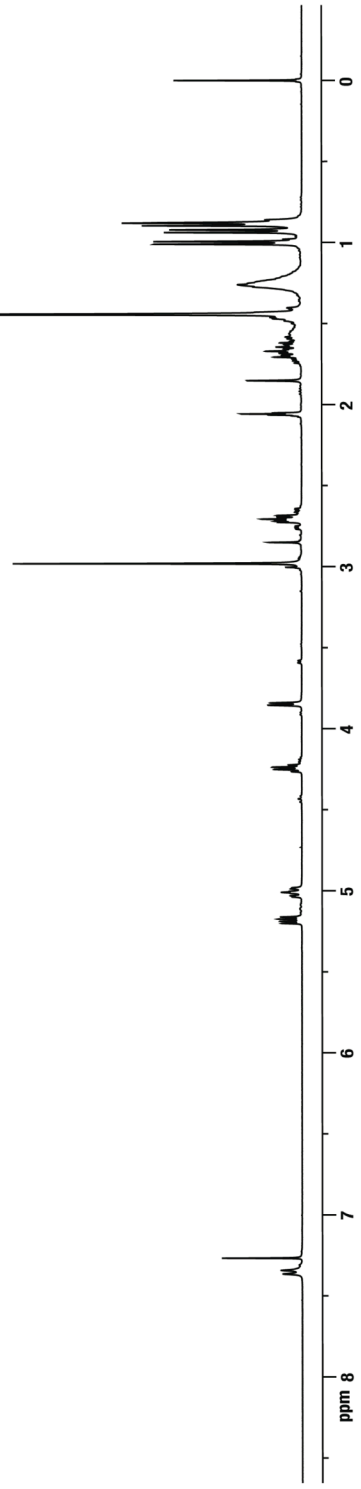
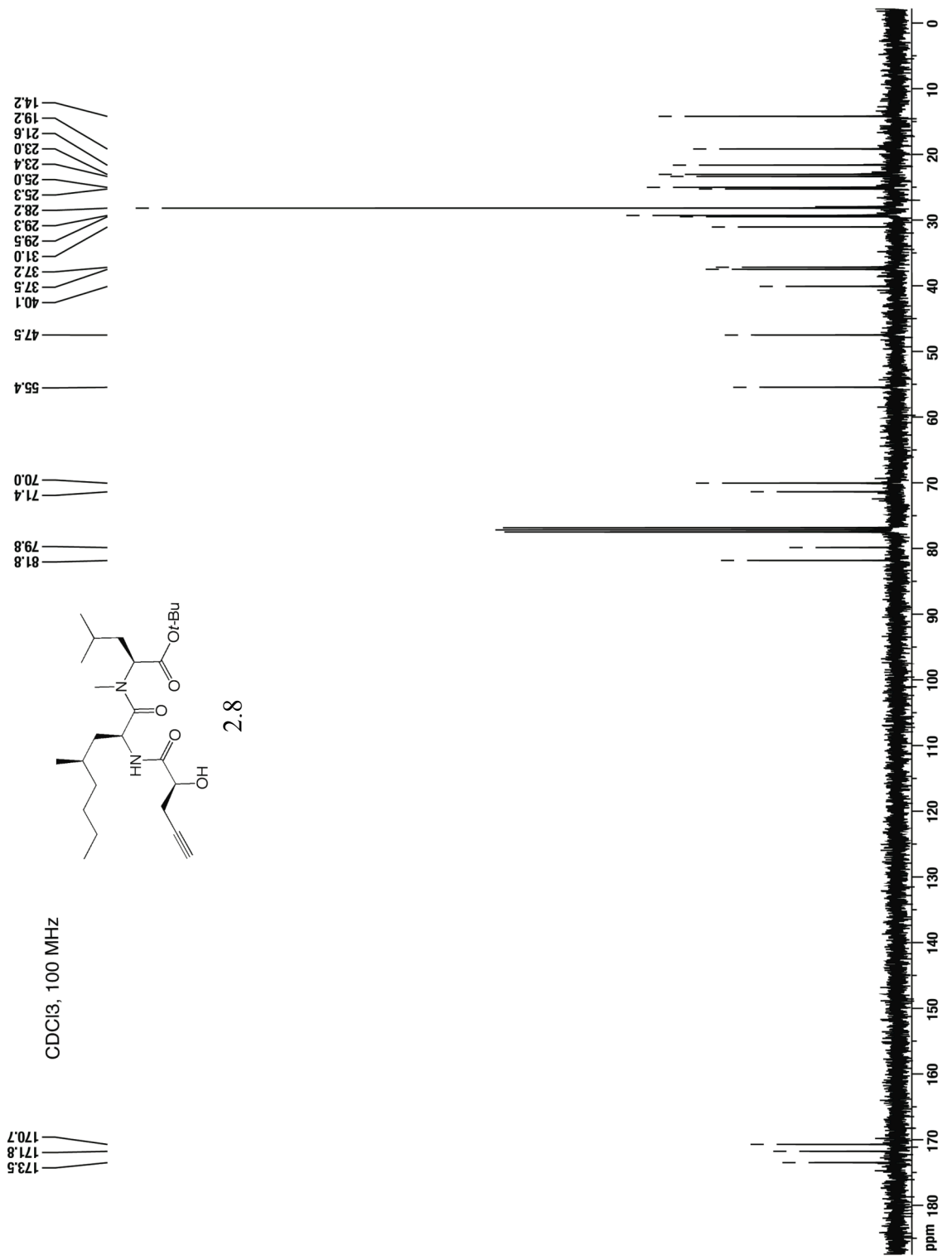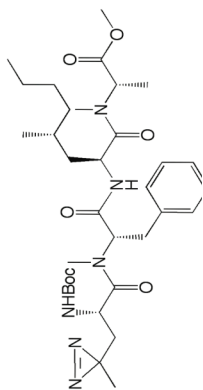CDCl3, 400 MHz
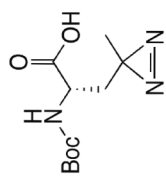
(S)-Boc-photo-leucine, 2.6

CDCl3, 400 MHz

2.7

19.9
23.7
28.4
32.7
34.6
38.5
46.8
52.5
58.6
80.0
127.0
128.6
128.9
136.7
154.9
170.9
171.9

2.7

CDCl3, 100 MHz

0 10 20 30 40 50 60 70 80 90 100 110 120 130 140 150 160 170 180

CDCl3, 400 MHz

2.8

Ot-Bu

OH

CDCl3, 100 MHz

2.8

14.2
19.2
21.6
23.0
23.4
25.0
25.3
28.2
29.3
29.5
31.0
37.2
37.5
40.1

47.5

55.4

70.0
71.4

79.8
81.8

170.7
171.8
173.5

CDCl3, 400 MHz

2.9

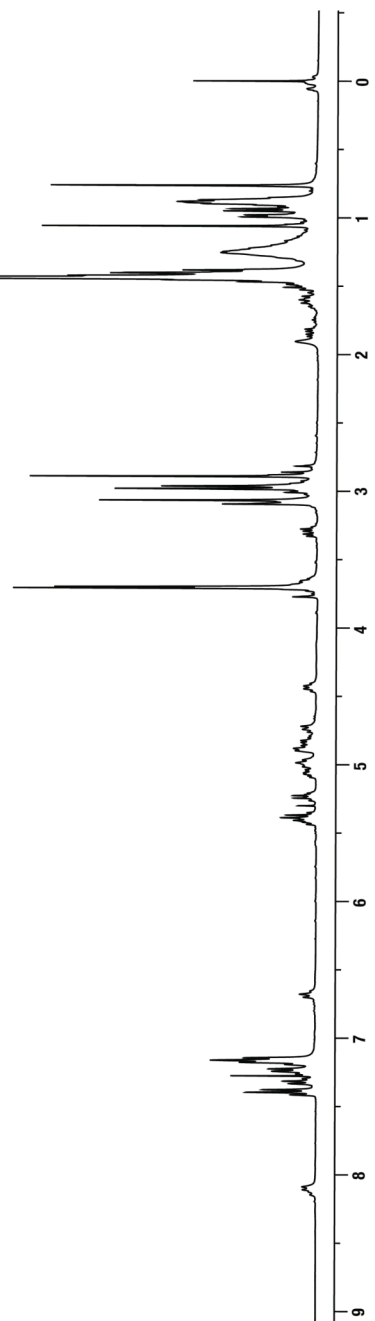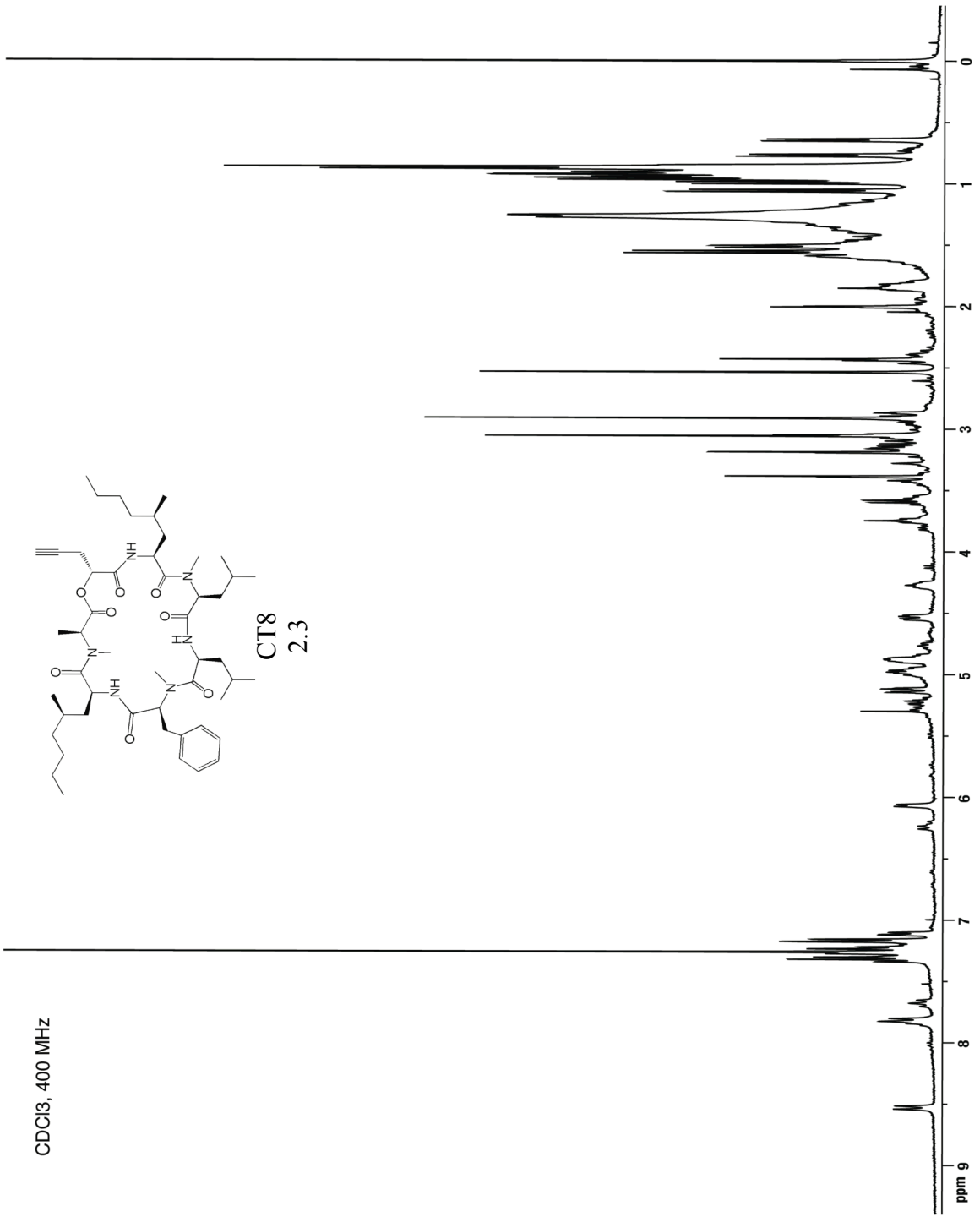CDCl3, 400 MHz

2.10

CT7
2.2

CDCl3, 400 MHz

2.11

CDCl3, 400 MHz

CDCl3, 400 MHz

CT8
2.3

Publishing Agreement

It is the policy of the University to encourage the distribution of all theses, dissertations, and manuscripts. Copies of all UCSF theses, dissertations, and manuscripts will be routed to the library via the Graduate Division. The library will make all theses, dissertations, and manuscripts accessible to the public and will preserve these to the best of their abilities, in perpetuity.

I hereby grant permission to the Graduate Division of the University of California, San Francisco to release copies of my thesis, dissertation, or manuscript to the Campus Library to provide access and preservation, in whole or in part, in perpetuity.

_____   11/12/2011
Author Signature   Date